2017

Activated Carbon Preparation and Modification for Adsorption

Yuhe Cao
South Dakota State University

ACTIVATED CARBON PREPARATION AND MODIFICATION FOR

ADSORPTION

BY

YUHE CAO

A dissertation submitted in partial fulfillment of the requirements for the

Doctor of Philosophy

Major in Biological Sciences

Specialization in Agricultural and Biosystems Engineering

South Dakota State University

2017

ACTIVATED CARBON PREPARATION AND MODIFICATION FOR

ADSORPTION

This dissertation is approved as a creditable and independent investigation by a candidate for the Doctor of Philosophy in Biological Sciences degree and is acceptable for meeting the dissertation requirements for this degree. Acceptance of this does not imply that the conclusions reached by the candidate are necessarily the conclusions of the major department.

Zhengrong Gu, Ph.D.
Dissertation Advisor   Date

Van Kelley, Ph.D.
Head of Department
Agricultural and Biosystems Engineering   Date

Dean, Graduate School   Date

This is lovingly dedicated to my wife, Beibei, and our parents who have been my

constant source for encouragement and inspiration.

ACKNOWLEDGEMENTS

It is the end of the three-and-a-half-year journey involving memorable times and many experiences in science and social life in Brookings, South Dakota. I would like to thank all the people who contribute this journey with their encouragements and supports. Probably I will forget some people in these acknowledgments and therefore I apologize on beforehand.

First and foremost, I am deeply grateful to my supervisors, Professor Zhengrong Gu, my advisor, thank you for giving me the opportunity to pursue my PhD in your group. You inspired and guided me with your immense knowledge, passion, motivation, and patience, while at the same time giving me the freedom to explore the world of unknown. I learned a lot from your inspiring ideas, broad knowledge, and attitudes towards scientific research. All of these help in shaping me to be a qualified PhD and will be a great treasure in my life. I appreciate your continuous support for my PhD study and related research and the large amount of time that you spent on my work, discussing the results, timely correcting my papers and my dissertation. Without your help and guidance, this dissertation would never be finished in time.

I would like to express my sincere gratitude to the committee members: Prof. Gibbons, Prof. Muthu and Prof. Held for their guidance and support in finishing this dissertation. Their insightful suggestions broadened my professional experience and prepared me for

future challenges. Thanks a lot for taking their precious time to evaluate my dissertation and attend my defense.

Many thanks to those who provided help with experiments: Dr. Parashu (XRD), Maheshwar (Raman), James D Hoefelmeyer (TEM), Joun Lee (XPS), James A Rice (NMR), and Al-Ahsan Talukder (SEM). I would like to express my special thanks to Prof. Qihua Fan who help me a lot for material characterization and data analysis.

My great appreciations also need to give to Prof. Kelley, Candy, Susan, Jasmine, Kristina, for their sincere helps during my study here. Many thanks to our technical supporting team: Scott and Jeff for their very kind help.

I need also express my feeling of gratitude to Mr. Joseph F. Nelson and the Joseph F. Nelson Graduate Scholarship Committee for selecting me as the Scholarship recipient. I am honored to be one of the recipients of the Joseph F. Nelson Graduate Scholarship, which really provided me the financial and spiritual supports. This will motivate me to work hard and achieve the excellence in my research area during my tenure at SDSU and beyond.

I would also thank my other colleagues and friends I met during my stay in SDSU: Hong Jin, Keliang, Xianhui, Shouyun, and Yaming. I am also grateful for Wendy Wang, for her helping with some of the materials preparation which was used in my research program.

I want to express my thanks to all of my REU students: Han Vu, Maria Andrea Castro and Tyler Ambrico. Thank you all for your great contributions to my dissertation. I am so proud of you for all the achievements you have made. I wish you great success with your future career.

Last but not the least, I would like to express my great gratitude to my family. This dissertation would not be possible without the spiritual and financial support and continuous encouragement from my family members. Particularly, I am deeply grateful to my beloved wife Beibei, without whom, this dissertation would never exist.

TABLE OF CONTENTS

LIST OF FIGURES

LIST OF TABLES

ABSTRACT

ACTIVATED CARBON PREPARATION AND MODIFICATION FOR

ADSORPTION

YUHE CAO

2017

Butanol is considered a promising, infrastructure-compatible biofuel. Butanol has a

higher energy content than ethanol and can be used in conventional gas engines without

modifications. Unfortunately, the fermentation pathway for butanol production is

restricted by its toxicity to the microbial strains used in the process. Butanol is toxic to

the microbes, and this can slow fermentation rates and reduce butanol yields. Gas

stripping technology can efficiently remove butanol from the fermentation broth as it is

produced, thereby decreasing its inhibitory effects.

Traditional butanol separation heavily depends on the energy intensive distillation

method. One of the main issues in acetone-butanol-ethanol fermentation is that butanol

concentrations in the fermentation broth are low, ranging from 1 to 1.2 percent in weight,

because of its toxicity to the microorganisms. Therefore distillation of butanol is even

worse than distillation of corn ethanol. Even new separation methods, such as solid-

extraction methods involve adding substances, such as polymer resin and zeolite or

activated carbon, to biobutanol fermentatioon broth did not achieve energy efficient separation of butanol due to low adsorption selectivity and fouling in broth. Gas-stripping - condensation is another new butanol recovery method, however, the butanol in gas-stripping stream is too low to be condensed without using expensive and energy intensive liquid nitrogen.

Adsorption can then be used to recover butanol from the vapor phase. Activated carbon (AC) samples and zeolite were investigated for their butanol vapor adsorption capacities. Commercial activated carbon was modified via hydrothermal H_2O_2 treatment, and the specific surface area and oxygen-containing functional groups of activated carbon were tested before and after treatment. Hydrothermal H_2O_2 modification increased the surface oxygen content, Brunauer-Emmett-Teller surface area, micropore volume, and total pore volume of active carbon. The adsorption capacities of these active carbon samples were almost three times that of zeolite. However, the un-modified active carbon had the highest adsorption capacity for butanol vapor (259.6 mg g^{-1}), compared to 222.4 mg g^{-1} after 10% H_2O_2 hydrothermal treatment. Both modified and un-modified active carbon can be easily regenerated for repeatable adsorption by heating to 150 ℃. Therefore, surface oxygen groups significantly reduced the adsorption capacity of active carbons for butanol vapor.

In addition, original active carbon and AC samples modified by nitric acid hydrothermal modification were assessed for their ability to adsorb butanol vapor. The

specific surface area and oxygen-containing functional groups of AC were tested before and after modification. The adsorption capacity of unmodified AC samples were the highest. Hydrothermal oxidation of AC with HNO_3 increased the surface oxygen content, Brunauer-Emmett-Teller (BET) surface area, micropore, mesopore and total pore volume of AC. Although the pore structure and specific surface area were greatly improved after hydrothermal oxidization with 4 M HNO_3, the increased oxygen on the surface of AC decreased the dynamic adsorption capacity.

In order to get high adsorption capacity adsorbents, we used corn stalk as precursor to fabricate porous carbon. ACs were prepared through chemical activation of biochar from whole corn stalk (WCS) and corn stalk pith (CSP) at varying temperatures using potassium hydroxide as the activating agent. ACs were characterized via pore structural analysis and scanning electron microscopy (SEM). These adsorbents were then assessed for their adsorption capacity for butanol vapor. It was found that WCS activated at 900 °C for 1 h (WCS-900) had optimal butanol adsorption characteristics. The BET surface area and total pore volume of the WCS-900 were 2330 m^2 g^{-1} and 1.29 cm^3 g^{-1}, respectively. The dynamic adsorption capacity of butanol vapor was 410.0 mg g^{-1}, a 185.1 % increase compared to charcoal-based commercial AC (143.8 mg g^{-1}).

Based on the adsorption experiments of butanol vapor, we found the chemical properties of the AC surface play an important role in adsorbing molecules. The adsorption of creatinine on active carbons was also studied, which is a toxic compound

generated by human. High levels of creatinine in the blood stream is normally caused by malfunction or failure of the kidneys. Activated carbons is taken by the patients orally to reduce creatinine level.

In order to figure out whether chemical modification could increase the adsorption capacity of creatinine, AC samples modified by nitric acid hydrothermal modification were assessed for their ability to adsorb creatinine. The pore structure and surface properties of the AC samples were characterized by N_2 adsorption, temperature programmed desorption (TPD), Fourier Transform Infrared spectroscopy (FTIR), and X-ray photoelectron spectrometer (XPS). It indicated that 4M HNO_3 hydrothermal modification with 180 °C was an efficient method in improvement of the creatinine adsorption. The improved adsorption capacity can be attributed mainly to an increase in the acidic oxygen-containing functional groups. The adsorption of creatinine over AC may involve an interaction with the acidic oxygen-containing groups on AC. Langmuir and Freundlich adsorption models were applied to describe the experimental isotherm and isotherm constants. Equilibrium data fitted very well to the Freundlich model in the entire saturation range (3.58-59.08 mg L^{-1}). The maximum adsorption capacities of AC modified with 180 °C is 62.5 mg g^{-1} according to the Langmuir model. Pseudo first-order and second-order kinetic models were used to describe the kinetic data and the rate constants were evaluated. The experimental data fitted well to the second-order kinetic model, which indicates that the chemical adsorption was the rate-limiting step, instead of mass transfer.

Chapter 1 Introduction and background

1.1   Introduction

The fluctuating price of oil, finite stocks of fossil fuels, and environmental consequences of fossil fuel use have prompted the demand for the production of biofuels from natural resources [1]. Butanol is considered a promising liquid fuel [2] because of its superior fuel properties, such as high energy density [3], low vapor pressure, low corrosivity to aluminum or polymer components in fuel systems [4], and high tolerance to water contamination for long-term storage [5]. In addition, butanol's fuel properties are close to gasoline and it can be used as blend fuel in spark ignition engines without any engine modification [6]. Microbial butanol can be produced by fermentation using different feedstocks, such as sucrose [7], starch [8, 9], lignocellulosic biomass [10], glycerol [11], and algae [12]. The concentration of butanol or total organic solvents is approximately 10-20 g/L in aqueous fermentation broth [13-15]. Distillation is generally applied for product recovery, but this is energy-intensive due to the low butanol concentration [16-18].

The product butanol is toxic to bacteria and will inhibit the fermentation process [19]. To overcome this problem, several in-situ product recovery techniques have been developed to remove butanol as it is made. These methods include liquid phase adsorption [20], liquid-liquid extraction [21], pervaporation [22], and gas stripping [23]. While advancements have been made in each of these areas, the expense of recovering

butanol from diluted solutions has hindered commercial deployment. Cells and organic compounds in the broth can foul adsorbents. Liquid-liquid extraction technology is limited by toxicity of the organic liquid solvents to the butanol-producing microbes, as well as emulsion formation and loss of extractant. Pervaporation can efficiently recover and concentrate butanol from fermentation broth, but membrane fouling with the microbes and non-volatile organic substances is a challenge [24].

Gas stripping has been suggested as one of the best techniques for butanol recovery [14, 23, 25], since butanol would be rapidly removed from the fermentation broth, and no harmful or expensive extractants or adsobents would be in contact with said broth. Gas stripping is a relatively simple process in which a gas is continuously bubbled through the fermentation culture to volatilize and carry out the chemical (as well as some water vapor), which are subsequently condensed. The challenge with applying gas stripping to fermentation is that the gas stream exiting the fermentor would also be very dilute. The condensation temperature required to condense butanol from a vapor stream is directly correlated with the butanol concentration. Therefore, a dilute butanol vapor would require exceptionally cold condensation temperatures, such as that of -60 ℃ [26]. These added costs would negate the benefits of gas stripping. To overcome this challenge, an alternative to direct condensation is to pass the gas stripping vapor first into an absorbent to concentrate the chemical. A smaller volume of gas can subsequently be used to displace the chemical from the absorbent, resulting in a higher concentration in this secondary vapor, such that cold water could be used to condense the product.

Active carbon (AC) is a porous material with large surface area, high porosity, and rapid adsorption capabilities, and has been employed to absorb various volatile organic compounds, including benzene, toluene, formaldehyde, n-hexane, and ethanol [27-32]. These studies focused on the adsorption behavior of AC without attention to regeneration. In general, physical adsorption occurs when the solvent is held on the surface and in the pores of the AC by Van der Waals force of attraction. Then, the adsorbed solvent can be easily desorbed by heating the AC. Hence, AC can potentially be used to capture butanol vapor released from fermentation broth via the gas stripping processes. Therefore, it is important to understand butanol adsorption and desorption curves for AC, as well as the relationship between AC properties (pore size, surface area, and functional group) and adsorption capacity. It has been widely recognized that chemical species adsorbed by AC is due predominantly to the surface complex formation between the species and the surface functional groups [33]. Therefore, it is essential to investigate the chemical modification of ACs and their adsorption behavior before and after treatment. Meanwhile, we try to use waste biomass-cornstalk as precursor to fabricate high specific surface area AC in order to get high butanol adsorption capacity AC samples.

Creatinine is a low-molecular-weight water-soluble uremic toxin that is the main indicator for renal health. In the efforts to replace extensive kidney dialysis procedures and develop an artificial kidney, a strong adsorbent is needed that can adsorb low and

middle weight uremic toxins. Creatinine will also be adsorbed in this process and its adsorption on the selected adsorbent needs to be understood. Charcoal-based commercial Activated Carbon (AC) was modified with HNO3 to improve its adsorption capacity for creatinine.

1.2 Gas stripping

Gas stripping does not require expensive investments on apparatus, does not harm the culture, does not remove nutrients and reaction intermediates and reduces butanol toxicity (inhibition), which can be used to remove liquid fuels such as butanol. This technique is simple and does not require expensive apparatus. The volatile properties of the fermentation permit easy product removal by gas stripping. Gas can be sparged through the fermentor/bioreactor through a rotating fermentor shaft and volatile butanol can be condensed and recovered from the condenser. The concentration of butanol in the recovered stream is higher than present in the fermentation broth [34]. The gas-stripping process has been described as one of the most important techniques for removing butanol from the fermentation broth [35] since a number of advantages over other removal processes, for example: it is simple and inexpensive to operate and does not suffer from fouling or clogging due to the presence of biomass.

Groot et al. studied production of butanol in a continuous reactor and recovery by gas stripping. The broth was sprayed on top of the separate packed-bed stripper [36] column

and withdrawn at the bottom. Oxygen free nitrogen was used as a strip gas in a closed circuit. The gas was introduced at the bottom of the column by a compressor, and the alcohol/water vapors were condensed in a condenser at -5°C and a cold trap at -40°C.

Fig. 1.1 shows a schematic diagram of butanol removal by gas stripping from the fermentation broth.
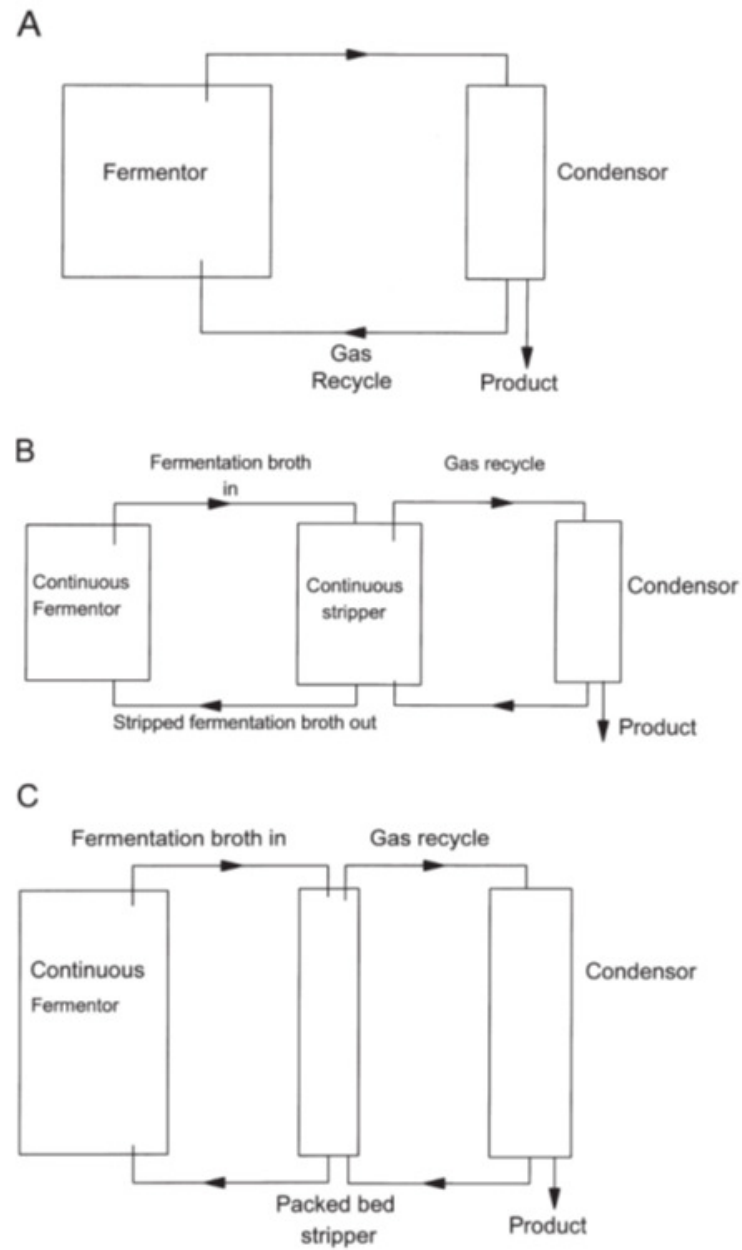
Fig. 1.1. Schematic diagrams of butanol/ABE removal from fermentation broth by gas stripping. (A) Removal from the fermentor; (B) removal using a separate stripper; (C) removal using a separate packedbed stripper[34].

1.3 Modification of activated carbon

The adsorption capacity of activated carbon is attributed to its textural properties and the chemical nature of its surface, i.e. the amount and nature of the oxygen-containing functional groups [37]. Research have focused on enhancing the effectiveness of activated carbon by modifying their surface chemical properties in order to enable the carbon to develop affinity for certain compounds. AC surface can display acidic, basic and/or neutral characteristics depending on the functional groups on its surface. Acidic and basic functional groups could be added onto the AC surface by chemical modification. Acidic groups such as carboxyl, quinone, carbonyl, lactone, hydroxyl and carboxylic anhydride are shown in Fig. 1.2. These groups can be created or increased by oxidation with oxygen at elevated temperatures (or by aging at mild temperatures) or with liquid oxidants, typically nitric acid and hydrogen peroxide. The increased acidic functional groups can increase the adsorption capacity of chemical compounds, however, it is detrimental to the physical aspects of AC such as BET surface area and pore volume [33].
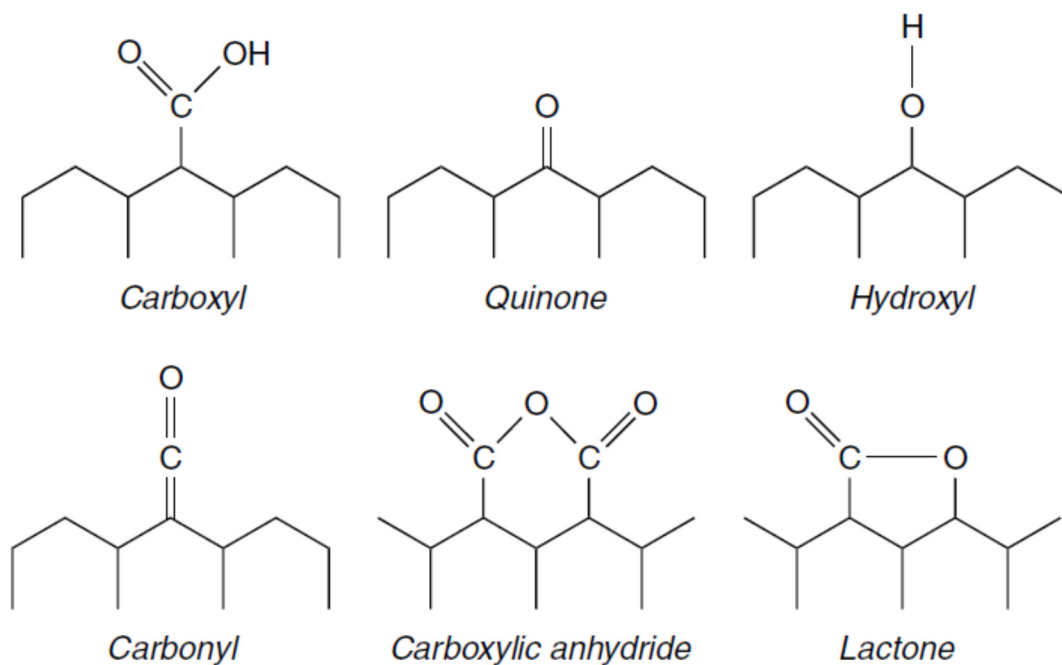
Fig. 1. 2. Simplified schematic of some acidic surface groups bonded to aromatic rings on AC. These groups are bonded to aromatic rings [38].

1.3.1 Nitric acid treatment of AC

Although oxidation would play beneficial effect on the adsorption, treatment with nitric acid reduced the BET surface area and total pore volume by 9.2% and 8.8% [39], respectively. AC treated with concentrated nitric acid and equimolar mixture of nitric/sulfuric acid for 38 and 24 h, respectively, experienced reduced BET surface area by 33.7% and 6.5% [40, 41]. They postulated partial or complete blockage with additional oxygen complexes and destruction of porous structure within AC as the reasons for the reduction, which is caused by severe nitric acid oxidation.

1.3.2 Hydrogen peroxide treatment of AC

H_2O_2 is a much lesser effective oxidant than HNO_3, concerning the number of oxygen surface groups created and the extent to which some of them are generated [42]. The surface chemistry of the AC was not significantly affected by treatment with H_2O_2 at room temperature and by using a low solution concentration [43]. Oxidation treatment at 363 K gives rise to a slight decrease in the surface area and the pore volume [44]. The decrease in surface area and volume brought about by stronger oxidation is generally explained by the restriction of the pore volume available for adsorption due to the formation of oxygen-containing groups at the entrance and/or on the walls of micro-pores and by the possible destruction of the pore walls and its collapse when oxygenated terminal groups are created.

1.4 Activated carbon preparation

Activated carbon (AC) is amorphous carbon, and it has a complex porous structure with disordered arrangements of carbon atoms forming micropores with a radius minor than 2 nm, mesopores with a radius of 2–50 nm and macropores with a radius bigger than 50 nm. Activated carbon has been widely used in adsorption due to its high surface area, high pore volume (micropore and mesopore volumes). There are mainly three steps for manufacturing AC: raw material preparation, low-temperature carbonization, and

activation. Two activation methods can be used to fabricate AC: physical and chemical process.

1.4.1 Physical activation

After initial treatment and pelletizing of the precursor, the bulk of the volatile matter was eliminated firstly at 400-500 °C, and then partial gasification at 800-1000 °C to develop the porosity and surface area. The partial gasification of carbonaceous materials was done in mild oxidizing gases such as steam, CO_2, or a combination of these. The activated carbon created by the activation process is used primarily for gas and vapor adsorption processes [38].

1.4.2 Chemical activation

Chemical activation occurs at a high temperature in the presence of agents such as KOH, K_2CO_3, NaOH, Na_2CO_3, $AlCl_3$, $ZnCl_2$, and H_3PO_4, which are used to degrade and dehydrate the cellulosic materials and, simultaneously, to prevent shrinkage during carbonization. The remaining chemicals are removed from the carbon by acid or water wash.

The physical activated carbon generally has a relatively lower specific surface area than the chemical activated carbon. Comparing both methods, chemical activation has

advantages such as low energy and operating cost, higher carbon yields and larger surface areas, which can also generate a higher development of microporous structure [45].

1.5 Corn stalk

Biomass wastes are very cheap and easily available, which are potential raw materials for the preparation of porous carbons with good electrochemical capacitive performance. Over recent years a considerable amount of literature has been published on porous carbon materials fabricated from biomass [46-52]. Corn stalk is an annually renewable biomass, available in abundant volumes throughout the world that is often left behind after corn grain is harvest [53]. In the United States, corn is the most widely grown crop [54] and it is estimated that approximately 153 million dry residual from this plant, which is available as biomass feedstock every year [55].

Corn stalk is made up of a cortex and a core, and the cortex is mainly made up of cellulose and lignin and the corn stalk core is mainly hemi-cellulose and a little lignin and cellulose [56]. Different parts of the biomass would produce different texture morphology. Cornstalk core is like a foam, which is porous. This natural porous structure can potentially generate hierarchical porous structure, which provides carbon with large surface for the molecule diffusion in carbon matrix. Cornstalk core was employed as a precursor to prepare nanoporous AC. Based on the spongy texture of the corn stalk pith,

we were expecting to obtain carbon materials with a relatively high surface area and hierarchical porous structure using KOH as the activating agent [57].

1.6 Creatinine adsorption

Presently, 26 million Americans have kidney disease and more than 450,000 of them are on dialysis [58]. People on dialysis are treated at least three times a week and each session lasts about four hours. They need to plan their life around their dialysis sessions substantially and traveling is made nearly impossible. This results in a low quality of life. We are researching an alternative method to reduce the concentration of toxins in the blood at a quicker rate, reducing the frequency of needed dialysis sessions, therefore giving people a better quality of life.

Activated carbon is an extremely porous carbon material with very large surface area available for adsorption or chemical reactions [59]. It is widely used as an adsorbent to remove various kinds of molecules from gaseous or aqueous media. It is already used in the medical field as to trap and adsorb chemicals in the digestive system to prevent poisoning or overdose [60]. It can also be used as an adsorbing agent for uremic toxins to lighten the workload of the kidneys and the dialysis.

Creatinine is a low molecular weight, water-soluble uremic toxin which is the end product of creatine metabolism [61]. Serum creatinine concentration is an important

indicator of renal health in humans because it is excreted unchanged by the kidneys. Therefore, this chemical was used as a marker for uremic toxin adsorbance of our activated carbon. Standard healthy concentrations in humans range from 135-206 µmol/L (15.3-23.3 mg/L). For people with kidney failure, the concentrations is around 2000 umol/L (226 mg/L). In the efforts to replace extensive kidney dialysis procedures and develop an artificial kidney, a strong adsorbent is needed that can adsorb low and middle weight uremic toxins. Creatinine will also be adsorbed in this process and its adsorption on the selected adsorbent needs to be understood. In this study, charcoal-based commercial AC was modified with HNO_3 to improve its adsorption capacity for creatinine. To the best of our knowledge, there was no such studies have been published on this concept.

Chapter 2 Objectives

It is interesting to have ACs with oxygen containing groups on the surface as they have large influence on the adsorption process. In this respect it is important to analyze the extent of these groups has on the textural characteristics of the active carbons. The objective of this dissertation is to analyze the possibility of obtaining active carbons having well developed textural characteristics and high content of oxygen groups. Furthermore, the adsorption behaviors of the prepared AC were investigated. In order to obtain high adsorption capacity AC, corn stalk was used as precursor for AC preparation.

- Evaluate the porous properties of the carbon materials which were modified by H_2O_2 and HNO_3, different concentrations, and different reaction temperatures by BET characterization
- Evaluate the porous properties of the carbon materials which were produced by corn stalk with different reaction temperatures by BET characterization
- Evaluate the adsorption capacity of the AC samples
- Analysis the micro-morphology structures of carbon materials by SEM characterization
- Analysis the functional groups on carbon materials by TPD, FTIR and XPS characterization

Chapter 3 Butanol vapor adsorption behavior on active carbons and zeolite crystal

3.1. Introduction

Biobutanol, produced in bioreactors, is a highly viable biofuel, even more so than ethanol. It has a higher combustion heat (83% that of gasoline as opposed to ethanol's 65%), is less miscible in water, and less hazardous to handle because of a higher boiling point (117°C) and flash point (29°C). Unfortunately, production is severely limited because of butanol's toxicity to the cyanobacteria that produce it. At concentrations between 1-2%, the butanol will strip away at the cyanobacteria's cell matrix, requiring constant filtration. With current methods, production energy is 1.5 times that of the butanol yielded [62]. Gas stripping and filtration with an activated carbon filter has been proposed as a means to adsorb some of these volatile organic compounds ventilated from a bioreactor and has the potential to provide a means of controlling the levels of these toxic compounds while increasing the yield of marketable products [26].

Active carbon can be modified to optimize adsorption/desorption activity. Pore size, pore structure, and total surface area are major components of active carbon adsorption capacity. Pores come in three classifications: micropores are the smallest, then mesopores, and lastly macropores are the largest. In general, a larger total surface area

correlates to a larger adsorption capacity as area available for reactions to take place increases [33].

However, another important feature is the surface functional groups present. For example, acid modification can increase the amount of acidic groups present, making active carbon ideal for the uptake of heavy metals or bases. Meanwhile, base modification will increase conjugated pi electron systems, making it ideal for uptake of aromatic organic acids [33]. With this in mind, our research aims to look at the effect of hydrogen peroxide modifications on the butanol adsorption/desorption activity of active carbon, with the hope that they will increase adsorption/desorption capacity.

In this study four types of AC (original and chemically modified active carbon by hydrothermal H_2O_2 reaction) were investigated for their absorption and desorption behavior with butanol vapor. In addition, the zeolite ZSM-5 was used as a control, since it is known that zeolites are good adsorbents for butanol recovery from aqueous solutions [63].

3.2 Materials and methods

3.2.1 Materials

Analytical grade butanol, 30% H_2O_2, hydrochloride acid, sodium hydroxide, and ethanol were purchased from Thermo Fisher Scientific Inc. The purity of butanol was >99.8%, which was used to generate vapor directly with helium gas bubbling. Commercial active carbon Sabre Series CR2050C-75 (unmodified AC) was donated by Carbon Resources. Different kinds of modified AC were obtained by reaction between commercial AC and different concentrations of H_2O_2. Another adsorbent, zeolite ZSM-5 (purchased from Sigma), was also used for comparison with the different kinds of AC.

3.2.2 Methods

3.2.2.1 Modification of active carbon

Commercial AC was packed into a Soxhlet extractor and washed with boiling water for 2 h. The wet AC was transferred to a beaker and dried at 105°C for 24 h. Then 5 g of unmodified AC was reacted with 40 ml H_2O_2 at 10%, 20% and 30% concentration (wt. %) in a sealed PTFE reactor (50 ml) at 120 °C for 1 h. After reaction, the reactant was cooled, filtered, and washed with deionized water under vacuum filtration until the pH value of the permeate was ~7. Finally, the leached reactants were dried in a vacuum oven at 105 °C overnight. The dried modified AC was ground and run through a sieve, and grains falling within US mesh sizes 50-100 were used as adsorbents.

3.2.2.2 Analytical methods for adsorbents

Nitrogen adsorption/desorption was carried out using Surface Area and Pore Size

Analyzers (ASAP 2010, Micromeritics, USA). The total pore volume was determined at

relative pressure P/P0, and the specific surface area was calculated from the Brunauer-

Emmett-Teller (BET) method. Density functional theory (DFT) was used to characterize

the micropore and pore size distribution.

3.2.2.3 Gas Chromatography Mass Spectrometer (GC-MS) analytical procedure

GC-MS was applied to analyze the outlet of the sample tube. Chromatographic

analysis was performed in a Shimadzu series GC-MS (Shimadzu Corporation, USA)

equipped with an RXI capillary column (30m$\times$0.15µm$\times$15mm). The initial temperature

(40 ℃) was held for 1 min and then raised to 200 ℃ at a rate of 45 ℃/min. All samples

were injected in split mode. The injection temperature was 150 ℃. The mass

spectrometer was operated in EI mode. Mass spectra was acquired in full scan mode with

repetitive scanning from 45 m/z to 500 m/z in 0.25 s. Ion source temperature was 250 ℃.

3.2.2.4 Adsorption and regeneration procedure

A Micrometrics Autochem II Chemisorption Analyzer, connected to a Shimadzu GC-

MS, was employed to investigate the adsorption and desorption behavior of different

adsorbents. Figure 3.1 shows the schematic diagram of the adsorption system used for

testing adsorbents. The flow rate of the vapor, carrier, and reference were set at 5, 5, and

10 cm3/min, respectively. Experiments were performed at atmospheric total pressure

using helium as carrier gas, assuming that helium is not adsorbed on active carbon.

Butanol was heated to 50 °C and, as it passed through the sample tube was adsorbed on

the adsorbent. Un-adsorbed butanol passed through the analysis chamber and then into

the GCMS. The reference chamber recorded the thermal conductivity detector (TCD)

readings and plotted them against time. The GC-MS records the intensity of the signal

produced by the adsorbate as a function of time approximately once every 10.5 minutes,

and the integral of the curve provides the volume of adsorbate present after adsorption.

At least 20 data points were obtained by the GC-MS over the course of the chemisorption

analysis. For regeneration, the temperature-programmed desorption (TPD) process pre-

programmed into the Micromeritics analyzer was used. The flow rate of the vapor,

carrier, and reference were set at 0, 10, and 10 cm^3/min, respectively. The temperature

ramp was set at 15°C/min, starting from 25-150 °C with a 1 h end temperature hold.
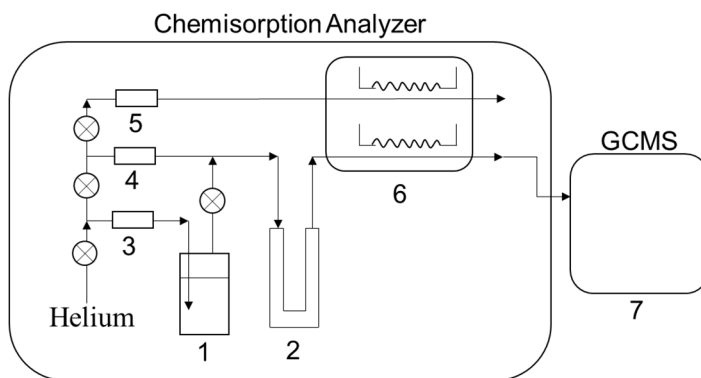
Fig. 3. 1. Schematic diagram of the experimental adsorption system: 1, butanol bath; 2, sample tube; 3, vapor flow rate meter; 4, carrier flow rate meter; 5, reference flow rate meter; 6, TCD detector; 7, GC-MS.

3.2.2.5 Surface functional group characterization

TPD analysis was also performed to investigate the oxygen content of the four AC samples. The carbon sample (0.05 g) was placed in a U-shaped quartz tube inside an electrical furnace and heated at 10 °C/min up to 1000 °C using a constant flow rate of helium (the flow rate of the vapor, carrier, and reference were set at 0, 10, and 10 cm3/min respectively). The TCD signals were monitored during the thermal analysis, and the corresponding TCD spectra was obtained.

3.2.2.6 Butanol quantification

To test the impact of surface modification on the butanol adsorption and desorption capacities of AC, a Shimadzu GC-MS was used. A standard curve was first created by injecting 1 µl volumes of various butanol concentrations in ethanol (1, 5, 10, 20, 30, 50, 60, 75, 93, 170, 235, and 290 mg/ml) and measuring the area beneath the curves. Figure 3.2A shows the intensity peaks for these butanol: ethanol mixtures. The initial retention times for ethanol and butanol were 1.58 min and 2.23 min, respectively. The peak areas

versus butanol concentrations were plotted to generate the standard curve shown in Figure 3.2B, with an R^2 of 0.99.

To quantify butanol vapor adsorbed on the adsorbent, the butanol concentration of the outlet stream was measured by passing 0.5 ml of outlet stream gas exiting the adsorption column into the GC-MS. Since the GC-MS needs time to cool down, the outlet of the sample tube was measured every 10.5 minutes. The outlet butanol vapor concentration as a function of time gave the breakthrough curve, and the adsorption capacity of the packed column was calculated for each experiment by the following equation:

$$Q = \frac{M_{adsorption}}{W} = \frac{T_q C_i F_A}{W} \qquad (1)$$

The time Tq is estimated according to the equation (2):

$$T_q = \int \left(1 - \frac{C_o}{C_i}\right) dt \qquad (2)$$

Where Q is the adsorbed amount (mg mg-1); $M_{adsorption}$ is the mass of butanol adsorbed (mg); F_A is the volumetric flow rate of the carrier gas (ml min-1); W is the net weight of adsorbent (mg); C_i represents the butanol concentration at the inlet (µg ml-1); C_o is the butanol concentration at the outlet (µg ml-1).

A
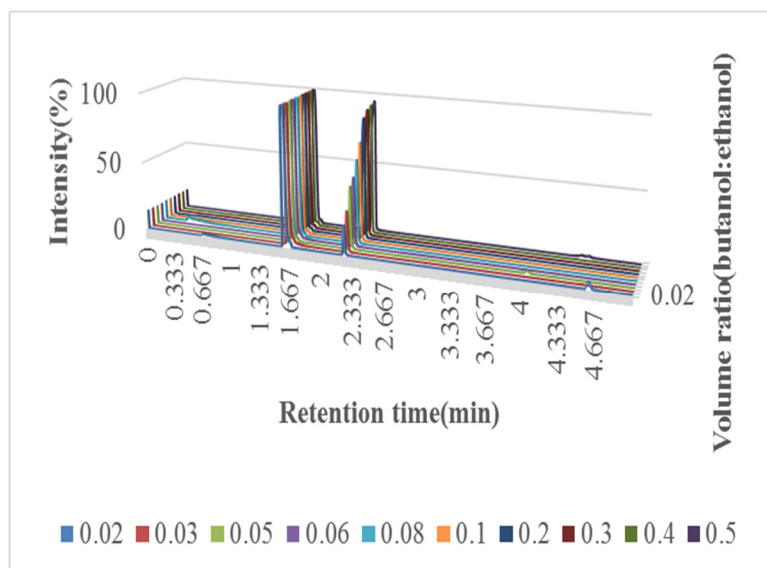
B
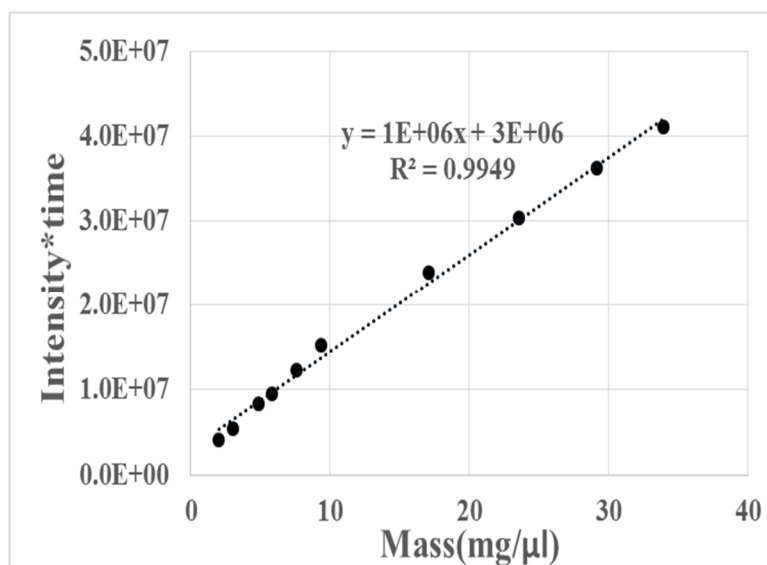
Fig. 3. 2. (A) GC profile for different butanol concentration. (B) Standard curve of butanol concentration via GCMS.

3.3. Results and Discussion

3.3.1 Physicochemical properties of adsorbents

3.3.1.1 Oxygen-containing functional groups

To investigate the functional groups on the surface of the AC samples, temperature-programmed desorption was employed. The carrier gas helium and the detected gases (CO_2, CO, NO, H_2O, etc.) have different thermal conductivities, and the area under each TCD peak is proportional to the amount of gas produced. At the beginning of each measurement, the TCD base line was zeroed using carrier gas and reference gas. According to Figure 3.3, which shows the TPD spectra of the AC before and after the oxidative treatments with different concentration of H_2O_2, there were small peaks for all AC samples from 35 ℃ to 100 ℃, which were caused by the air trapped in the pores of the AC samples.
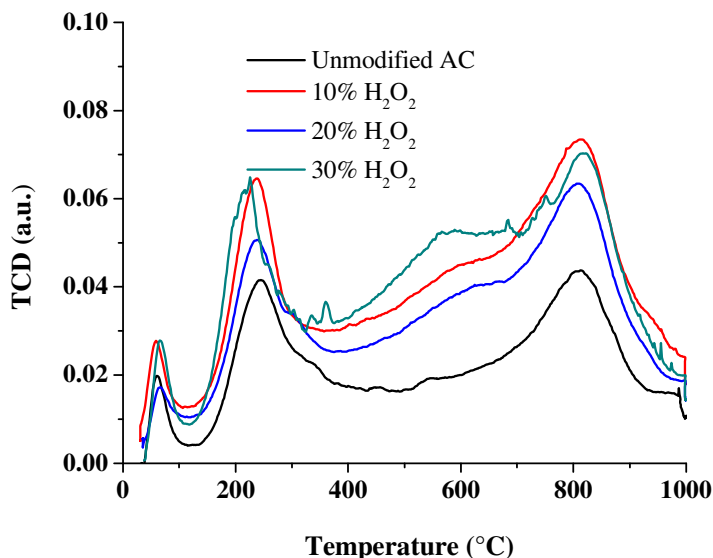
Fig. 3. 3. TCD signals for TPD spectra of AC samples.

After H_2O_2 treatment, the TCD signal intensities were generally higher than for unmodified AC. The evolution of CO_2 at temperatures of 100-400 ℃ is usually assigned to the degradation of carboxylic functional group, while at higher temperature (427 ℃), CO_2 release is attributed to the decomposition of anhydride and lactone groups [64-66]. Both CO_2 and CO were formed from 400 ℃ to 1000 ℃ [67], and the CO may have been derived from the decomposition of phenols, ethers and carbonyls/quinones [68-70]. Based on the peaks that appeared from 100 ℃ to 1000 ℃, it can be concluded that the H_2O_2 treatments of AC were effective in forming acidic oxygen surface groups. The total amount of these groups was greatest in the 30% H_2O_2 treatment, followed by 10% and 20% H_2O_2 treatments, with unmodified AC having the lowest amount of acidic oxygen surface groups.

3.3.1.2 Micropores of the adsorbents

The micropore (smaller than 2 nm) volume was higher for all H_2O_2 hydrothermally treated AC samples compared to the untreated AC control (Table 3.1). This was likely due to new micropores being generated by etching of the carbon walls by the H_2O_2 hydrothermal treatments, as we observed a slight mass loss of carbon in these treatments (data not shown). Meanwhile, the formation of oxygen groups caused blockage of some macropores (larger than 50 nm) and mesopores (between 2 nm and 50 nm), thereby effectively transforming them into micropores. P.C.C. Faria et al. [71], V. Gómez-Serrano et al. [72], and P. Chingombe et al. [73] reported a similar effect caused by carbonyl and carboxylic groups formed during oxidation when using nitric acid. The generated functional groups and the opening of the closed micropores also increased the micropore region of AC samples.

Table 3. 1 Surface area and pore structure parameters.

Sample	S_{BET}[a] $(m^2\ g^{-1})$	V_{Total}[b] $(cm^3\ g^{-1})$	V_{Micro}[c] $(cm^3\ g^{-1})$	V_{Meso}[d] $(cm^3\ g^{-1})$	$D_{Average}$[e] (nm)
Unmodified AC	1157	0.72	0.39	0.27	2.49
ZSM-5	400	0.32	0.11	0.19	3.20
10% H_2O_2	1362	0.86	0.46	0.33	2.53
20% H_2O_2	1216	0.71	0.43	0.22	2.34
30% H_2O_2	1205	0.76	0.41	0.28	2.52

[a] BET (Brunauer-Emmett-Teller) surface area

[b] Total pore volume, measured at P/P^0=0.995

[c] Micropore volume, based on density functional theory (DFT)

[d] Mesopore volume, based on density functional theory (DFT)

[e] Average pore diameter of absorbents, calculated by $4V_{Total}/S_{BET}$

In contrast to our work, Pereira et al. found that the micropore volume of AC decreased 10% (from 0.382 to 0.343 cm^3 g^{-1}) when hydrogen peroxide oxidation was employed [74]. However in that study oxidation was performed at room temperature, while in this work we conducted hydrothermal H_2O_2 oxidation at 120 °C. The sealed reaction system used herein generated steam, which can help develop pore structure. In addition, the evenly distributed pressure in the sealed system was likely favorable for pore development.

While hydrothermal H_2O_2 oxidation did increase micropore volume compared to the control, the effect diminished at higher H_2O_2 concentrations. Thus at 30% H_2O_2 treatment, micropore volume was only 0.41 cm^3 g^{-1}, compared to 0.39 cm^3 g^{-1} for untreated AC. While low (i.e., 10%) concentrations of H_2O_2 can generate more micropores by serving as an expanding agent and an oxidant, higher concentrations may result in H_2O_2 self-decomposition or convert large micropores into mesopores. Oxygen-containing functional groups formed by higher H_2O_2 levels may also decrease the micropore volume. As for the ZSM-5 adsorbent, the micropore volume was only 0.11 cm^3 g^{-1}, or one-third of the unmodified AC sample.

3.3.1.2 Mesopores of the adsorbents

The adsorption/desorption isothermal curves of the five adsorbents are shown in Figure 3.4A. There are loops in the five curves between 0.4-1.0 P/P_0, which demonstrates that all the adsorbents contained mesopores.

The TPD profiles of the modified AC samples (Figure 3.3), indicate that oxidation with H_2O_2 generated many oxygen-containing functional groups. It also showed that oxidation with 10% H_2O_2 was not strong enough to cause wall collapse, but compared to untreated AC, some wall etching increased the mesopore volume from 0.27 to 0.33 cm^3 g^{-1} (Table 3.1). DFT model simulation results according to the nitrogen adsorption/desorption curve, indicate that the volume of pores between 2 nm and 50 nm are decreased by using 20% H_2O_2 (Figure 3.4B). As H_2O_2 concentration increased from 10% to 20%, the more robust oxidation caused walls of the mesopore to collapse, thereby reducing mesopore volume from 0.33 into 0.22 cm^3 g^{-1} (Table 3.1). Additionally, the 20% H_2O_2 level caused more surface oxygen functional groups to form on carbon walls, which further blocked mesopore volume.

A
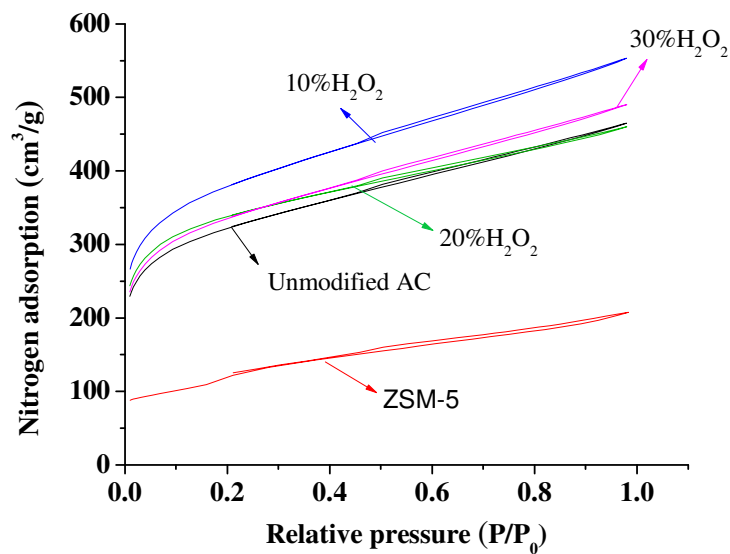
B
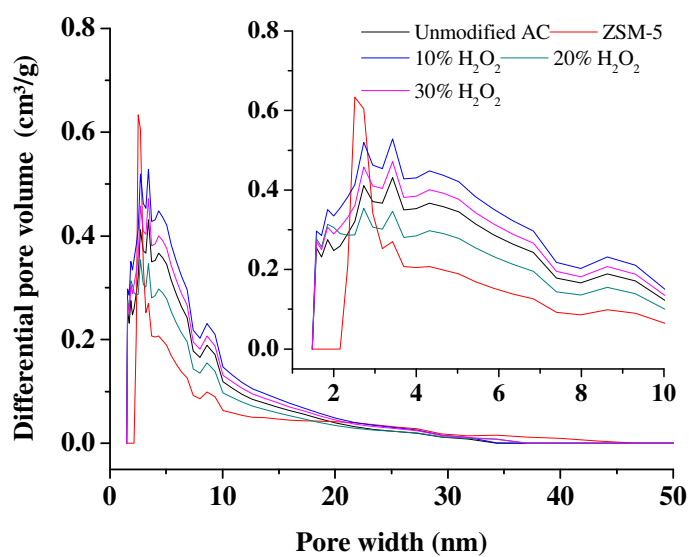
Fig. 3. 4. (A) Nitrogen isothermal adsorption of the absorbents. (B) The DFT pore size distribution curves of the absorbents.

As H_2O_2 concentration increased to 30%, mesopore volume was partially restored by creating additional pores in the collapsed walls, widening some micropores to mesopores, and opening some closed mesopores in the carbon matrix. Therefore compared with the untreated AC, the mesopore volume only increased slightly with 30% H_2O_2 hydrothermal treatment from 0.27 to 0.28 cm^3 g^{-1} (Table 3.1). In comparison, the mesopore volume of ZSM-5 was only 0.19 cm^3 g^{-1} (Table 3.1), which is smaller than all AC samples.

3.3.1.3 Total pore volume and BET surface area of the adsorbents

Similar to the trends for micropores and mesopores, hydrothermal treatment of AC with 10% H_2O_2 substantially increased total pore volume from 0.72 cm^3 g^{-1} in untreated AC to 0.86 cm^3 g^{-1} (Table 3.1). This net increase of 0.14 cm^3 g^{-1} was similar to the combined increase in micro and meso pore volume of 0.13 cm^3 g^{-1} after modification. Therefore, the increase in total pore volume was primarily due to the increase in micro and meso pores. Further increasing the H_2O_2 concentration to 20% resulted in a total pore volume of 0.71 cm^3 g^{-1} (Table 3.1), which was similar to the untreated AC. Again, this net difference can be explained by the 0.04 cm^3 g^{-1} increase in micropores and the 0.05 cm^3 g^{-1} decrease in mesopores between untreated AC and 20% H_2O_2 treated AC (Table 3.1). Similar correlations can be drawn for the untreated AC versus the 30% H_2O_2 treated AC (Table 3.1).

Some researchers [71, 74] have used oxidized AC for dye adsorption, and reported that higher H_2O_2 concentrations resulted in greater oxidation effectiveness. However, the BET surface area of these AC samples decreased from 972 to 949 m^2 g^{-1} [71] and from 1032 to 908 m^2 g^{-1} [74]. P.C.C. Faria et al. [71] noted that differences in the textural properties of the activated carbons cannot explain the disparity in dye adsorption, leading to the conclusion that surface chemistry plays a key role in adsorption. M. F. R. Pereira et al. [74] found that oxygen-containing groups have a negative effect on adsorption of anionic dyes, but a positive effect for cationic dyes.

In this study we found that surface area increased after H_2O_2 oxidation (Table 3.1), and hypothesize that this was because we used hydrothermal H_2O_2 oxidation, instead of oxidation at room temperature [71, 74]. In the study reported herein, the AC samples were also reacted in a sealed reactor at 120 °C. The hydrothermal H_2O_2 treatment appears to provide a critical reaction environment, which accelerated pore texture development and increased the BET surface area.

In summary, hydrothermal H_2O_2 treatment resulted in different pore structures, with different abilities for butanol adsorption, depending on the H_2O_2 concentration used. As can be seen in Table 3.1, 10% H_2O_2 treatment resulted in the greatest improvements to AC texture. Surface area, micro and meso pore volume, and total pore volume were

increased to the greatest extent. This indicates that a moderate concentration of H_2O_2 can generate additional micropores, while not causing carbon walls of mesopores to collapse. In addition, as can be seen from Figure 3.3, AC treated with 10% H_2O_2 resulted in more oxygen-containing functional groups compared with the 20% H_2O_2 treatment, however, it had the lowest butanol adsorption capacity of the four AC samples (Figure. 3.5A). Thus, in addition to pore structure and surface area, functional groups also affect butanol vapor adsorption. Compared to these AC samples, ZMS-5 had less BET surface area (400 m^2 g^{-1}), micropore volume (0.11 cm^3 g^{-1}), and total pore volume (0.32 cm^3 g^{-1}), as well as the lowest adsorption capacity for butanol vapor.

A
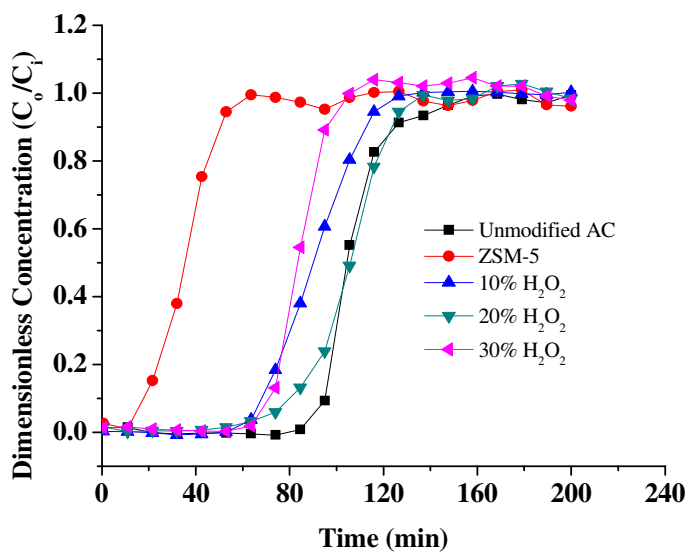
B
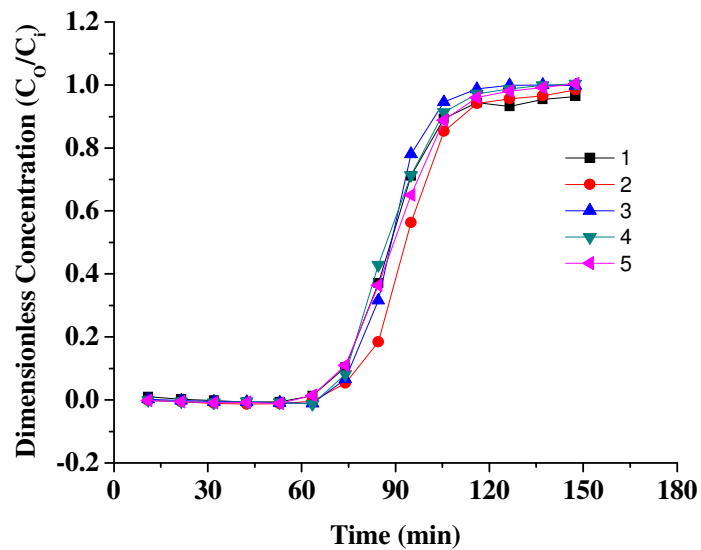
C
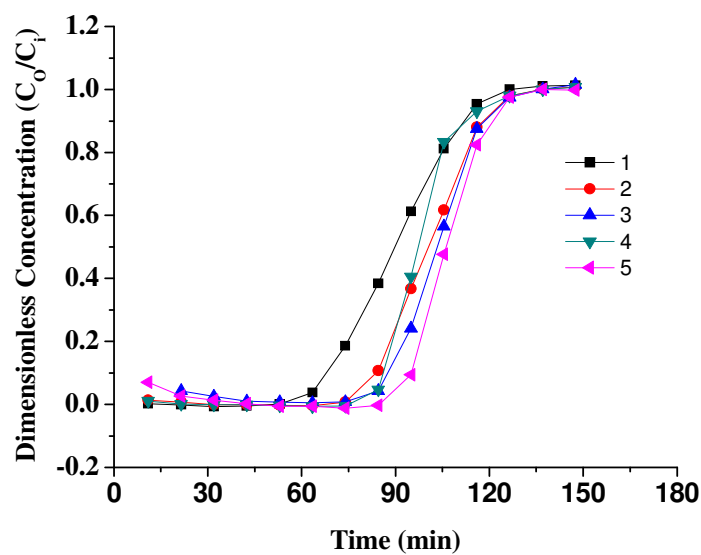
Fig. 3. 5. (A) Butanol adsorption by different absorbents. (B) Repeated adsorption of butanol with unmodified AC. (C) Repeated adsorption of butanol with 10% H_2O_2 modified AC.

3.3.2 Adsorption and desorption of butanol on the adsorbents

Figure 3.5A shows the breakthrough curves for butanol adsorption under atmospheric conditions and 24 ℃. ZSM-5 was easily saturated by butanol vapor at 63.5 min. All four AC samples had longer saturation times, with the longest being 168.0 min for unmodified AC.

The adsorption capacity (Q value in Table 3.2) indicates that the three H_2O_2 treated ACs had reduced butanol adsorption compared to untreated AC (259.6 mg g^{-1}), but all were significantly higher than ZSM-5 (83.0 mg g^{-1}). Although the AC modified by 10% H_2O_2 had a larger BET surface area compared with the 20% and 30% H_2O_2 modified AC samples, it had a lower adsorptive capacity (222.4 mg g^{-1}) due to more oxygen content on the surface (Figure 3.3). Therefore, adsorption of butanol is affected by BET surface area as well as the surface functional groups.

Table 3. 2. Adsorption process parameters.

Parameter	Unmodified AC	ZSM-5	10%H_2O_2	20%H_2O_2	30%H_2O_2
F_A [f]$(ml\ min^{-1})$	10	10	10	10	10
T_q [g](min)	108.2	34.6	90.4	103.2	103.1
C_i [h]$(\mu g\ ml^{-1})$	12.0	12.1	12.3	12.0	12.3
$M_{adsorption}$ [i](mg)	12.98	4.15	11.12	12.38	12.68
W [j](mg)	50	50	50	50	50
Q [k]$(mg\ g^{-1})$	259.6	83.0	222.4	247.6	253.6

[f] Volumetric flow rate of the carrier gas

[g] Stoichiometric time determined from the breakthrough curve

[h] Butanol concentration at the inlet

[i] Mass of butanol adsorbed

[j] Net weight of adsorbent

[k] Dynamic adsorption capacity of the adsorbent

The major factor determining adsorption capacity is pore size. Based on the relative changes in micro and meso pore in Table 3.1 and adsorption capacity in Table 3.2, it is apparent that micropore volume is more important. In comparison to ZSM-5, micropore volumes of the ACs were 355-418% higher, while mesopore volumes were only 116-195% higher than ZSM-5. In comparison, adsorption capacity in ACs were 298-313% higher than in ZSM-5. Thus adsorption capacity is mainly attributed to the micropores in the adsorbents. This is logical, as the kinetic diameter of butanol is 0.5 nm [75], and micropores (smaller than 2 nm) provide a more stable environment to store butanol molecules.

Desorption TCD profiles of unmodified AC and AC treated with 10% H_2O_2 were obtained via programmed temperature ramping. As is shown in Figure 3.6, butanol vapor will evolve once desorption starts, even at low temperature (30 ℃). Butanol desorption was highest at 110 ℃, and was completed when the temperature reached 150 ℃. In addition, nearly all of the butanol was removed after 30 min. It also can be seen that the

peak of the unmodified AC is higher than that of 10% H_2O_2 modified AC, which is

corresponded to the adsorption amount calculated.
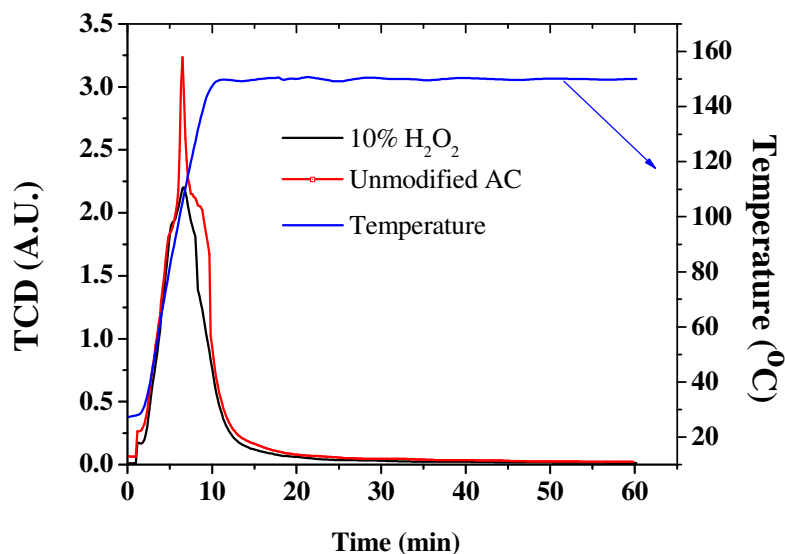
Fig. 3. 6. Desorption TCD profiles of unmodified AC and 10% H_2O_2 modified AC.

3.3.3 Regeneration of the adsorbent

To investigate the influence of oxidation on repeated adsorption/desorption cycles,

unmodified AC (Figure 3.5B) and AC modified with 10% H_2O_2 (Figure 3.5C) were

evaluated. The break through curves for unmodified AC (Figure 3.5B) almost overlapped

over five rounds of adsorption and desorption, which means that unmodified AC has non-

changed adsorption ability after heating regeneration at 150 ℃. Due to the acidic oxygen

surface groups generated by10% H_2O_2, the amount of adsorbed butanol from the first round was smaller than these of regenerated AC (the second to fifth adsorption rounds). It indicates that the adsorption capacity increased after regeneration. To investigate the mechanism of this phenomenon, the products from the regeneration was measured.

Figure 3.7A shows butanol desorption of the AC modified by 10% H_2O_2 treatment. The outlet was monitored by GC-MS when the TCD signal (1.95) was highest during the desorption process. There was a small amount of butanal produced via oxidation of butanol during regeneration as shown in Figure 3.7B. Meanwhile the surface oxygen of the AC sample was consumed. After that reaction, the regenerated AC demonstrated much higher dynamic capacity for adsorbing butanol with longer time for the breakthrough (the second to fifth adsorption rounds).

A
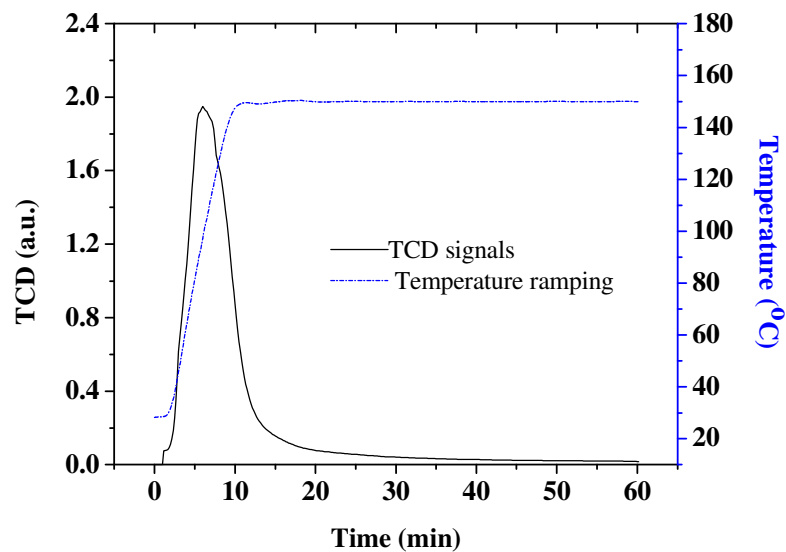
B
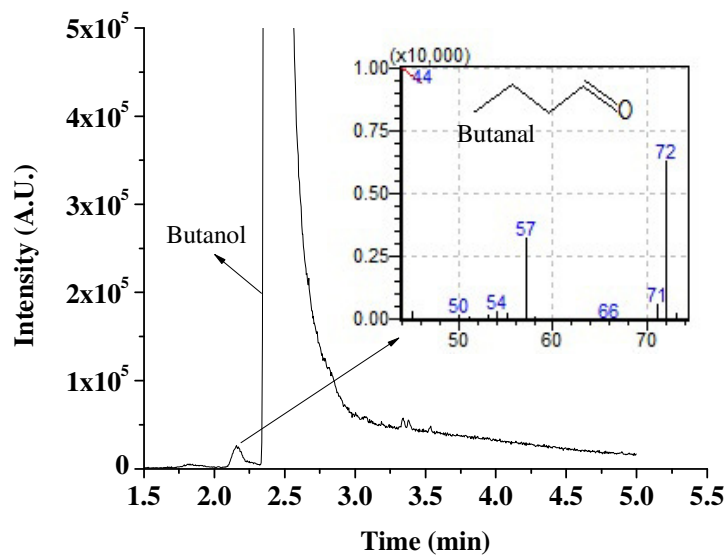
Fig. 3. 7. (A) Butanol desorption of 10% H_2O_2 modified AC (B) GC-MS profile of the outlet at 6.0 min (97 ℃).

3.4. Conclusion

Butanol vapor was adsorbed by AC samples and the zeolite ZSM-5. The adsorption capacity of unmodified AC was 259.6 mg g^{-1}, which was almost three times that of zeolite ZSM-5. Treatment of AC with 10% H_2O_2 increased BET surface area by 205 m^2 g^{-1}, micropore volume by 0.07 cm^3 g^{-1}, and mesopore volume by 0.06 cm^3 g^{-1}. However, the adsorption capacity decreased to 222.4 cm^3 g^{-1}. Hence, the oxygen-containing function groups generated by oxidation decreased the adsorption ability of AC, because adsorption capacity is related to the pore structure and surface functional groups. Micropores in the adsorbents played an important role in butanol vapor adsorption. The unmodified AC sample were easily regenerated for repeatable adsorption by heating. Although the unmodified AC achieved the best adsorption and desorption performance, surface functional groups of AC samples play a key role in butanol vapor adsorption. This work provides some guidance for designing absorbents for use in industry.

Chapter 4 Adsorption of butanol vapor on active carbons with nitric acid

hydrothermal modification

Adapted from Cao, Y.; Wang, K.; Wang, X.; Gu, Z.; Gibbons, W.; Vu, H., Adsorption of butanol vapor on active carbons with nitric acid hydrothermal modification. Bioresource technology 2015, 196, 525-32.

4.1 Introduction

High fuel prices and climate change are two critical challenges in the world. Fossil fuels, particularly petroleum-based fuels such as gasoline, diesel fuel, liquefied petroleum gas, and natural gas are mainly used for transportation, and will become increasingly difficult to access in the next few decades [76, 77]. Liquid biofuels such as biobutanol [78], bioethanol [79], and biodiesel [80] have the potential to reduce the need for petroleum fuels. These biofuels can also reduce greenhouse gas emissions compared to petroleum-based fuels [81].

Biobutanol has several advantages over other biofuels such as ethanol, including higher energy density and lower water miscibility, flammability, and corrosiveness. Butanol is also considered an infrastructure compatible fuel, as it can be blended in any ratios with gasoline without requiring engine modifications [82]. Butanol can also be transported using the same pipelines and distribution networks that are currently used for petroleum products. Butanol is primarily produced via the bacterial acetone-butanol-ethanol (ABE) fermentation pathway [83, 84].

One of the chief limitations of butanol is that it is highly inhibitory to the microbes used to produce it. Levels as low as 13.0 g/L can cause reduced growth and metabolism [85]. Butanol recovery from dilute fermentation broth is quite expensive, and this has been a major hurdle to commercialization. Distillation [86] is widely used to recover volatile fermentation products, but is not practical for butanol due to high energy requirements [87]. Membrane distillation [88] and pervaporation [89] have been suggested, but membrane fouling by organic compounds in the fermentation slurry has been an issue. Liquid phase adsorption [90-92] and liquid-liquid extraction [93] are often limited by the toxicity of the liquid absorbents to the microbial culture.

A more economical method of recovering butanol from dilute fermentation streams may be gas stripping [23, 88, 94]. Gas stripping is a relatively simple process in which a gas is continuously bubbled through the fermentation culture to volatilize and carry out the chemical (as well as some water vapor), which are subsequently condensed [95]. The challenge with applying gas stripping to butanol fermentation is that the gas stream exiting the fermentor would also be very dilute. The condensation temperature required to condense butanol from a vapor stream is directly correlated with the butanol concentration. Therefore, a dilute butanol vapor would require exceptionally cold condensation temperatures, such as that of liquid nitrogen [94]. These added costs would negate the benefits of gas stripping. To overcome this challenge, an alternative to direct

condensation is to pass the gas stripping vapor first into an absorbent to concentrate the chemical. A smaller volume of gas can subsequently be used to displace the chemical from the absorbent, resulting in a higher concentration in this secondary vapor, such that cold water could be used to condense the product.

Activated carbon (AC) has been widely employed to adsorb volatile organic compounds (benzene, toluene, formaldehyde, n-hexane, butanol, and ethanol) from gas streams that are generated from a wide range of industries [96]. AC has a large surface area, high porosity, a variety of pore sizes and structures, and rapid adsorption capabilities. Thus AC may provide an economical option for recovering and concentrating butanol in gas stripping vapor. However, prior work on the adsorption behavior of AC has not adequately addressed the effects of adsorption temperature, concentration, and regeneration, which are critical for butanol recovery through vapor adsorption (Cao et al., 2015).

It is possible to treat AC to alter the surface functional groups present. For example, acid modification can increase the amount of acidic groups present, making AC ideal for the uptake of heavy metals or bases. Meanwhile, base modification will increase conjugated pi electron systems, making it ideal for uptake of aromatic organic acids [97]. The performance of AC in most applications is related to its pore structure, specific surface area, and surface functional groups, with modification of its properties being the

target of treatment [98]. Butanol is neutral with a hydroxyl group. According to the hydrogen-bonding interaction, we hypothesized that butanol adsorption capacity could be increased by generating carboxyl and hydroxyl groups on the surface of the active carbons, which would potentially form hydrogen-bonding interaction with butanol. The aim of this study was to investigate the effects of nitric acid hydrothermal modification on the butanol adsorption /desorption activity of AC.

4.2 Materials and methods

4.2.1 Materials

HNO_3, butanol, hydrochloride acid, sodium hydroxide, and ethanol were purchased from Thermo Fisher Scientific Inc. All of these chemicals were analytical grade. Commercial AC Sabre Series CR2050C-75 (unmodified AC) was donated by Carbon Resources. Several types of modified AC were generated by reacting the commercial AC at different concentrations of HNO_3.

4.2.2 Methods

4.2.2.1 Modification of AC

The commercial AC was washed by boiling water with a Soxhlet extractor for 2 h. The wet AC was dried at 105°C for 24 h. Five g of the dried AC was reacted with 30 ml HNO_3 at 2M, 4M and 6M concentrations in a sealed PTFE reactor (50ml) at 120 °C for 1 h. After reaction, the reactant was cooled and filtered, then washed with deionized water under vacuum filtration until the pH value of the permeate was ~7. Finally, the washed AC was dried in a vacuum oven at 105 °C overnight. Then the dried AC was ground and run through a sieve, and grains falling within US mesh sizes 50-100 were used as absorbents.

4.2.2.2 Analytical methods for absorbents

Isotherm adsorption of N_2 was carried out using an ASAP 2010 Micropore Analyzer. The total pore volume was determined at relative pressure 0.995 P_0, and the specific surface area was calculated from the BET method. The micropore and mesopore volume and the pore size distribution were determined by the density functional theory (DFT) for samples based on the N_2 isotherm adsorption data.

Temperature-programmed desorption (TPD) was performed using a Micrometrics Autochem II Chemisorption Analyzer to investigate the oxygen content of these four AC samples. The carbon sample (0.1 g) was placed in a U-shaped quartz tube inside an electrical furnace and heated at 10 °C/min up to 1000 °C using a constant flow rate of

helium (the flow rate of the vapor, carrier, and reference were set at 0, 60, and 60

cm^3/min respectively). The thermal conductivity detector (TCD) signals were monitored

during the thermal analysis, and the corresponding TCD spectra was obtained.

4.2.2.3 Gas Chromatography Mass Spectrometer (GC-MS) analytical procedure

GC-MS was applied to analyze the outlet of the sample tube. Chromatographic

analysis was performed in a Shimadzu series GC-MS (Shimadzu Corporation, USA)

equipped with an RXI capillary column (30m×0.15μm×15mm). The initial temperature

(40 ℃) was held for 1 min and then raised to 200 ℃ at a rate of 45 ℃/min. All samples

were injected in split mode. The injection temperature was 150 ℃. The mass

spectrometer was operated in EI mode. Mass spectra were acquired in full scan mode

with repetitive scanning from 45 m/z to 500 m/z in 0.25 s. Ion source temperature was

250 ℃.

4.2.2.4 Dynamic adsorption and regeneration experiments

The Micrometrics Autochem II Chemisorption Analyzer, connected to the Shimadzu

GC-MS, was also employed to investigate butanol adsorption and desorption on different

absorbents. Fig. 4.1 shows the schematic diagram of the adsorption system used for

testing the adsorbents. The flow rate of the vapor, carrier, and reference were set at 5, 5,

and 10 cm^3/min, respectively. Experiments were performed using helium as carrier gas, assuming that helium does not interfere with butanol adsorption on AC [99]. Pure butanol was heated to 50 °C and sparged with helium at 5 cm^3/min. The gas outflow passed through the sample tube with carrier gas at 5 cm^3/min. The butanol from the outflow was adsorbed by the loaded AC, and what remained passed through the analysis chamber and then into the gas chromatograph. The reference chamber recorded the TCD readings and ploted it against time. The GC-MS recorded the intensity of the signal produced by the adsorbate as a function of time approximately once every 10.5 min, and the integral of the curve provided the volume of adsorbate present after adsorption. At least 20 data points were obtained by the GC-MS over the course of the analysis.

For regeneration, the TPD process pre-programmed into the Micromeritics analyzer was used. The flow rate of the vapor, carrier, and reference were set at 0, 10, and 10 cm^3/min, respectively. The temperature ramp was set at 15 °C/min, starting from 25 °C to the set temperature with a 1 h end temperature hold.
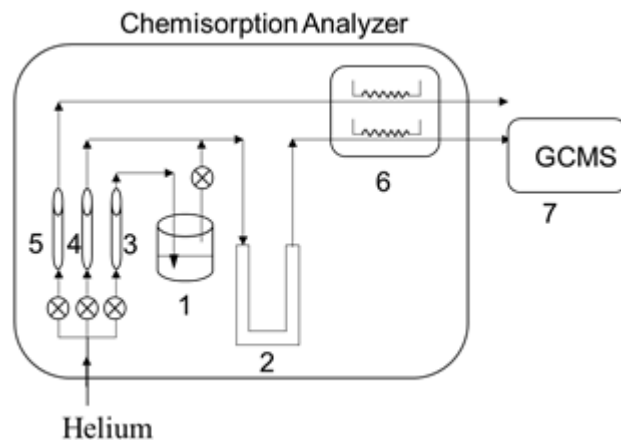
Fig. 4. 1. Schematic diagram of the experimental adsorption system: 1, butanol bath; 2, sample tube; 3, vapor flow rate meter; 4, carrier flow rate meter; 5, reference flow rate meter; 6, TCD detector; 7, GC-MS.

4.2.2.5 Butanol quantification

To test the impact of surface modifications on the adsorption and desorption capacities of AC, a standard curve using a GC-MS was created as described previously [99]. Ethanol was used as solvent to prepare different concentrations of butanol (1.0, 5.0, 10.0, 20.0, 30.0, 50.0, 60.0, 75.0, 93.0, 170.0, 235.0, and 290.0 mg/ml) which were analyzed in a Shimadzu GC-MS to generate a standard curve that was subsequently used to measure butanol levels from the outlet of the sample tube.

To quantify butanol vapor that was not adsorbed onto the adsorbent from the packed

column, 0.5 ml of the outlet stream exiting the adsorption column was injected into GC-MS. Since the GC-MS needed time to cool down, the outlet of the sample tube was measured every 10.5 minutes. Determination of the outlet butanol vapor concentration as a function of time allowed us to determine the breakthrough curve and experimentally calculate the dynamic adsorption capacity of the packed column for each experiment. The adsorbed amounts were calculated with the following equation:

$$Q = \frac{M_{adsorption}}{W} = \frac{T_q C_i F_A}{W} \qquad (1)$$

The time T_q is estimated according to the equation (2):

$$T_q = \int \left(1 - \frac{C_o}{C_i}\right) dt \qquad (2)$$

Where Q is the adsorbed amount (mg mg^{-1}); $M_{adsorption}$ is the mass of butanol absorbed (mg); F_A is the volumetric flow rate of the carrier gas (ml min^{-1}); W is the net weight of adsorbent (mg); C_i represents the butanol concentration at the inlet (µg ml^{-1}); C_o is the butanol concentration at the outlet (µg ml^{-1}).

4.3. Results and Discussion

4.3.1 Physicochemical properties of active carbons

Pore structure and surface area parameters were obtained by the N_2 adsorption method, while micropore volume was determined using the density functional theory

(DFT). Fig. 4.2A shows the N_2 adsorption/desorption isothermal curves of the four adsorbents. The isotherms were similar for both the original AC and the AC treated with 2 M HNO_3, but when AC was treated with higher HNO_3 concentrations (4 and 6 M), N_2 uptake increased. Table 4.1shows that the BET surface areas were larger (1486 and 1277 m^2 g^{-1}, respectively) for these latter treatments in comparison to the original AC (1157 m^2 g^{-1}). Table 4.1also shows that the pore structures were affected by the higher HNO_3 concentrations. The total pore volumes of the modified AC increased 0.24 and 0.13 cm^3 g^{-1} for the 4 M and 6 M HNO_3 modifications, respectively, in comparison to untreated AC. Total pore volume for the 2 M HNO_3 treatment was similar to the control. Formation of new pores or opening of inaccessible pores are two possible explanations for the increased BET surface areas [100].

A
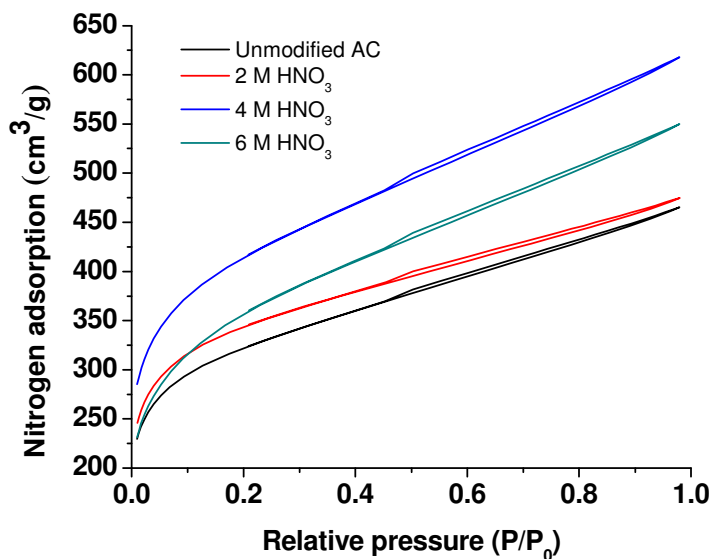
B
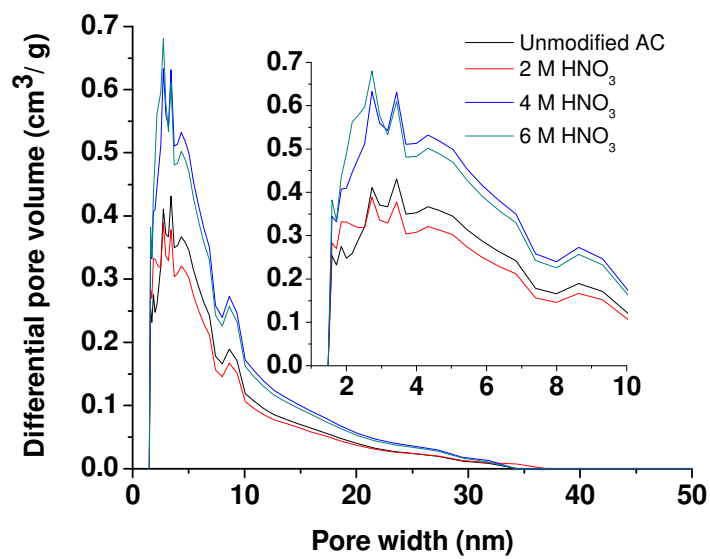
C
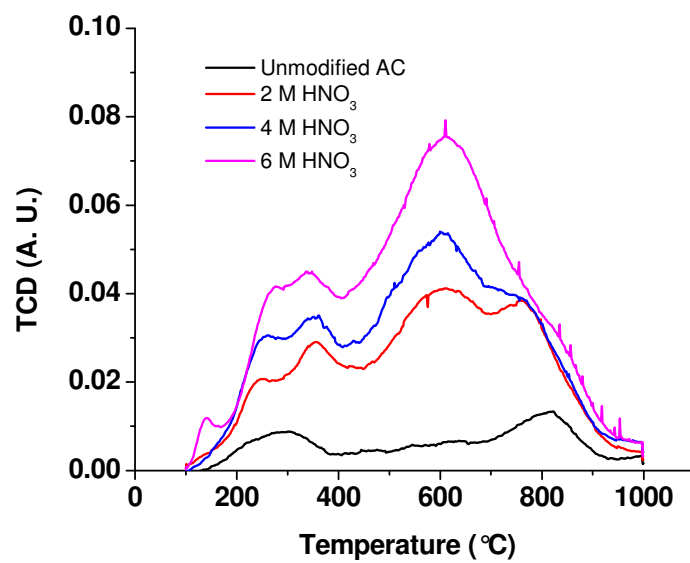
Fig. 4. 2. (A) N_2 isothermal adsorption/desorption on the absorbents; (B) DFT pore size distribution curves of the absorbents; (C) TCD signals for temperature-programmed desorption of AC samples.

The nitric acid hydrothermal treatment increased the micropore volumes of modified ACs from 0.39 cm^3 g^{-1} in AC to 0.43, 0.49 and 0.43 cm^3 g^{-1} by using 2, 4 and 6 M HNO_3 modifications, respectively. Increased micropore volume and BET surface area both contributed to enhanced accessibility to the inner part of the micropores by defect creation and/or opening of blocked micropores. Although the micropore volume increased slightly, the total pore volume of the 2M HNO_3 modified AC was similar to the control (0.72 vs 0.73 cm^3 g^{-1}), perhaps because this treatment caused mesopore volume to drop (from 0.27 to 0.24 cm^3 g^{-1}). This may have been caused by intensive erosion of mesopore walls by HNO_3, resulting in partial destruction or collapse of the porous structure [97, 98, 101]. Some of the mesopore may have changed into micropore. Table 4.1 shows that the average pore diameter of the AC decreased from 2.49 into 2.36 nm following treatment with 2 M HNO_3. In addition, the oxygen containing groups introduced by HNO_3 modification were probably fixed at the active sites at the entrance of the mesopores [102]. These oxygen containing groups could hinder access to the pores.

Table 4. 1 Surface area and pore structure parameters of the absorbents.

Sample #	S_{BET}[a] $m^2\ g^{-1}$	V_{Total}[b] $cm^3\ g^{-1}$	V_{Micro}[c] $cm^3\ g^{-1}$	V_{Meso}[d] $cm^3\ g^{-1}$	$D_{Average}$[e] nm
Unmodified AC	1157	0.72	0.39	0.27	2.49
2mol/L HNO_3	1236	0.73	0.43	0.24	2.36
4mol/L HNO_3	1486	0.96	0.49	0.39	2.58
6mol/L HNO_3	1277	0.85	0.43	0.36	2.66

[a] BET (Brunauer-Emmett-Teller) surface area

[b] Total pore volume, measured at $P/P_0=0.995$

[c] Micropore volume, based on density functional theory (DFT)

[d] Mesopore volume, based on density functional theory (DFT)

[e] Average pore diameter of absorbents, calculated by $4V_{Total}/S_{BET}$

By contrast, mesopore volume increased greatly for samples modified by 4 and 6 M HNO_3 (Table 4.1). As is shown in Fig. 4.2B, DFT model simulation results according to the nitrogen adsorption/desorption curve indicate that the volume of pores between 2 nm and 50 nm were increased from 0.27 to 0.39 (4 M HNO_3) and 0.36 $cm^3\ g^{-1}$ (6 M HNO_3), respectively. Higher concentrations of HNO_3 reacted much more strongly, causing more robust oxidation and etching of the carbon matrix of AC, and generating additional micropores and mesopores by eroding carbon walls via strong oxidation. Widening of micropores into mesopores also may have contributed to the greater increase in mesopores. This resulted in the average pore diameter of the ACs modified by 4 and 6 M HNO_3 increasing to 2.58 and 2.66 nm, respectively (Table 4.1).

In summary, 4 M HNO_3 treatment of AC resulted in the largest changes in AC texture, surface area, micropore volume, and total pore volume. This suggests that a proper concentration of HNO_3 can generate more micropores and mesopores. Due to erosion of reactive sites on the AC, total pore volume increased at higher concentrations of oxidative acid (e.g. 4 and 6 M HNO_3).

Temperature-programmed desorption (TPD) was employed to investigate the functional groups generated by HNO_3 modification. The carrier gas helium and the detected gases (CO, O_2 and CO_2) have different thermal conductivities. TCD signals from the evolved gases were recorded and the areas under the peak were proportional to the amount of gases produced. The TCD readings were zeroed using carrier gas and reference gas at the beginning of each measurement.

Fig. 4.2C displays the TPD spectra arising from oxygenated groups released as CO and CO_2 from the surface of AC that had been hydrothermally treated with different concentration of HNO_3. The TPD profile measured for the untreated AC was also included. The quantity of oxygenated groups released during treatment was directly related to the HNO_3 concentration used to treat AC. Generally, carboxylic functional groups decompose and release H_2O at lower temperatures (100 ℃ to 400 ℃), while anhydride and lactone groups decompose at higher temperatures (427 ℃) [103-105]. In this study, the peaks formed between 400-1000 ℃ were assumed to be CO_2 and CO

[106], and the CO was possibly derived from the decomposition of phenols, ethers and carbonyls/quinones [107-109].

4.3.2 Adsorption of butanol on the adsorbents

4.3.2.1 Adsorption of different concentrations of butanol on unmodified AC

To observe the effects of butanol vapor concentration (11.9, 15.9, 19.9, 23.9 and 31.9 $\mu g \ ml^{-1}$) on the breakthrough characteristic of AC, experiments were conducted at atmospheric conditions and 25 °C. As shown in Fig. 4.3A, the breakthrough time considerably decreased from about 85 min to less than 30 min as the butanol concentration increased from 11.9 to 31.9 $\mu g \ ml^{-1}$.

The widely used Langmuir isotherm has found successful application in many real adsorption processes and is expressed as:

$$q_e = \frac{q_m B P_e}{1 + B P_e} \qquad (3)$$

which can be rearranged to obtain a linear form

$$\frac{P_e}{q_e} = \frac{P_e}{q_m} + \frac{1}{q_m B} \qquad (4)$$

where q_m refers to the monolayer adsorption capacity, q_e is amount of adsorption at

equilibrium, P_e is the partial pressure of butanol vapor at equilibrium and B is the

Langmuir constant.

A
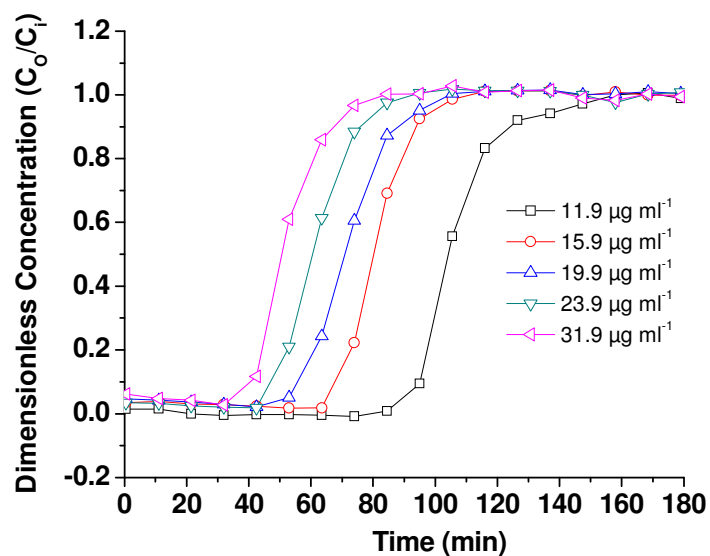
B
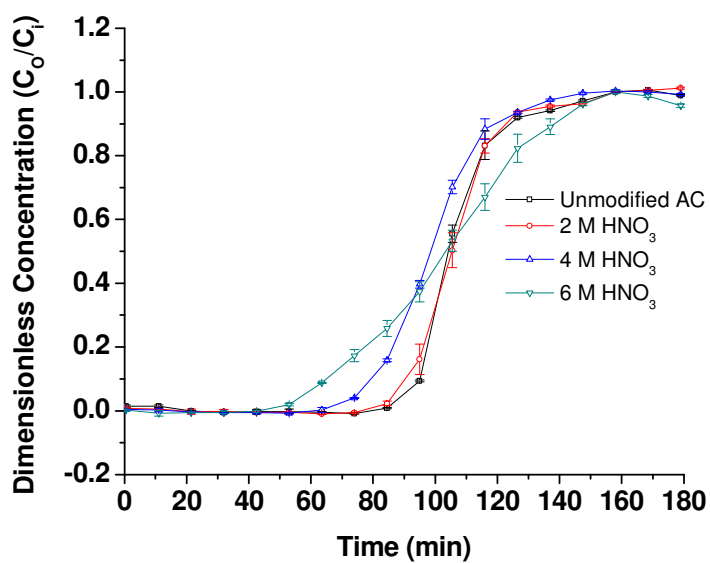
C
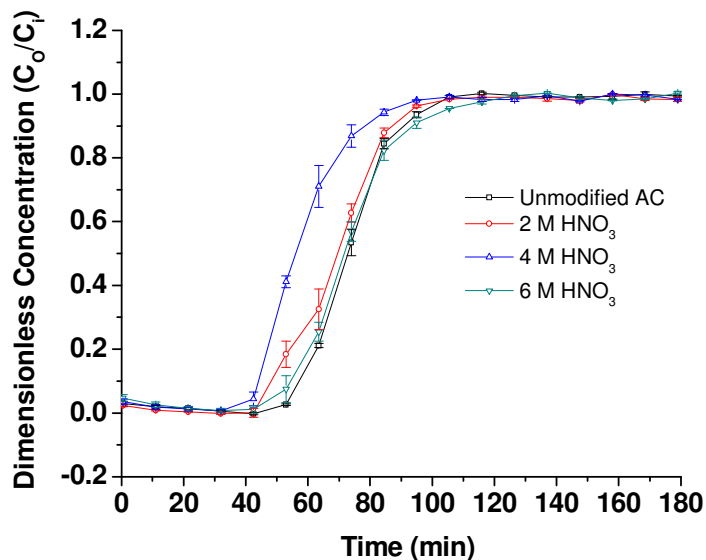
Fig. 4. 3. (A) Butanol adsorption capabilities of unmodified AC at different butanol concentrations; (B) Adsorption capabilities of different absorbents at 25 ℃; (C) Adsorption capabilities of different absorbents at 30 ℃.

A linearized plot of P_e/q_e versus q_e was obtained from the model shown in Fig. 4.4. The fit is good for unmodified AC with butanol vapor under the concentration ranges studied (correlation coefficient, $R^2 > 0.988$). This indicates that the calculated maximum monolayer capacity q_m of butanol vapor onto the unmodified AC is 359.7 mg g^{-1} and the Langmuir isotherm parameter B is 5.24 kPa^{-1}.
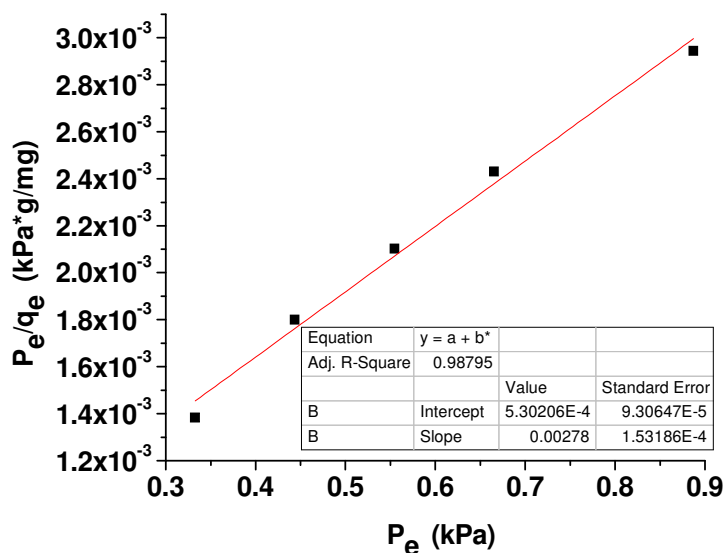
Fig. 4. 4. Langmuir plot for unmodified AC with different butanol vapor inlet concentrations.

4.3.2.2 Adsorption of butanol on the adsorbents at 25 ℃

Fig. 4.3B shows the breakthrough curves for 11.9 µg ml-1 butanol under atmospheric conditions and 25 ℃ when adsorbed by the various AC samples. All samples had almost the same saturation time (158 min). The adsorption behavior of untreated AC and AC modified by 2 M HNO3 were very similar, as the breakthrough curves almost overlapped. The breakthrough time (Co/Ci =0.05, which is defined as the time that the ratio of outlet to the inlet butanol concentration reaches 0.05) for 2 M HNO3 modified AC was slightly lower (88.5 min) than the unmodified AC (90.0 min). Values for the key adsorption parameters listed in Table 4.2 were within the margin of error for the control and the 2 M HNO3 AC treatment, suggesting that it was not strong enough to change

adsorption significantly. This is consistent with the relative lack of change in micropore, mesopore, and total pore volumes noted in Table 4.1.

Table 4. 2 Key adsorption parameters for butanol adsorption at 25 $^{\circ}$C.

Items	Unmodified AC	2 M HNO_3 treated AC	4 M HNO_3 treated AC	6 M HNO_3 treated AC
F_A [a]$(ml\ min^{-1})$	10	10	10	10
T_q [b](min)	107.47±0.85	106.51±0.97	99.45±1.12	102.56±1.01
C_i [c]$(\mu g\ ml^{-1})$	11.90	11.90	11.90	11.90
$M_{adsorption}$ [d](mg)	12.79±0.10	12.67±0.12	11.83±0.13	12.20±0.12
W [e](mg)	50	50	50	50
Q [f]$(mg\ g^{-1})$	255.8±2.0	253.4±2.4	236.6±2.6	244.0±2.4

[a] Volumetric flow rate of the carrier gas

[b] Stoichiometric time determined from the breakthrough curve

[c] Butanol concentration at the inlet

[d] Mass of butanol adsorbed

[e] Net weight of adsorbent

[f] Dynamic adsorption capacity of the adsorbent

On the other hand, after treatment of AC with higher concentrations of HNO_3 (4 and 6 M), butanol breakthrough times were reduced to 75.0 and 58.0 min, respectively. It can be observed (Fig. 4.3B) that the profile corresponding to the 4 M HNO_3-modified AC was steeper than that of 6 M HNO_3-modified AC, which implies a slower butanol adsorption rate for the latter. The AC modified by 4 M HNO_3 had a greater total pore volume (+0.11 $cm^3\ g^{-1}$) and a higher percentage of micropores compared to mesopores

than 6 M HNO_3-modified AC. Oxygen-containing functional generated during HNO_3 treatment could also cause resistance to butanol diffusion into micropores, making it butanol breakthrough more rapid. Thus the order of butanol breakthrough was 6 M HNO_3<4 M HNO_3<2 M HNO_3<unmodified for these AC samples.

It is well-known that both the porous structure and the surface chemistry of AC are important factors affecting adsorption of different compounds. Increasing the surface area of sorbents will generally lead to improved adsorption, but the effects of functional surface groups on the adsorptive characteristics of ACs is closely related to the chemical nature of the adsorbates. As can be seen from Fig. 4.5, the water contact angle for unmodified AC was 99°, and it decreased to 35 ° after modification with 2M HNO_3. Water contact angles could not be measured on the surface of the 4 and 6 M HNO_3-modified ACs since water droplets spread out too rapidly. Conversely, butanol spread very rapidly on the surface of the unmodified-AC, while butanol contact angles of 13°, 16°, and 17° were measured for AC treated with 2, 4, and 6 M HNO_3, respectfully. This indicates that HNO_3 modification changed AC from a hydrophobic into hydrophilic material, and the higher HNO_3 concentration resulted the higher surface hydrophilicity. Butanol has higher affinity for hydrophobic active carbons than hydrophilic active carbon. Hence, the slightly decreased butanol adsorption was partially due to the increased oxygen functional groups, which decreased the affinity of butanol.
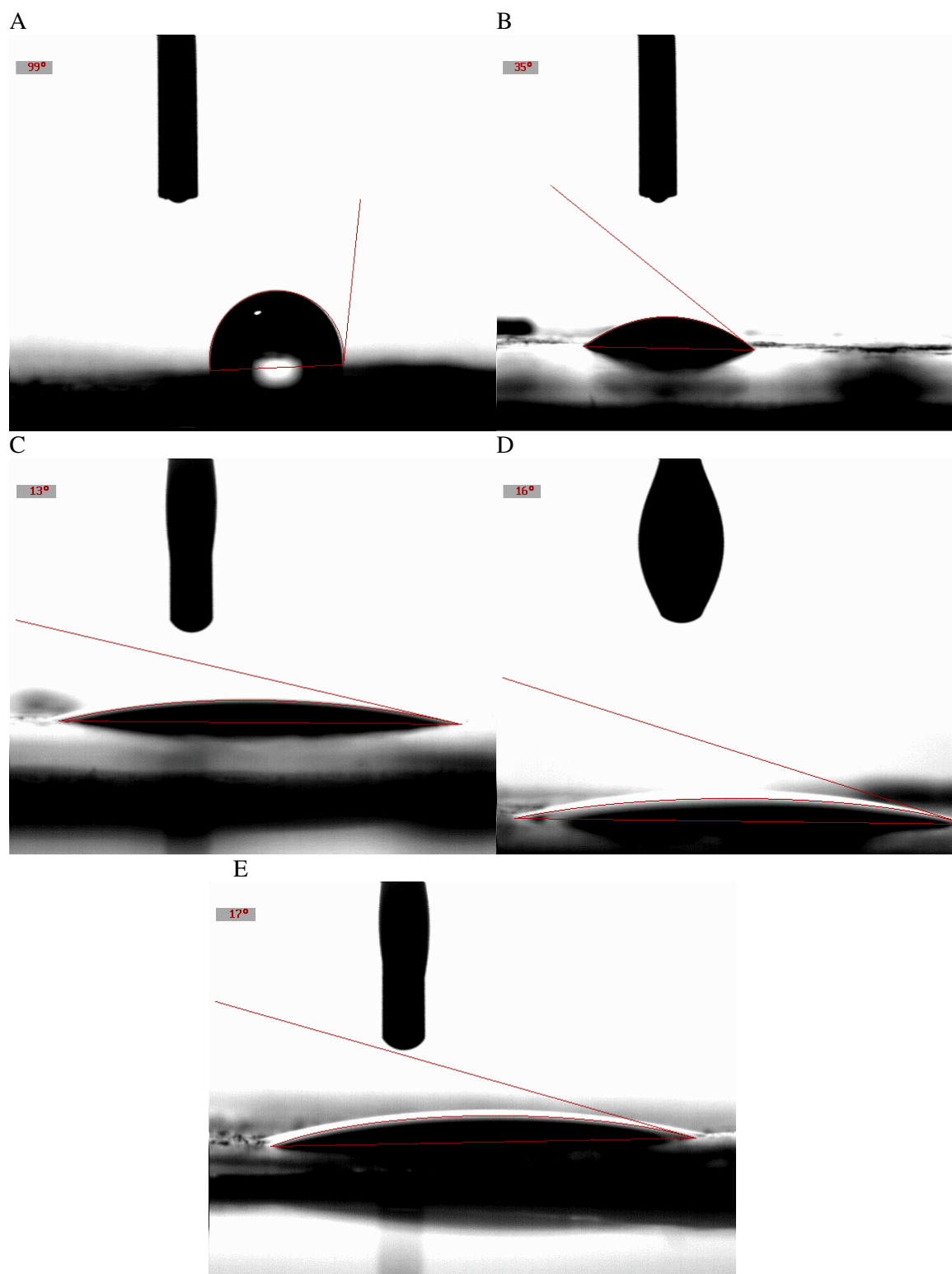
Fig. 4. 5. (A) Water contact angle for unmodified AC; (B) Water contact angle for 2 M HNO_3 modified AC; (C) Contact angle for 2 M HNO_3 modified AC with butanol; (D) Contact angle for 4 M HNO_3 modified AC with butanol; (E) Contact angle for 6 M HNO_3 modified AC with Butanol.

Although the AC modified by 4 M HNO_3 had largest BET surface area and highest total pore volume, it had the lowest dynamic saturate adsorption capacity (236.6 mg g^{-1}, Table 4.2). The the kinetic diameter of butanol is 0.5 nm [110], and the high proportion of micropores (smaller than 2 nm) in the AC modified by 4 M HNO_3 (0.49 cm^3 g^{-1}) provided a more stable environment to store butanol molecules. However, partial micropores were not able to adsorb the butanol molecules effectively since they were covered with oxygen-containing functional groups, which repelled the butanol molecules. Therefore, adsorption of butanol is not only dependent on the BET surface but also on the surface functional groups.

4.3.2.3 Adsorption of butanol on the adsorbents at 30 ℃

Fig. 4.3C shows the breakthrough curves for butanol under atmospheric conditions and 30 ℃. The breakthrough time of these four adsorbents was much lower compared with adsorption at 25 ℃. Increasing the adsorption temperature decreased both breakthrough time and total adsorption. The unmodified AC still had the highest

adsorption capacity (170.0 mg g^{-1}, Table 4.3), while the 4 M HNO$_3$-modified AC had the lowest adsorption capacity (139.4 mg g^{-1}, Table 4.3). The adsorption capacity of the 2 M HNO$_3$-modified AC (168.2 mg g^{-1}) was statistically similar to the untreated control, but higher than the 6 M HNO$_3$-modified AC (163.8 mg g^{-1}). Thus the trends in adsorption behavior were similar for both 25 and 30 ℃.

Table 4. 3 Key adsorption parameters for butanol adsorption at 30 ºC.

Items	Unmodified AC	2 M HNO$_3$ treated AC	4 M HNO$_3$ treated AC	6 M HNO$_3$ treated AC
F_A [a](ml min^{-1})	10	10	10	10
T_q [b](min)	71.45±0.95	70.71±1.03	58.53±1.31	68.82±1.10
C_i [c](µg ml^{-1})	11.90	11.90	11.90	11.90
$M_{adsorption}$ [d](mg)	8.50±0.11	8.41±0.12	6.97±0.16	8.19±0.13
W [e](mg)	50	50	50	50
Q [f](mg g^{-1})	170.0±2.2	168.2±2.4	139.4±3.2	163.8±2.6

[a] Volumetric flow rate of the carrier gas

[b] Stoichiometric time determined from the breakthrough curve

[c] Butanol concentration at the inlet

[d] Mass of butanol adsorbed

[e] Net weight of adsorbent

[f] Dynamic adsorption capacity of the adsorbent

Higher adsorption temperatures were also investigated for the unmodified AC. Fig. 4.6 shows the breakthrough curve shifted further to the left as the temperature was increased to 35 ℃, indicating an early saturation of the unmodified AC. Therefore, lower

temperature seems to have higher adsorption for the butanol vapor. Since both higher and lower adsorption temperatures require much more energy than the room temperature 25 ℃, the optimal adsorption temperature for butanol vapor is 25 ℃.
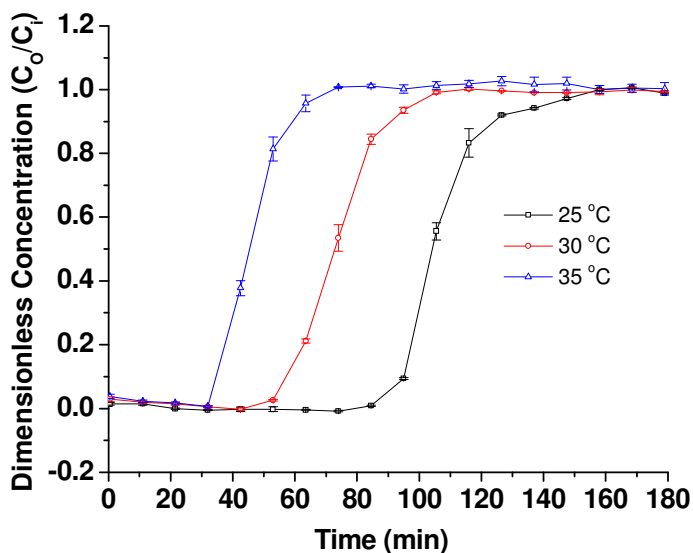
Fig. 4. 6. Adsorption capabilities of unmodified AC at different temperatures.

4.3.3 Regeneration of the adsorbent

Heating was used to recover butanol and regenerate adsorbent from saturated AC samples. Fig. 4.7A shows the TPD of butanol saturated, unmodified AC at 110, 130, and 150 ℃. The TCD signal shows that butanol desorption was positively correlated with regeneration temperature, with the highest amount of butanol evolved at 150 ℃. In a subsequent adsorption cycle with the unmodified AC that had been regenerated at 130 ℃, we observed a decrease in adsorption ability compared to fresh, unmodified AC (Fig.

4.7B). In this case the breakthrough time decreased from 95 to 50 min, and the saturation

time decreased from 158 to 126.5 min. This indicates that 130 ℃ is not high enough to

remove all of the adsorbed butanol vapor.

A
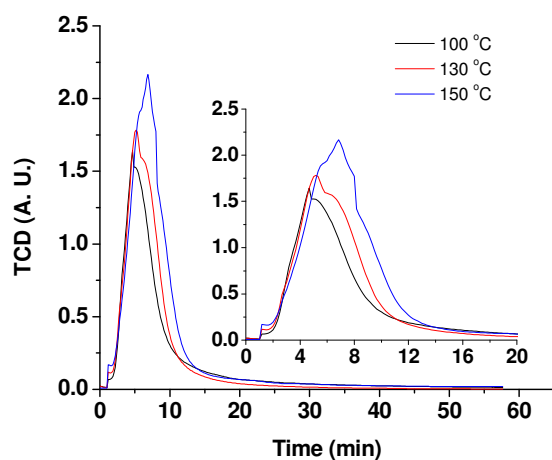
B
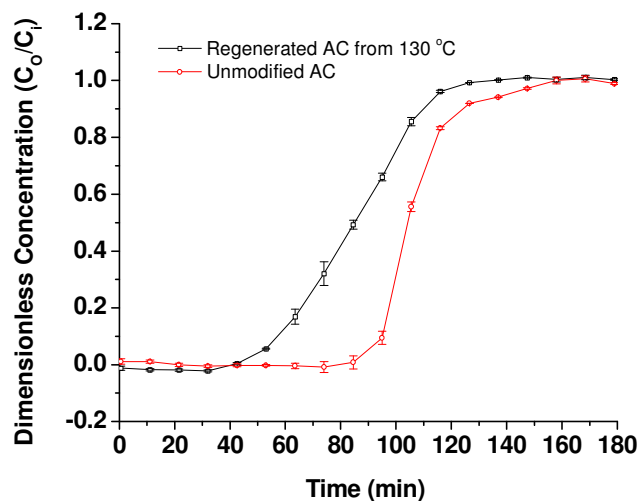
Fig. 4. 7. (A) Butanol desorption of unmodified AC at different temperatures; (B)

Adsorption curves for fresh and regenerated (at 130 ℃) unmodified AC.

In a separate test we used a regeneration temperature of 150 ℃ to assess adsorption ability of unmodified AC for four cycles of adsorption/desorption. As is shown in the Fig. 4.8A, the breakthrough curves for the four cycles were identical, indicating that 150 ℃ is an appropriate desorption temperature for butanol saturated AC. The almost overlapped adsorptions mean that the unmodified AC has non-changed adsorption ability after heating regeneration at 150 ℃.

A

B
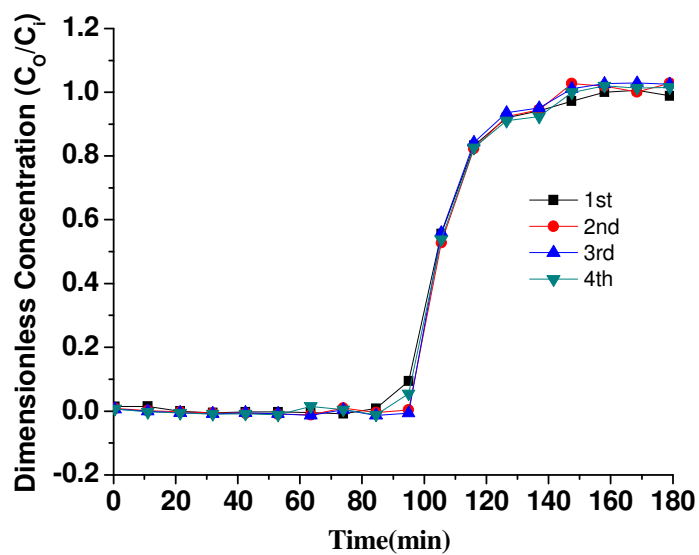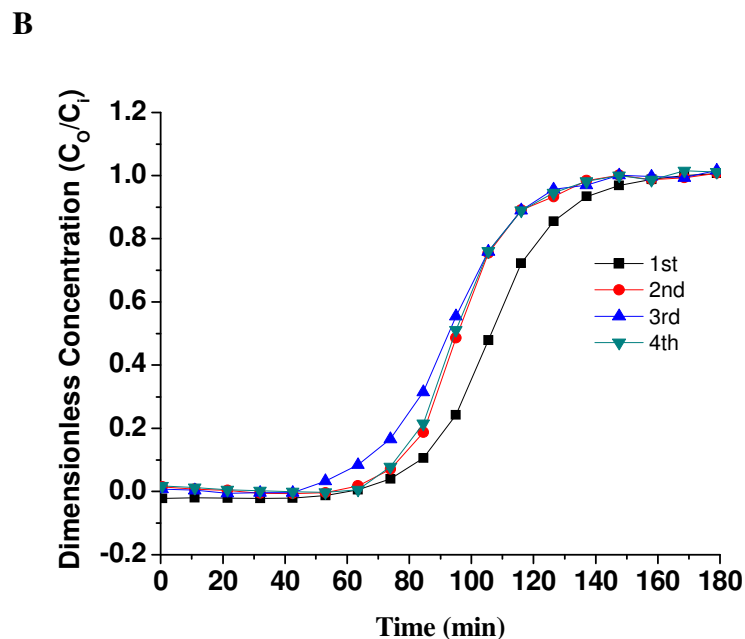
Fig. 4. 8. (A) Repeated adsorption of butanol with unmodified AC; (B) Repeated adsorption of butanol with 6 M HNO$_3$ modified AC.

To investigate the influence of oxidation on repeated adsorption/desorption cycles, AC modified with 6 M HNO$_3$ was evaluated. The outlet was monitored by TCD and GC-MS during desorption. As shown in Fig. 4.8B, the adsorption capacity appeared to decrease after the first adsorption and desorption round, but was stable for the second to fourth cycles. From the TCD signals (Fig. 4.9) for the desorptions, it can be concluded that the adsorption capacities for butanol were almost the same for the second to fourth cycles. However, the breakthrough curve (Fig. 4.8B) for the first adsorption indicates that it has loaded more butanol than the subsequent adsorption cycles. We hypothesize that surface oxides reacted with butanol and formed new functional groups on the surface in

the first round, which partially blocked butanol chemical adsorption sites for cycles two though four.
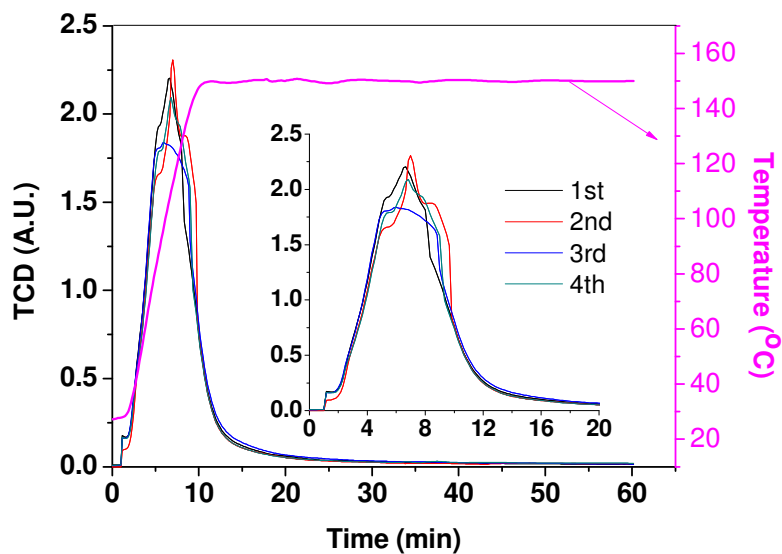
Fig. 4. 9. Butanol desorption of 6 M HNO3 modified AC.

Fig. 4.10A is the GC-MS profile of the outlet at 100 ℃ for the first regeneration. Besides the butanol peak, there were four peaks. According to the MS profiles (Fig. 4.10B) and a similarity search in the GC-MS standard library, peak 1 was 1-butene, peak 2 was butane, peak 3 was butanol, peak 4 was formic acid butyl ester, and peak 5 was n-Butyl ether. The mass spectral similarities were 98%, 98%, 98%, 98%, and 94%, respectively. Thus, it can be inferred that the modified AC catalytically reacted with

butanol. The exact mechanism of the reaction cannot be explained at the present stage of investigation. A detailed analysis will be needed in the future.

A
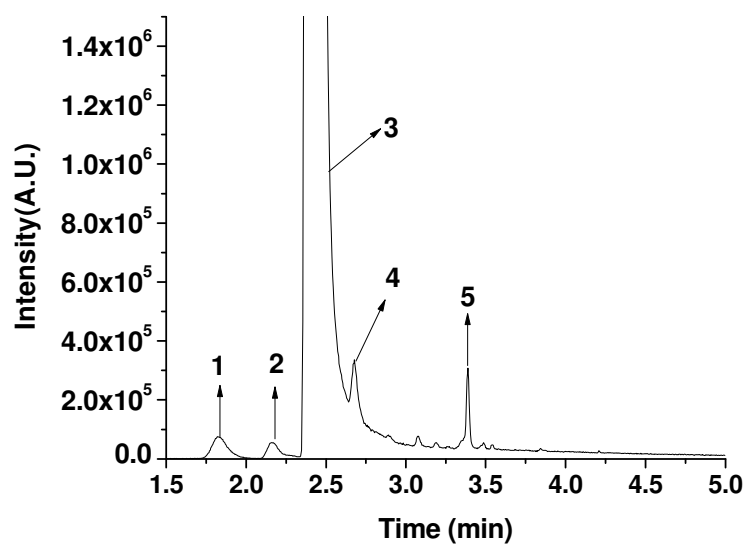
B
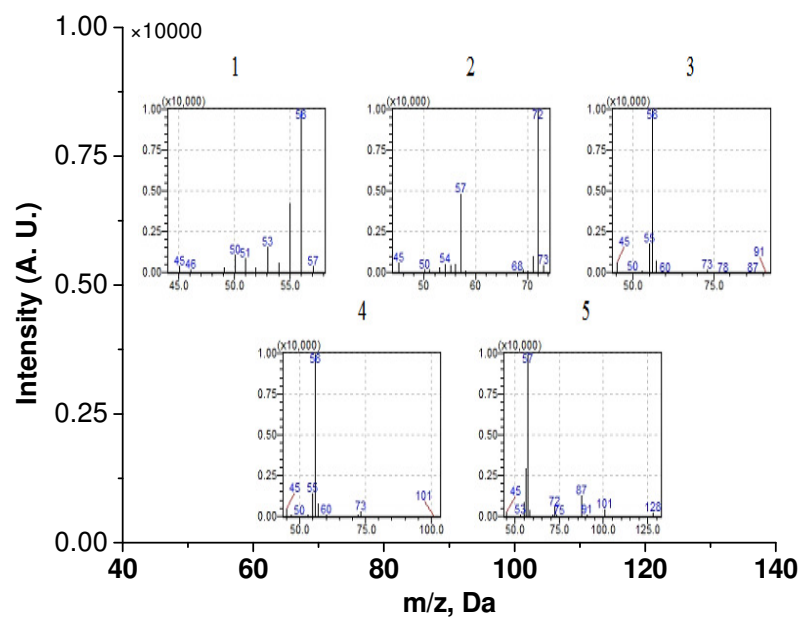
Fig. 4. 10. (A) GC profile of the outlet at 6.0 min (97 ℃) for butanol desorption of 6 M HNO$_3$ modified AC. (B) MS profiles of the compounds from the outlet at 6.0 min (97 ℃) during desorption.

4.4. Conclusion

Hydrothermal modification with 4 M HNO$_3$ increased BET surface area by 329 m^2 g^{-1}, micropore volume by 0.10 cm^3 g^{-1}, and mesopore volume by 0.12 cm^3 g^{-1}. However, the adsorption capacity (dynamic saturate) decreased from 255.8 to 236.6 mg g^{-1}. The oxygen-containing functional groups generated by HNO$_3$ hydrothermal treatment decreased the butanol adsorption ability of the AC. Overall, the adsorption capacity is not only related to the pore structure but also the surface functional groups. The butanol absorbed by the modified AC cannot be fully recovered after the first adsorption because it partially reacts with the functional groups on the surface.

Chapter 5 Preparation of active carbons from corn stalk for butanol vapor adsorption

Adapted from Cao, Y.; Wang, K.; Wang, X.; Gu, Z.; Ambrico, T.; Gibbons, W.; Fan, Q.; Talukder, A.-A., Preparation of active carbons from corn stalk for butanol vapor adsorption. Journal of Energy Chemistry 2017, 26(1): 35-41.

5. 1 Introduction

Growing concerns about environmental impact and increased fossil fuel consumption have prompted more research on alternative fuels than ever before. Bio-fuels are one such alternative because of their limit environmental impact, relatively low cost, and resource availability [111-113]. Butanol is an infrastructure-compatible fuel with higher energy density, lower water miscibility, and less corrosivity than many other biofuels. Biobutanol is produced primarily via the bacterial acetone-butanol-ethanol (ABE) fermentation pathway [83]. However, butanol levels as low as 13.0 g/L can cause reduced growth and metabolism since it is highly inhibitory to the microbes that produce it [85]. The dilute product and high boiling point of butanol (118 °C) make the solvent recovery process energy-intensive and costly. Separation methods related to the ABE fermentation process were studied, such as liquid phase adsorption [114-116], liquid-liquid extraction [21], pervaporation [117], and distillation [118]. High energy requirements, membrane fouling, and toxicity of the liquid adsorbents to the microbes are limitations for these recovery processes. Gas stripping technology [23, 85, 119, 120] is a relatively sample process in which a gas is continuously bubbled through the fermentation culture to volatilize and extract the butanol (as well as some water vapor). The gaseous products are

subsequently condensed [121]. This method can efficiently remove butanol from the fermentation broth as it is produced, thereby decreasing its inhibitory effects. The challenge for applying gas stripping to butanol fermentation is that the exiting gas stream is very dilute, exceptionally low condensation temperatures would be required for adequate butanol recovery [122]. To overcome this challenge, the dilute vapor can be adsorbed by an adsorbent, then a small volume of gas can be used to displace the concentrated chemical, resulting in a high concentration vapor, such that cold water could be used to condense the product [123]. Commercial AC (Active carbons) and zeolite ZSM-5 were used as adsorbents to measure the adsorption capacities of butanol vapor [124]. The adsorption capacity of the commercial AC was 259.6 mg g^{-1}, almost three times that of zeolite ZSM-5. Active carbons are extremely porous and thus have a very large surface area available for adsorption, a promising characteristic for high butanol vapor adsorption. To improve butanol adsorption, AC with high surface area and high porosity is required.

The use of agricultural waste for AC production has been described in the literature [125]. The use of agricultural waste as active carbon precursors also turns waste into wealth [126]. Corn is widely planted in USA; the corresponding by-product corn stalk (CS) is produced in large quantities annually, which is a precursor resource for AC. Corn stalk is made up of a cortex and a core. The cortex is comprised mostly of cellulose and lignin; the corn stalk pith (CSP) is comprised mostly of hemi-cellulose [56]. Different parts of the biomass would therefore produce different texture morphology. Activating

agents such as KOH, $ZnCl_2$, K_2CO_3 and H_3PO_4, were used to prepare AC from corn cob, corn stalk and cotton stalk (Table 5.1). Results indicate that different biomasses may produce different ACs. For example, different parts of the plant give different Brunauer-Emmet-Teller (BET) surface areas. It is possible to obtain carbon materials with a relatively high surface area using KOH as the activating agent [127]. There is still a need to optimize the production process of ACs with highly developed surface area and with suitable porosity from corn stalk [127]. In this study, different ACs were prepared from both WCS (whole corn stalk) and CSP. Their adsorption properties, specifically for butanol vapor, were characterized. AC with a 2330 $m^2\,g^{-1}$ surface area and 410.0 mg g^{-1} adsorption capacity for butanol vapor was prepared from WCS. These values are significantly higher than values obtained from ACs prepared from corn cob or cotton stalk (Table 5.1).

Table 5. 1 Carbonization of agricultural residues.

Raw material	Chemical treatment	$S_{BET}(m^2\,g^{-1})$	Reference
Corn cob	H_3PO_4	1274	[128]
Corn stalk	H_3PO_4	600	[129]
Cotton stalk	$ZnCl_2$	795	[130]
Corn cob	KOH	1320	[131]
Corn cob	K_2CO_3	1541	[132]
Corn stalk	KOH	2330	This work

| Corn stalk pith | KOH | 1650 | This work |

5.2. Experimental

5.2.1 Preparation of ACs

The corn stalk was collected from a farm located in Brookings, South Dakota, USA. The leaves and husks were manually stripped from the stalks and then the stalk sample was air dried. After air drying, the cortex was further peeled away to leave the core. Then the corn stalk and the corn stalk pith were cut into pieces of 25 mm length and precarbonized at 400 °C for 1 h in a tube furnace. The carbonized material was mixed with a KOH solution at a mass ratio of 4.2:1 (char: KOH). The mixture was then dried in an oven at 105 °C for 24 h. After drying, the activation was carried out at 800, 900, or 1000 °C for 1 h under 500 ml min^{-1} N_2 flow. The temperature ramping rate was 20 °C/min for all the carbonization and activation steps. The obtained samples were cooled down in the furnace under N_2 flow. The ACs were then washed with 6 M HCl at 110 °C in a hydrothermal reactor for 1 h. The ACs were washed with deionized water under vacuum filtration until the pH value of the permeate was ~7. Finally, the washed AC was dried in a vacuum oven at 105 °C overnight. Corn stalk-derived ACs were denoted as WCS-800, WCS-900, and WCS-1000 based on their activation temperature. Similarly, AC samples prepared from corn stalk pith were named as CSP-800, CSP-900, and CSP-1000.

5.2.2 Characterizations of Adsorbents

The pore structure of the sample is characterized by nitrogen adsorption at 77 K using an ASAP 2020 Micropore Analyzer. The total pore volume was determined at a relative pressure of 0.995 P_0 (P_0 being atmospheric pressure), and the specific surface area was calculated from the BET method. The micropore and mesopore volume and the pore size distribution were determined by the density functional theory (DFT) for samples based on the N_2 isotherm adsorption data. The micro-morphology was detected by SEM (HITACHI S-3400N).

5.2.3 Dynamic adsorption and regeneration experiments

The butanol vapor adsorption/desorption measurements were carried out by Micrometrics Autochem II Chemisorption Analyzer, connected to the Shimadzu GC-MS. Fig. 5.1 shows the schematic of the adsorption system used for testing the adsorbents [123]. Helium was used as carrier gas, given that helium does not interfere with the adsorption of butanol by AC. The butanol vapor was generated by first heating the pure liquid butanol to 50 °C, and then bubbling helium into it. The outflowing gas passed through the sample tube with AC in it. The butanol vapor from the outflow was adsorbed by the AC. Any remaining butanol vapor passed into an analysis chamber monitored by a gas chromatograph. The GC-MS recorded the intensity of the signal produced by the adsorbate as a function of time approximately once every 10.5 min, and the integral of

the resulting curve provided the stoichiometric time, T_q. T_q was then used in equation (1) to determine the total mass of butanol adsorbed per gram adsorbent.
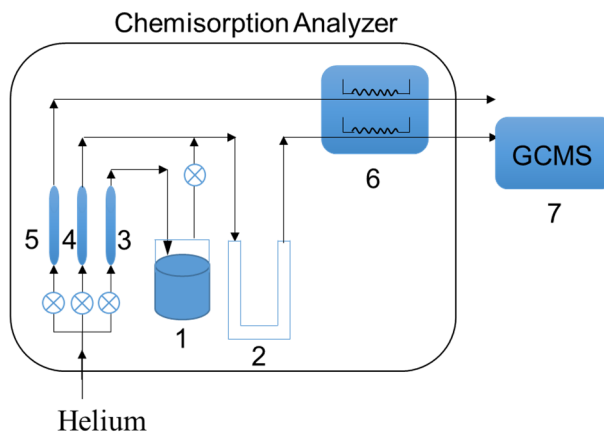
Fig. 5. 1. Schematic diagram of the experimental adsorption system: 1, butanol bath; 2, sample tube; 3, vapor flow rate meter; 4, carrier flow rate meter; 5, reference flow rate meter; 6, TCD detector; 7, GC-MS.

Breakthrough time is defined as the time when the outlet concentration of butanol vapor is 5% of the inlet concentration. Determination of the outlet butanol vapor concentration as a function of time allowed us to determine the breakthrough curve and experimentally calculate the dynamic adsorption capacity of the packed column for each experiment. The adsorbed amounts were calculated with the following equation:

$$Q = \frac{M_{adsorption}}{W} = \frac{T_q C_i F_A}{W} \qquad (1)$$

The time T_q is estimated according to the equation (2):

$$T_q = \int \left(1 - \frac{C_o}{C_i}\right) dt \qquad (2)$$

Where Q is the adsorbed amount (mg g^{-1}); $M_{adsorption}$ is the mass of butanol absorbed (mg); F_A is the volumetric flow rate of the carrier gas (ml min^{-1}); W is the net weight of adsorbent (mg); C_i represents the butanol concentration at the inlet (μg ml^{-1}); C_o is the butanol concentration at the outlet (μg ml^{-1}).

For regeneration, the temperature-programmed desorption (TPD) process was pre-programmed into the Micromeritics analyzer, the same device used for measuring adsorption. The flow rate of the vapor, carrier, and reference were set at 0, 10, and 10 cm^3/min, respectively. The temperature ramp was set at 15 °C/min, starting from 25 °C to 150 °C with a 1 h end temperature hold.

5.3. Results and discussion

5.3.1 Characteristics of porosity in ACs

The pore structure of the ACs (see Fig. 5.2A) were estimated using the nitrogen adsorption isotherm. The total BET surface area and pore volume distribution is listed in Table 5.2. The nitrogen adsorption isotherm of all these ACs showed type I nitrogen

isotherms at 77 K, according to the IUPAC classification [26]. WCS-900 has the highest

N_2 adsorption due to it having the largest BET surface area (2330 $m^2 g^{-1}$, Table 5.2) and

highest total pore volume (1.29 $cm^3 g^{-1}$, Table 5.2). All the ACs, except CSP-800 and

WCS-1000, showed large adsorption-desorption hysteresis cycles. It indicates that both

CSP-800 and WCS-1000 have low mesopore volume for 0.08 $cm^3 g^{-1}$, as shown in Table

5.2. The total pore volume of the ACs prepared from CSP increased with increasing

activation temperature, while the micorpore volume remained the same (0.47 $cm^3 g^{-1}$).

The mesopore volume increased appreciably, from 0.08 to 0.25 $cm^3 g^{-1}$. Therefore,

average pore diameter increased with the increasing temperature (1.93 nm for CSP-800,

2.20 nm for CSP-900 and 2.41 nm for CSP-1000). BET surface area increased as follows

for CSP AC samples: CSP-800 (1413 $m^2 g^{-1}$) < CSP-900 (1606 $m^2 g^{-1}$) < CSP-1000 (1654

$m^2 g^{-1}$).
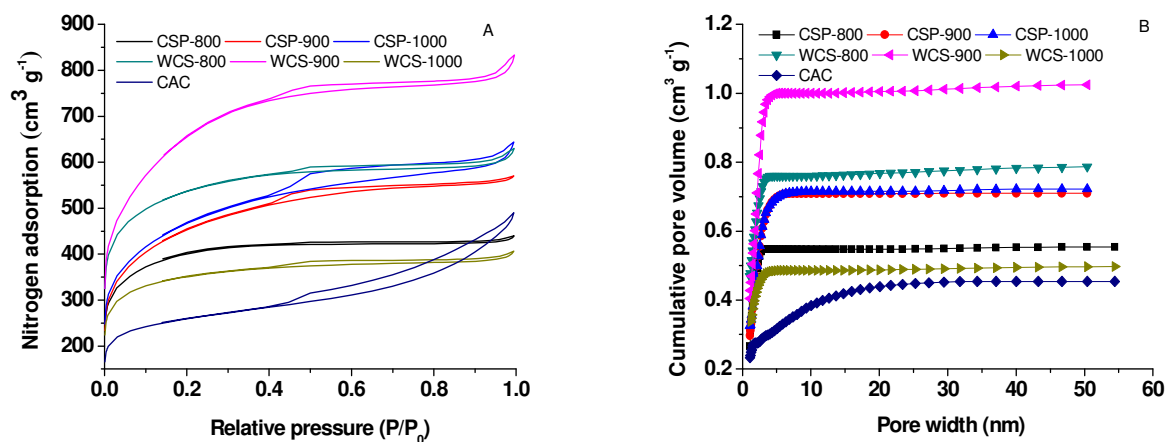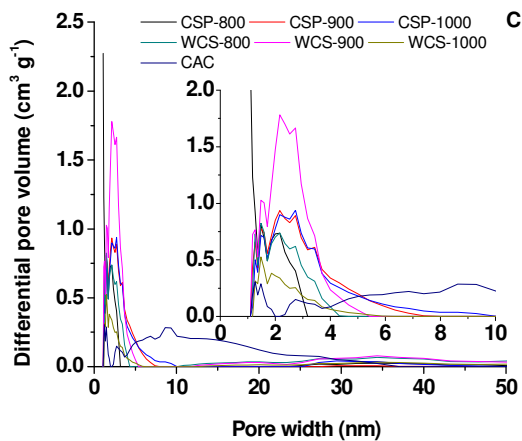
Fig. 5. 2. (A) N2 adsorption–desorption isotherms of ACs; (B) Cumulative pore volumes of the absorbents; (C) DFT pore size distribution curves of the absorbents.

Table 5. 2 Surface area and pore structure parameters of the adsorbents.

Sample #	S_{BET}[a]	V_{Total}[b]	V_{Micro}[c]	V_{Meso}[d]	$D_{Average}$[e]	Yield
	$m^2\ g^{-1}$	$cm^3\ g^{-1}$	$cm^3\ g^{-1}$	$cm^3\ g^{-1}$	nm	%
CSP-800	1413	0.68	0.47	0.08	1.93	22±1.3
CSP-900	1606	0.88	0.47	0.24	2.20	18±1.7
CSP-1000	1654	1.00	0.47	0.25	2.41	13±1.9
WCS-800	1884	0.97	0.63	0.16	2.07	29±1.2
WCS-900	2330	1.29	0.65	0.37	2.21	21±1.5
WCS-1000	1233	0.63	0.42	0.08	2.04	15±1.8
CAC	909	0.76	0.28	0.17	3.34	--

[a] BET (Brunauer-Emmett-Teller) surface area

[b] Total pore volume, measured at P/P_0=0.995

[c] Micropore volume, based on density functional theory (DFT)

[d] Mesopore volume, based on density functional theory (DFT)

^e Average pore diameter of absorbents, calculated by $4V_{Total}/S_{BET}$

As shown in Table 5.1, it is clear that there is a strong dependence of the specific surface area on the raw material. The specific surface area of WCS-900 was 724 $m^2 g^{-1}$ greater than the AC prepared from CSP at 900 °C. Additionally, WCS-900 obtained highest micropore and mesopore volumes, at 0.65 and 0.37 $cm^3 g^{-1}$ respectively. The micropore volume of WCS-900 at 900 °C was also significantly greater (0.18 $cm^3 g^{-1}$) than that of CSP-900. The WCS-800 also obtained higher pore volume (0.97, 0.63 and 0.16 $cm^3 g^{-1}$ for the total pore, micropore and mesopore volume, respectively) and BET surface area (+471 $m^2 g^{-1}$) than CSP-800. The pore volume for WCS was decreased significantly at the highest temperature (1000 °C). The micropore and mesopore volume obtained for WCS-1000 was 0.42 and 0.08 $cm^3 g^{-1}$, respectively. The major components (percent, w/w) were cellulose (8.5%), hemicelluloses (69.6%) and lignin (10.20%) on a dry weight basis of the CSP [56]. The WCS contains 34.4% lignin, 28.9% hemi-cellulose, 33.1% cellulose reported by Peterson and Hixon.[133] Different carbon source resulted in different carbon structure has been investigated by our previous study [134]. The biomass (CSP and WCS) was precarbonized at 400 °C for 1 h before activation with KOH, which produced different biochar. As is shown in Table 5.2, the micropore volume of CSP ACs with different activation temperature kept at 0.47 $cm^3 g^{-1}$. And the mesopores (around 0.24 $cm^3 g^{-1}$) were fully developed when the temperature increased from 900 to 1000 °C. In addition, macropores (larger than 50 nm) were generated more and more with temperature increasing, which are attributed to predominating of pore widening at high

base loading with high temperature. Therefore, the surface area of CSP based AC increased 48 $m^2 g^{-1}$ when the activation temperature increased from 900 to 1000 °C. Compared with CSP, WCS contains more lignin and cellulose than CSP. The lignin-based biochar from the WCS was carbonized quickly when temperature increased from 900 °C to 1000 °C, which formed robust carbon and was not easy to develop new pore structure [134]. Therefore, less micropores and mesopores were generated by using WCS as precursor at 1000 °C. This indicates that cellulose and lignin (the main components of the cortex) are not optimal materials for producing AC with a high BET surface area at 1000 °C under the conditions used in this study. The pore structure of the commercial activated carbon (CAC, Fisher Chemical) was also investigated. The BET surface area and total pore volume of CAC was 909 $m^2 g^{-1}$ and 0.76 $cm^3 g^{-1}$, respectively (Table 5.2). CAC also had less micropore volume (0.28 $cm^3 g^{-1}$) than any of the AC samples. Table 5.1 shows that the WCS could generate higher yield of active carbon compared with the CSP at the same activation temperature. This is due to the higher lignin content in WCS, which produced much more carbon than the low lignin-contained CSP [135]. The yield of active carbon was decreasing with the activation temperature increasing, which was caused by higher rate of carbon burnoff at higher temperature [134].Fig. 5.2B shows the cumulative pore volumes for the AC samples. The curves for CSP-900 and CSP-1000 almost overlap, indicating that their pore size distributions were almost the same. The cumulative pore volumes (diameter < 5 nm) of the ACs prepared from the biomass increased sharply, then remained stable. The cumulative pore volume of CAC increased remarkably from 0 to 25 nm. It indicates the pore size distribution of CAC was wider

than the AC prepared from the biomass.

Fig. 5.2C shows the pore size distributions for the ACs. Most of the pores from ACs prepared by KOH activation were smaller than 8 nm. As for the ACs prepared from CSP, the average pore diameter increased with increasing temperature preparation (1.93 nm for CSP-800, 2.20 nm for CSP-900 and 2.41 nm for CSP-1000). The AC prepared from WCS obtained the smallest average pore diameter (2.04 nm) at 900 °C, while the average pore diameter of CAC was the largest (3.34 nm) among those ACs. Mesopores of CAC ranged from 6 to 30 nm, which is far more than the other ACs (with the same pore size range). Judging from the change in the pore structure, in terms of the specific surface area and the pore volume, different components of the biomass produced different ACs using the same activation method.

The scanning electron microscope (SEM) is widely used to study the morphological features and surface characteristics of adsorbent materials. To compare the ACs prepared from different parts of the biomass, the microstructures of the WCS-900 and CSP-900 were observed by SEM and are shown in Fig. 5.3. This figure indicates that the adsorbents had irregular and porous surfaces; such morphology confers a relatively high surface area. This observation is supported by the BET surface areas of the different AC samples. WCS-900 seems to have more flat pieces than CSP-900, which should come from the cortex. The AC flat pieces are beneficial for mass transfer[136] and butanol

diffusion, which could enhance the vapor adsorption.
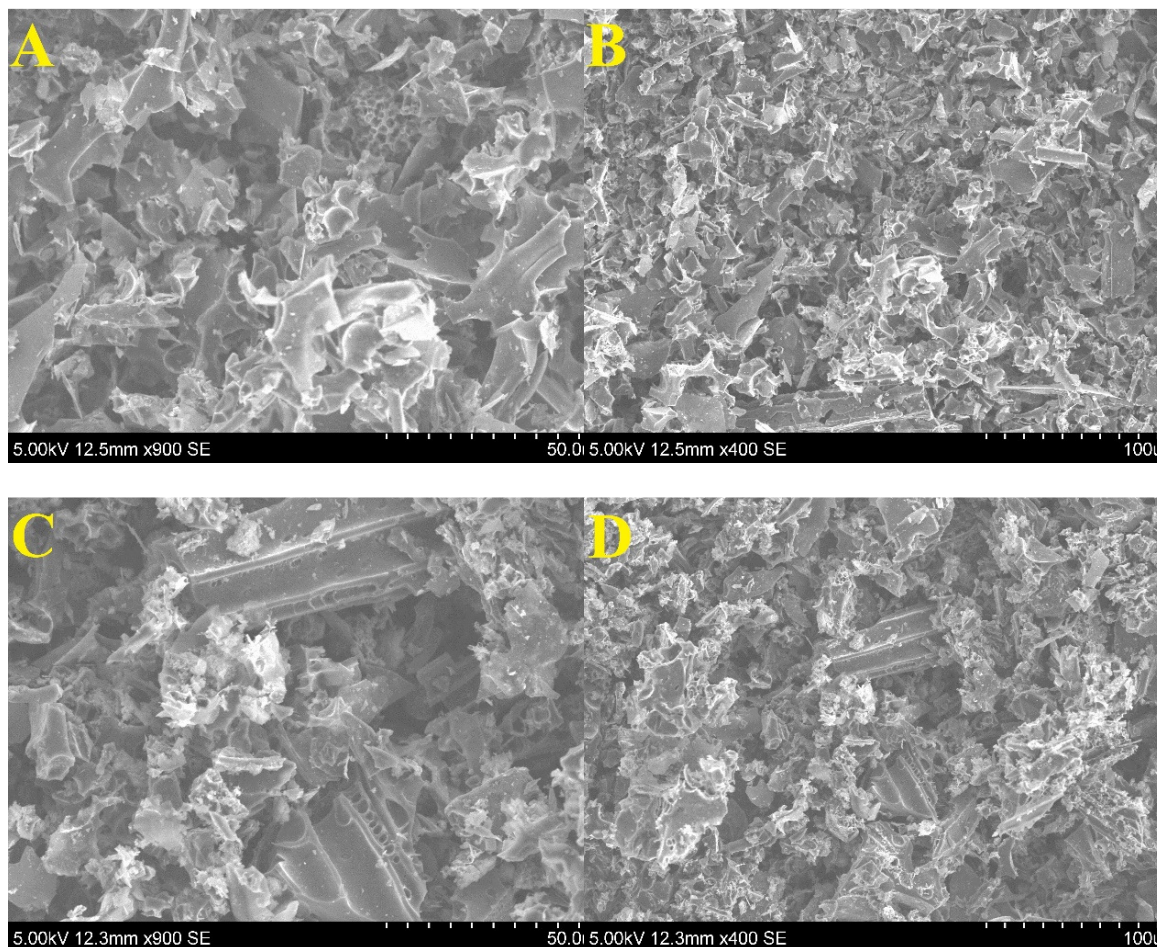
Fig. 5. 3. Scanning electron microscopy images of WCS-900 (A and B) and CSP-900 (C and D). (A and C) SEM image with a scale bar of 50 µm; (B and D) SEM image with a scale bar of 100 µm.

5.3.2. Adsorption of butanol vapor on the adsorbents

Fig. 5.4 shows the breakthrough curves for butanol under atmospheric conditions and 25 °C. The breakthrough time of WCS-900 was 190.8 min (Table 5.3), the longest of any

of the ACs. CSP-1000 and WCS-800 have the same breakthrough time (127.9 min, Table

5.3), which was slightly shorter than the breakthrough time for CSP-900 (128.4 min,

Table 5.3). The dynamic adsorption capacity of CSP-900 (287.9 mg g^{-1}) was also a little

greater than CSP-1000 (279.2 mg g^{-1}) and WCS-800 (280.2 mg g^{-1}). CSP-800 and WCS-

1000 had similar breakthrough time for 86.1 and 86.7 min, respectively. These two

adsorbents had similar micropore volumes (0.47 and 0.42 cm^3 g^{-1} for CSP-800 and WCS-

1000, respectively) and mesopore volumes (both were 0.08 cm^3 g^{-1}). Similar pore

structure conferred a similar breakthrough time for the two. The dynamic adsorption

capacity of WCS-1000 was 8.9 mg g^{-1} greater than that of CSP-800 (191.7 mg g^{-1}). This

increased adsorption capacity may have been due the fact that less oxygen-containing

surface functional groups—which decrease the affinity of butanol to the AC surface—

were present because they are known to decompose at 1000°C [123, 124]. The

commercial AC had the shortest breakthrough time (34.2 min), which might be due to

low micropore and mesopore volumes. It was easier for the butanol molecules to

breakthrough because there was less space to occupy. It can be observed that the profiles

for both the CSP and WCS samples were steeper than that of CAC, implying that CAC

has a lower butanol adsorption rate. Based on the observations of the different

breakthrough curves, it was concluded that the pores of the prepared ACs were easier for

butanol vapor to enter. Butanol molecules breaking through indicated saturation of the

adsorbent.
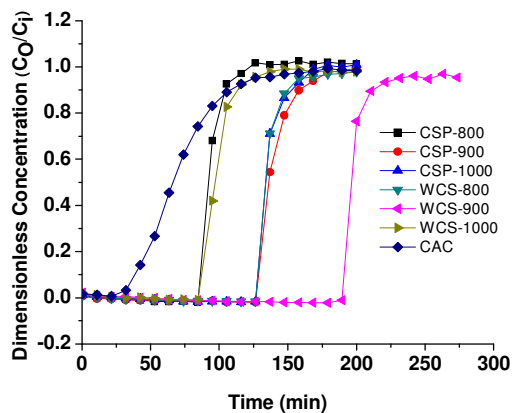
Fig. 5. 4. Breakthrough curves of different adsorbents.

Table 5. 3 Calculation of adsorption process.

Items	CSP-800	CSP-900	CSP-1000	WCS-800	WCS-900	WCS-1000	CAC
F_A [a] (ml min^{-1})	10	10	10	10	10	10	10
T_q [b] (min)	126.5	200.0	179.0	189.5	242.0	147.5	179.0
C_i [c] (µg ml^{-1})	10.1	10.1	10.1	10.1	10.1	10.1	10.1
$M_{adsorption}$ [d] (mg)	9.6	14.4	14.0	14.0	20.4	10.0	7.2
W [e] (mg)	50	50	50	50	50	50	50
Q [f] (mg g^{-1})	191.7	287.9	279.2	280.2	410.0	200.6	143.8
T_b [g] (min)	86.1	128.4	127.9	127.9	190.8	86.7	34.2

[a] Volumetric flow rate of the carrier gas

[b] Stoichiometric time determined from the breakthrough curve

[c] Butanol concentration at the inlet

[d] Mass of butanol adsorbed

[e] Net weight of adsorbent

[f] Dynamic adsorption capacity of the adsorbent

[g] Breakthrough time

Important factors governing the butanol adsorption capacity include the micropore volume mesopore volume, total pore volume, and BET surface area. Further investigations of these factors and their effects on the butanol vapor adsorption capacity were presented in Fig. 5.5. Linear fits were used to evaluate the contributions from these factors. Poor correlations were shown for the micropore volumes and total pore volumes—R^2 coefficients were 0.66 and 0.80 (Fig. 5.5A-B), respectively. The BET surface areas and the butanol vapor adsorption capacities have a stronger correlation (R^2=0.91, Fig. 5.5C). Furthermore, the butanol vapor adsorption capacities have been shown to be proportional to the pore volume (pore size <50 nm). A higher correlation coefficient (R^2=0.96, Fig. 5.5D) was noted for the linear equation, indicating that pores smaller than 50 nm play a significant role in butanol vapor adsorption. The major factor determining adsorption capacity is pore size. Micropores (smaller than 2 nm) provide a more stable environment to store butanol molecules. The mesopores working as transitional pores [137] also have ability to carry the molecules [138], which made contribution to the butanol adsorption capacity of the adsorbent. While the butanol molecules are not easy to be trapped in larger pores (>50 nm). Therefore, pores smaller than 50 nm can be used to capture the butanol molecules.
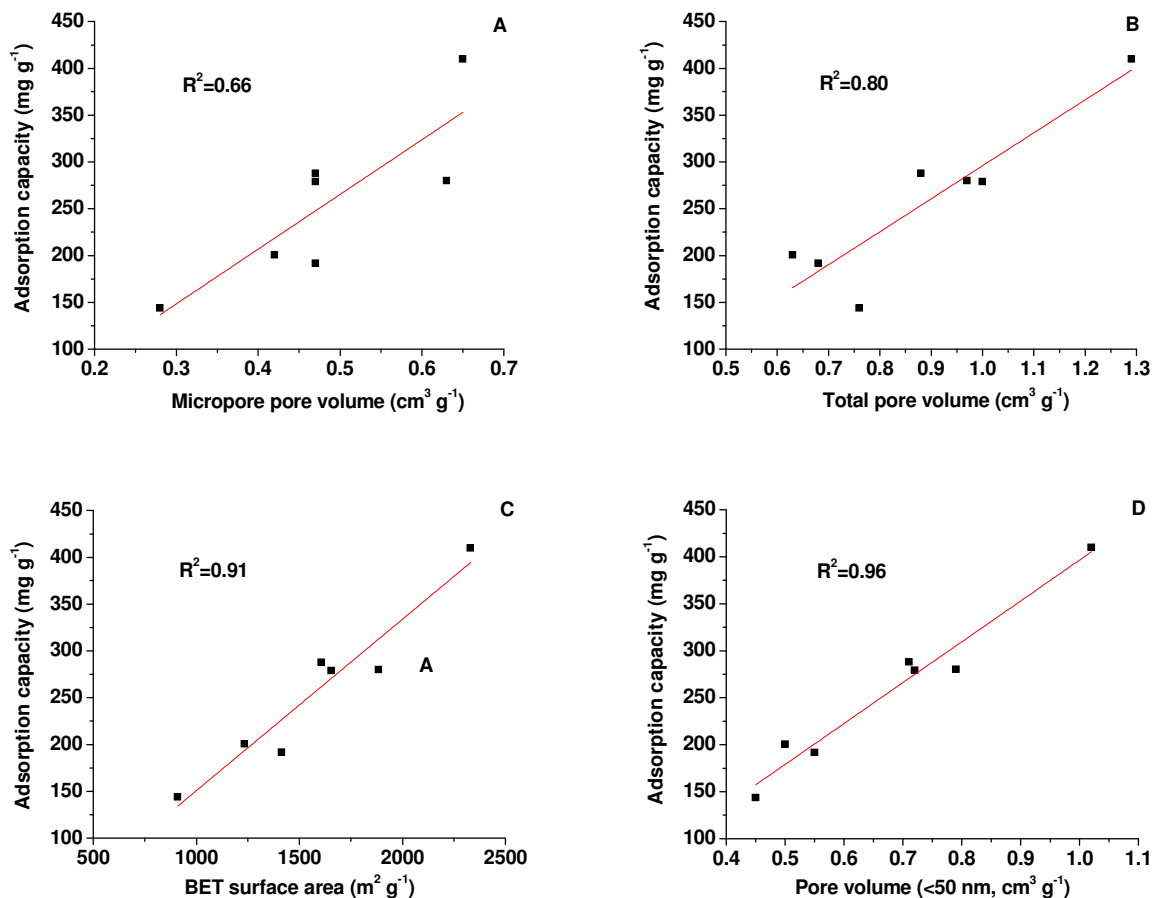
Fig. 5. 5. Correlations between pore structure parameters and butanol vapor dynamic adsorption capacities: (A) Micropore volume. (B) Total pore volume. (C) BET surface areas. (D) Pore volume (<50 nm).

5.3.3. Regeneration of the adsorbent

WCS-900 has the highest butanol vapor adsorption capacity. Repeated adsorption/desorption cycles were performed to investigate the reusability of the adsorbent. Heating was used to desorb the butanol from saturated AC sample [123]. As is shown in Fig. 5.6, the breakthrough curves for the first two cycles were almost identical.

The adsorption capacity for the first cycle was 410.0 mg g^{-1}, then it slightly decreased to 406 mg g^{-1} during the second cycle, as is shown in Table 5.4. Fig. 5.6 shows that the breakthrough curves (from the third cycle to the fifth cycle) almost overlapped. It can be concluded that the adsorption capacities for butanol were almost the same for the third to fifth cycles (386.0 mg g^{-1}, Table 5.4). Over five cycles, WCS-900 retained 94% of its initial adsorption capacity, indicating high re-usability of the adsorbent.
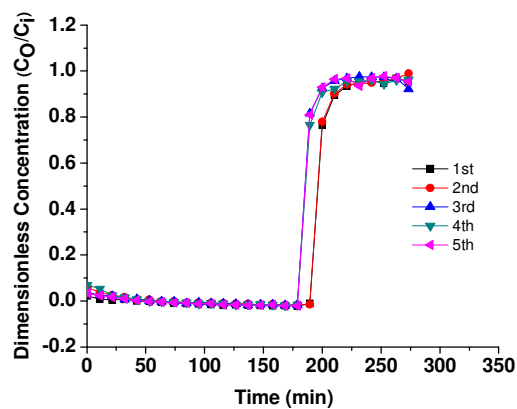
Fig. 5. 6. Repeated adsorption of butanol vapor with WCS-900.

Table 5. 4 Calculation of repeating adsorption process for WCS-900.

Items	1st round	2nd round	3rd round	4th round	5th round
F_A (ml min^{-1})	10	10	10	10	10
T_q(min)	202.5	200.8	189.8	191.2	190.6
C_i (μg ml^{-1})	10.1	10.1	10.1	10.1	10.1
$M_{adsorption}$ (mg)	20.5	20.3	19.2	19.3	19.3
W (mg)	50	50	50	50	50
Q (mg g^{-1})	410.0	406.0	384.0	386.0	386.0

5.4. Conclusions

High surface area active carbons were produced by simple thermo-chemical activation of corn stalk pith and the whole corn stalk with KOH as an activating agent. The active carbon with the highest BET surface area (2330 m^2 g^{-1}) was obtained by using mass-impregnation ratio of 1:4.2 (KOH pallet: Char) at 900 °C for 1 h. In addition, there is high adsorptive capacity (410.0 mg g^{-1}) for butanol vapor of this activated carbon, which was 185.1% higher than the commercial AC. Therefore, WCS-900 is a promising adsorbent that can be produced at a low-cost and is a viable alternative to CAC as an adsorbent for butanol. The adsorption capacity can be maintained at 94% for five cycles. There was a good correlation between the amount of butanol vapor adsorbed and pore volume (<50 nm). It can be concluded that butanol adsorption was mainly governed by pores smaller than 50 nm of the adsorbents.

Chapter 6 Adsorption of creatinine on active carbons with nitric acid hydrothermal modification

Adapted from Cao, Y.; Gu, Y.; Wang, K.; Wang, X.; Gu, Z.; Ambrico, T.; Castro, M. A.; Lee, J.; Gibbons, W.; Rice, J. A., Adsorption of creatinine on active carbons with nitric acid hydrothermal modification. Journal of the Taiwan Institute of Chemical Engineers 2016, 66, 347-356.

6.1 Introduction

Creatinine (2-amino-1-methyl-5H-imidazol-4-one, $C_4H_7N_3O$) is a typical uremic toxin in the human metabolism products. The accumulation of creatinine in the blood causes a series of toxic symptoms such as diabetic nephropathy, eclampsia, glomerulonephritis, muscular dystrophy, and preeclampsia, meanwhile which also reduces the kidney function and accelerates the renal decline [139].

Creatinine is commonly removed by haemodialysis. However, creatinine cannot be effectively removed by a single haemodialysis process. Haemoperfusion, the direct contact of the patients' blood with sorbents, can efficiently remove toxins without introducing any other substances into the blood [140]. Porous materials such as active carbon and polymeric resin are mainly used in haemoperfusion [141] to adsorb the creatinine. To date, porous materials like active carbon [142], zeolites [143-145], carbon nanotubes [146], molecularly imprinted polymers [147-149], and metal-organic frameworks [150] for artificial kidney application of creatinine adsorption have been investigated.

Among those adsorbents, activated carbon (AC) has a long record as a cheap sorbent in blood purification in the case of intoxications, acute and chronic renal failure as well as liver failure [151-153]. Moreover, carbon materials have chemically inert surface and excellent biocompatibility, they are more powerful sorbents than their inorganic or organic counterparts because they do not require special coatings [154].

On the other hand, creatinine not only exists in serum, but also in the alimentary canal (stomach and intestine) [155]. Active carbon can be used as oral sorbents to reduce the creatinine concentration in serum. Creatinine and other waste nitrogenous waste products (urea, etc) which diffuse into the gastrointestinal tract from the blood are bound to active carbon and excreted in the feces, creating a concentration gradient for continued diffusion, giving place to a process this intestinal dialysis. Therefore, active carbon can adsorb the creatinine, uric acid and other toxins in gastrointestinal tract quickly, lightening the burden of kidney excreting toxins [156, 157].

Both porous structure and surface chemistry of ACs may play an important role in determining their adsorption performance. Since the performance of AC in most applications is influenced by its surface chemistry, the modification of its properties has been the target of a variety of treatments. Nitric acid has been used to introduce carbon-oxygen surface groups in AC to increase the adsorption capacity for phenol [158] and

sulfur compounds [159] in aqueous phase. Nitric acid modified AC samples were also used for vapor adsorption [123], which decreased the butanol adsorption capacity due to the increased oxygen-containing functional groups on the adsorbents' surface [99]. It indicates that different adsorbates may have different interaction with the oxidized AC samples. To improve the adsorption performance of AC for removing creatinine, hydrothermal modification of the commercial AC was conducted in the present study by using 4 M HNO_3 at 120 °C, 150 °C and 180 °C, respectively. To our knowledge, similar research has not been reported so far.

6.2 Materials and methods

6.2.1 Materials

HNO_3 and creatinine (Assay Percent Range: 99+%, $C_4H_7N_3O$) were purchased from Thermo Fisher Scientific Inc. All of these chemicals were analytical grade. Commercial AC was purchased from Thermo Fisher Scientific Inc. Different kinds of modified AC were obtained by reaction between commercial AC and 4M HNO_3 at different temperatures.

6.2.2 Methods

6.2.2.1 Modification of AC

The commercial AC was washed by boiling water with a Soxhlet extractor for 2 hours. The wet AC was dried at 105 °C for 24 hours. 3 g of the dried AC was reacted with 40 ml 4 M HNO_3 in a sealed PTFE reactor (50ml) at 120, 150, and 180 °C for 1 hour respectively. These samples are denoted as 120-AC, 150-AC, and 180-AC. After reaction, the reactant was cooled and filtered, and washed with deionized water under vacuum filtration until the pH value of the permeate was ~7. Finally, the washed AC was dried in a vacuum oven at 105 °C overnight.

6.2.2.2 Chemical and textural characterization for absorbents

The characterization of the porous texture of the ACs was carried out by the analysis of the adsorption isotherm adsorption of N_2 using an ASAP 2020 Micropore Analyzer. The total pore volume was determined at relative pressure 0.995 P_0, and the specific surface area was calculated from the BET method. The micropore and mesopore volume and the pore size distribution were determined by the density functional theory (DFT) for samples based on the N_2 isotherm adsorption data.

Temperature-programmed desorption (TPD) was performed using a Micrometrics Autochem II Chemisorption Analyzer to investigate the oxygen content of these four AC

samples. The carbon sample (0.05 g) was placed in a U-shaped quartz tube inside an electrical furnace and heated at 10 °C/min up to 1000 °C using a constant flow rate of helium (the flow rate of the vapor, carrier, and reference were set at 0, 60, and 60 cm^3/min respectively). The thermal conductivity detector (TCD) signals were monitored during the thermal analysis, and the corresponding TCD spectra was obtained.

In order to analyze the functional groups on the surface, FTIR analysis of AC samples were carried out by using UV-3600 spectrophotometer within the range of 600-4000 cm^{-1}. The AC samples were dried in an oven at 110 °C for overnight before the FTIR analysis. XPS analysis was carried out using Kratos Axis Ultra X-ray photoelectron spectrometer with concentric hemispherical electron energy analyzers combined with the established delay-line detector (DLD). The incident radiation monochromatic Al Kα X-ray (1486.6 eV) at 150W (accelerating voltage 15kV, emission current 10mA) was projected 45º to the sample surface and the photoelectron data was collected at takeoff angle of θ= 90º. The absolute energy scale was calibrated to Cu $2p_{3/2}$ peak binding energy at 932.6 eV using sputter etched 99.9999% pure copper foil. The base pressure in the analysis chamber was maintained at 1.0×10^{-9} torr. Low energy electrons were used for charge compensation to neutralize the sample. Carbon powders were pressed onto 99.999% pure Indium foil for analysis. Survey scans were taken at pass energy of 160 eV, and carried out over 1200 eV ~-5 eV binding energy range with 1.0 eV steps and a dwell time of 200 ms. High resolution scans of C 1s, O 1s, and N 1s were taken at pass energy of 20 eV with 0.1 eV steps and a dwell time of 1000ms. The spectra analyses

were carried out using CasaXPS version 2.3.17dev6.4k. Shirley type background was routinely used to account for inelastically scattered electrons that contribute to the broad background. Transmission corrected RFS/Kratos library relative sensitivity factors (RSFs) was used for elemental quantification. The spectra were calibrated using adventitious carbon C 1s peak at 285.0 eV.

6.2.2.3 Quantification of creatinine

To determine the amount of creatinine adsorbed by the adsorbents, a standard curve was used to calculate the creatinine amount in the solution. Creatinine was dissolved in distilled water, and creatinine solutions with different concentrations (2, 4, 8, 10, 20, 40, 60, 80, 100, 120, 140, and 160 mg L^{-1}) were prepared. The ultraviolet (UV) region of 120 mg/L creatinine solution is scanned from 200 to 400 nm by a Shimadzu UV 2450 spectrophotometer (Tokyo, Japan). As is shown in Fig. 6.1, the wavelength of maximum absorbance is 230 nm. Therefore, the absorbance of the solution was measured at 230 nm. The standard curve was plotted according to the concentration and absorbance, which is shown in Fig. 6.2. Regression of the standard absorbance with concentration typically resulted in an $R^2 \geqslant 0.99$.
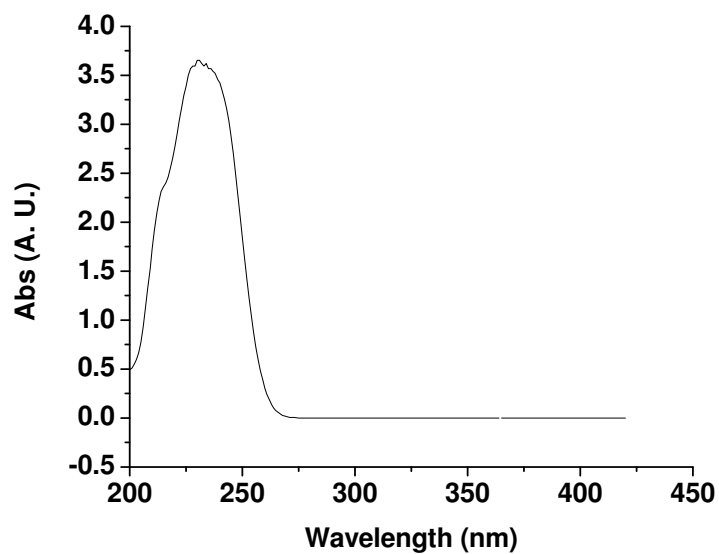
Fig. 6. 1. UV adsorption of creatinine.
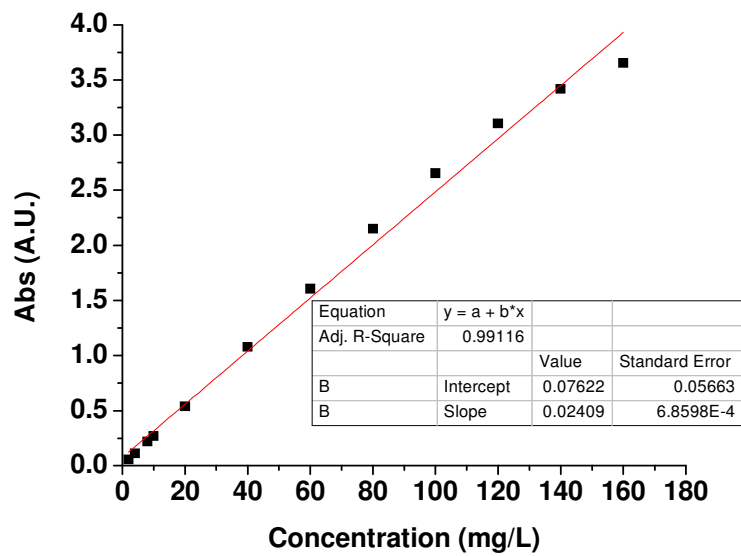
Fig. 6. 2. Standard curve for creatinine mass concentration.

6.2.2.4 Batch equilibrium

The creatinine was dissolved in deionized water to the required concentration. In experiments of equilibrium adsorption isotherm, AC sample (50 mg) of and creatinine solution (20 mL) were place in a 100 mL Erlenmeyer flask and shaken for 2 h by an incubator at the constant temperature of 37 °C. Each used a range of initial creatinine concentration was 40, 60, 80, 100, 120, 140 and 160 mg L^{-1} at pH 7. The AC sample was removed via a Millipore membrane filter (0.20 µm) and the permeate was measured in the UV Spectrometer at 230 nm to determine the concentration of creatinine in the solution. Every value reported contained at least three separate measurements, and standard deviation was less than 5%. The amount of adsorption at equilibrium q_e (mg/g) was calculated as follows:

$$q_e = \frac{(C_0 - C_e) \times V}{W} \quad (1)$$

Where C_0 and C_e (mg/L) are the initial and equilibrium creatinine concentration respectively. V (L) is the volume of the solution and W (g) is the weight of AC used.

6.2.2.5 Batch kinetic

In experiments of batch kinetic adsorption, 50 mg of different AC samples were weighed and both the samples and the 160 mg L^{-1} creatinine solution were heated to 37 °C in an incubator. The 160 mg L^{-1} creatinine solution was mixed in the incubator constantly at 100 rpm. Once the samples warmed, 20 mL of creatinine solution were

added to each sample in Erlenmeyer flasks and samples were removed at 1, 3, 5, 15, 30, 60 or 120 min via membrane filters. The creatinine concentration was determined as above-mentioned measuring method.

6.2.2.5 Data analysis

The widely used Langmuir isotherm has found successful application in many real adsorption processes and is expressed as:

$$q_e = \frac{QbC_e}{1+bC_e} \qquad (2)$$

which can be rearranged to obtain a linear form

$$\frac{C_e}{q_e} = \frac{1}{Qb} + \frac{C_e}{Q} \qquad (3)$$

where Q (mg g^{-1}) refers to the monolayer adsorption capacity, q$_e$ is amount of adsorption at equilibrium, C$_e$ (mg L^{-1}) is the creatinine concentration at equilibrium and b is the Langmuir constant.

The Freundlich isotherm, used for isothermal adsorption, is a special case for heterogeneous surface energy in which the energy term in the Langmuir equation varies as a function of surface coverage strictly due to variation of the adsorption [160]. The Freundlich equation is given as:

$$ln q_e = ln k_f + \frac{1}{n} ln C_e \qquad (4)$$

where C_e is the equilibrium concentration of adsorbate (mg L^{-1}), q_e is the amount of the creatinine adsorbed by the adsorbents at equilibrium (mg g^{-1}), k_f ((mg/g) (dm^3/mg)$^{1/n}$) and n are indicators of adsorption capacity and adsorption intensity, respectively. k_f and n can be determined from the linear plot of ln q_e versus ln C_e.

In order to investigate the mechanism of adsorption, the pseudo first-order and second-order equations were used to test the experimental data. The first-order rate expression of Lagergren [13] is given as:

$$log(q_e - q) = log q_e - \frac{k_1 t}{2.303} \qquad (5)$$

where q_e and q are the amounts of urea nitrogen adsorbed onto adsorbent at equilibrium and at time t, respectively, and k_1 (min^{-1}) is the rate constant of first-order adsorption. The second-order kinetic model is expressed as:

$$\frac{t}{q} = \frac{1}{k_2 q_e^2} + \frac{t}{q_e} \qquad (6)$$

Where k_2 (g mg^{-1} min^{-1}) is the rate constant of second-order adsorption.

6.3 Results and discussion

6.3.1. Physicochemical properties of active carbons

6.3.1.1 Pore structure characterization

Nitrogen adsorption-desorption isotherms of unmodified AC, 120-AC, 150-AC and 180-AC are shown in Fig. 6.3A. All nitrogen adsorption isotherms are of type II according to the classification by Brunauer et al [161]. The N_2 adsorption capacity on the ACs increased in the order of 120-AC < 150-AC < 180-AC < AC. A hysteresis loop was observed at the relative high pressure for each AC sample, indicating the presence of mesopores, which can also be found from the density functional theory (DFT) mesopores size distribution of the ACs, as is shown in Fig. 6.3B. It indicates that the pore volumes for micropores (smaller than 2nm) and mesopores (from 2nm to 50 nm) were slightly decreased for 120-AC and 150-AC samples. Fig. 6.3C shows the cumulative pore volumes for the AC samples, the curves for 120-AC and 150-AC, 180-AC and AC are almost overlapped respectively, which indicates their pore size distributions are almost the same for each pair. However, compared with the untreated AC, the total pore volume decreased from 0.76 to 0.70, 0.70, and 0.72 cm^3 g^{-1} for 120-AC, 150-AC and 180-AC respectively, which is shown in Table 6.1. The pores less than 50 nm (micropore volume plus mesopore volume) was decreased from 0.45 to 0.41 cm^3 g^{-1} for both 120-AC and 150-AC, while there is no change for AC treated with 180 °C. With the total pore volume decreased after the modification, the BET surface areas for the AC-120, AC-150, and AC-180 decreased from 909 (unmodified AC) to 847, 869, 883 m^2 g^{-1}, respectively (Table 6.1).
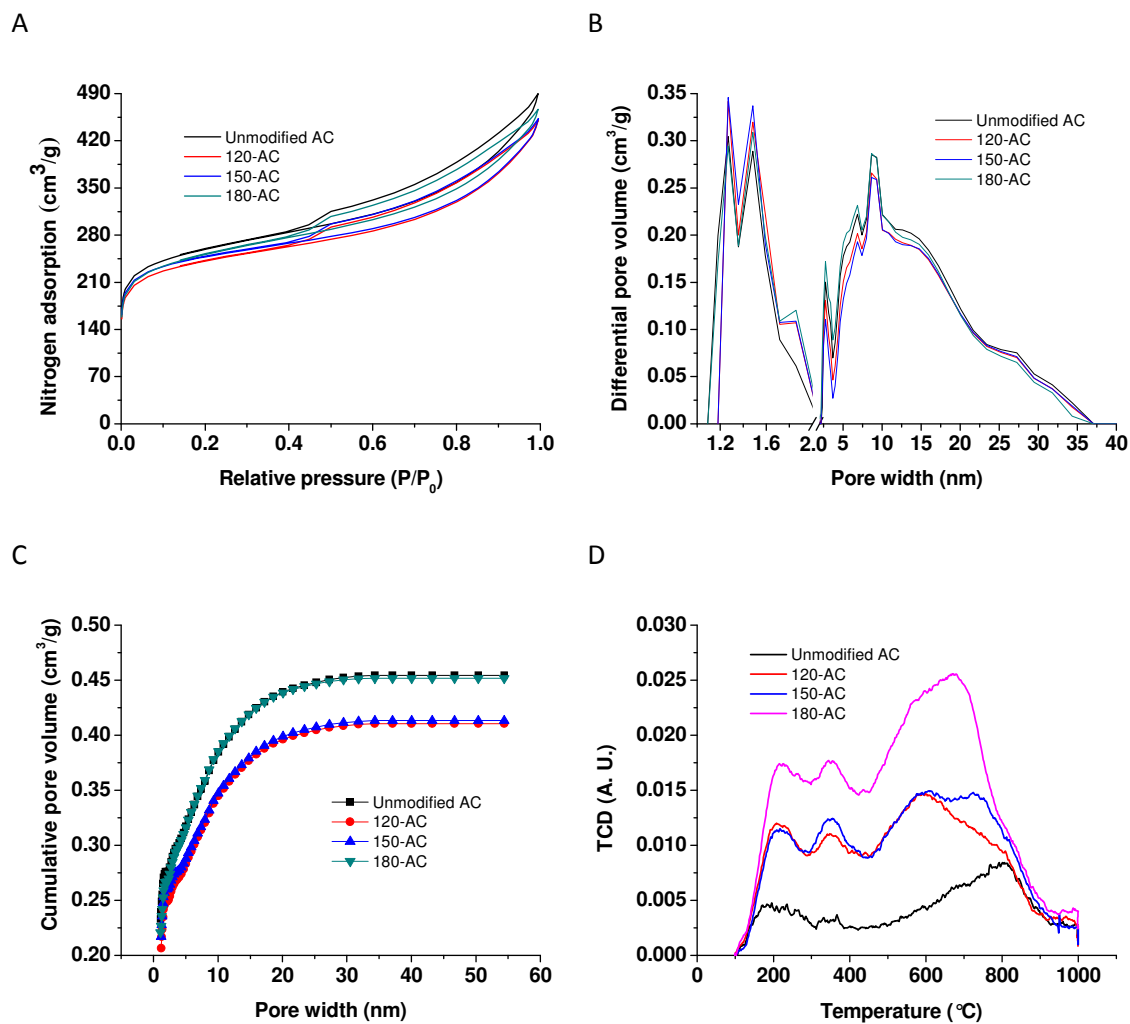
Fig. 6. 3. (A) N$_2$ adsorption–desorption isotherms of ACs; (B) DFT pore size distribution curves of the absorbents; (C) Cumulative pore volumes of the absorbents; (D) TPD profiles of ACs.

Table 6. 1 Surface area and pore structure parameters of the absorbents.

Sample #	S_{BET}[a] $m^2\ g^{-1}$	V_{Total}[b] $cm^3\ g^{-1}$	V_{Micro}[c] $cm^3\ g^{-1}$	V_{Meso}[d] $cm^3\ g^{-1}$	$D_{Average}$[e] nm
Unmodified AC	909	0.76	0.28	0.17	3.34
120-AC	847	0.70	0.25	0.16	3.31
150-AC	869	0.70	0.26	0.15	3.22
180-AC	883	0.72	0.27	0.18	3.26

[a] BET (Brunauer-Emmett-Teller) surface area

[b] Total pore volume, measured at $P/P_0=0.995$

[c] Micropore volume, based on density functional theory (DFT)

[d] Mesopore volume, based on density functional theory (DFT)

[e] Average pore diameter of absorbents, calculated by $4V_{Total}/S_{BET}$

The nitric acid hydrothermal treatment decreased the micopores volume for 0.03, 0.02 and 0.01 $m^2\ g^{-1}$ at 120, 150, and 180 °C, respectively, which can be attributed to partial destruction of the porous structure of the original sample due to the erosion of micropore walls [158, 162]. The mesopore volume decreased from 0.16 to 0.15 $cm^3\ g^{-1}$ with reaction temperature increased from 120 to 150 °C, which caused mesopores partially transferred into micropores [99]. It is likely due to the partial destruction of the pore structure and the introduced oxygen-containing functional groups at the active sites at the entrance of the mesopores [158, 162]. This resulted in the average pore diameter of the 120-AC and 150-AC decreased from 3.34 (unmodified AC) into 3.31 and 3.22 nm, respectively (Table 6.1).

On the contrary, compared with 150-AC the mesopore volume slightly increased (0.01 cm^3 g^{-1}) for 180-AC. Higher temperature enhanced oxidation reaction much more greatly, causing more robust oxidation and etching of the carbon matrix of AC. It generated some new micropores, meanwhile, some of the micropores were widened into mesopores. Therefore, the average pore diameter of 180-AC (3.26 nm) was slightly larger than that of 150-AC (3.22 nm), as is shown in Table 6.1.

6.3.2.2 Oxygen-containing functional groups on ACs

Temperature-programmed desorption (TPD) was employed to investigate the functional groups generated by HNO_3 modification [123]. The carrier gas helium and the detected gases (CO, O_2 and CO_2) have different thermal conductivities. TCD signals from the evolved gases were recorded and the areas under the peak were proportional to the amount of gases produced. Therefore, the TPD profile roughly indicates the amount of oxygen-containing functional groups.

Fig. 6.3D displays the TPD spectra arising from oxygenated groups released as CO and CO_2 from the surface of ACs. The TPD profile measured for the untreated AC was also included. The quantity of oxygenated groups released during treatment was directly related to the temperature used to treat AC. Generally, carboxylic functional groups decompose and release H_2O at lower temperatures (100 °C to 400 °C), while anhydride

and lactone groups decompose at higher temperatures (427 °C) [103-105]. In this study, the peaks formed between 400-1000 °C were assumed to be CO_2 and CO [106], and the CO was possibly derived from the decomposition of phenols, ethers and carbonyls/quinones [107-109]. The order of oxygen-containing functional group's amount was AC-180>AC-150>AC-120>unmodified AC according to the TPD profiles. The level of oxygen functional groups that are created on the AC surface is dependent on the treatment conditions, including nitric acid concentration, temperature and amount of carbon loaded [163]. It indicates that higher temperature can generate more oxygen-containing functional groups due to more vigorous oxidation with higher temperature.

As is shown in Fig. 6.4, there are two major characteristic peaks in the range of 1800-1400 cm^{-1}, which are mainly absorption bands of C=O and aromatic ring. The peak centered at 1722 cm^{-1} can be contribution from the stretching vibrations of carboxyl groups (C=O) on the edges of layer planes or from conjugated groups in the lactone groups. The peak at 1563 cm^{-1} can be assigned to asymmetric COO^- vibration. The peak around 1158 cm^{-1} can be ascribed to the both C-O stretching and O-H bending modes in phenolic and carboxylic groups. Compared with the unmodified AC, it was observed that the 180-AC had higher absorption intensity at 1722, 1563 and 1158 cm^{-1}, indicating an increase in carboxyl, lactone, and hydroxyl groups [159]. After TPD, these absorptions decreased significantly. It means that high temperature decomposed those oxygen-containing functional groups.
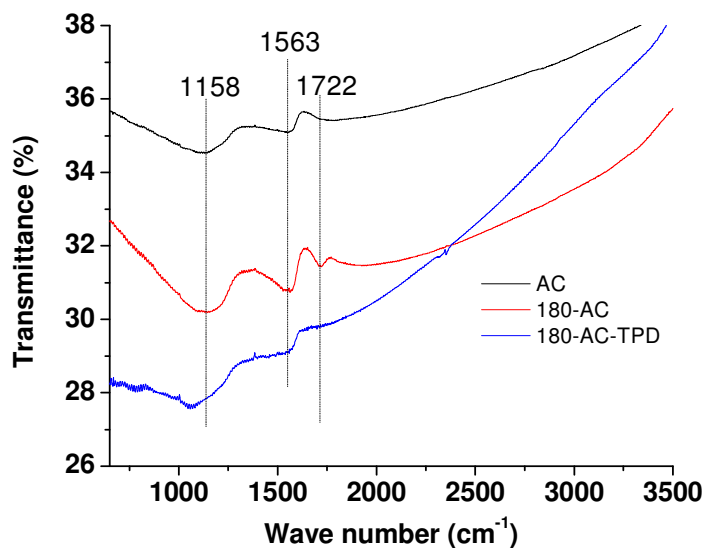
Fig. 6. 4. FTIR spectra of ACs.

It was found that the HNO_3 hydrothermal oxidation would change the total surface area and pore distribution to some extent as discussed above, but the surface morphology of ACs were almost the same, as is shown in Fig. 6.5. However, after HNO_3 treatment, oxygen content in the AC increased significantly, which has been verified by SEM-EDS (Table 6.2). The order of total oxygen content was unmodified AC (4.39, wt. %) < 120-AC (7.67, wt. %) <150-AC (8.50, wt. %) <180-AC (11.83, wt. %).

Table 6. 2 Elements Composition from Energy-dispersive X-ray Spectroscopy (EDS).

Samples	Elements	Line	Intensity (c/s)	Error 2-sig	Conc wt%
Unmodified AC	C	Ka	593.77	15.411	93.964
	O	Ka	6.98	1.671	4.394
120-AC	C	Ka	443.53	13.319	86.497
	O	Ka	12.66	2.251	7.670
150-AC	C	Ka	541.23	14.713	87.938
	O	Ka	15.00	2.450	8.502
180-AC	C	Ka	455.80	13.502	85.480
	O	Ka	17.85	2.672	11.833
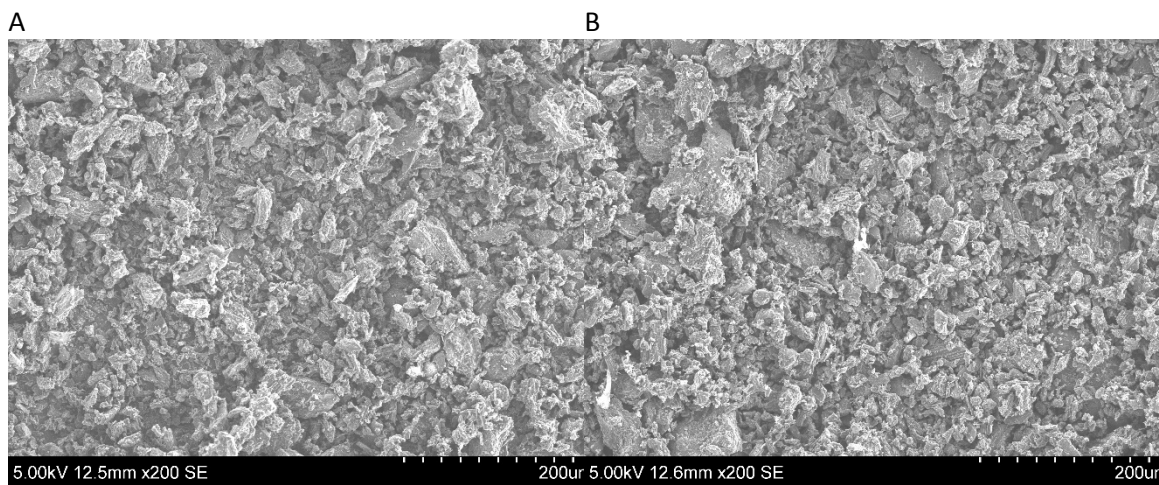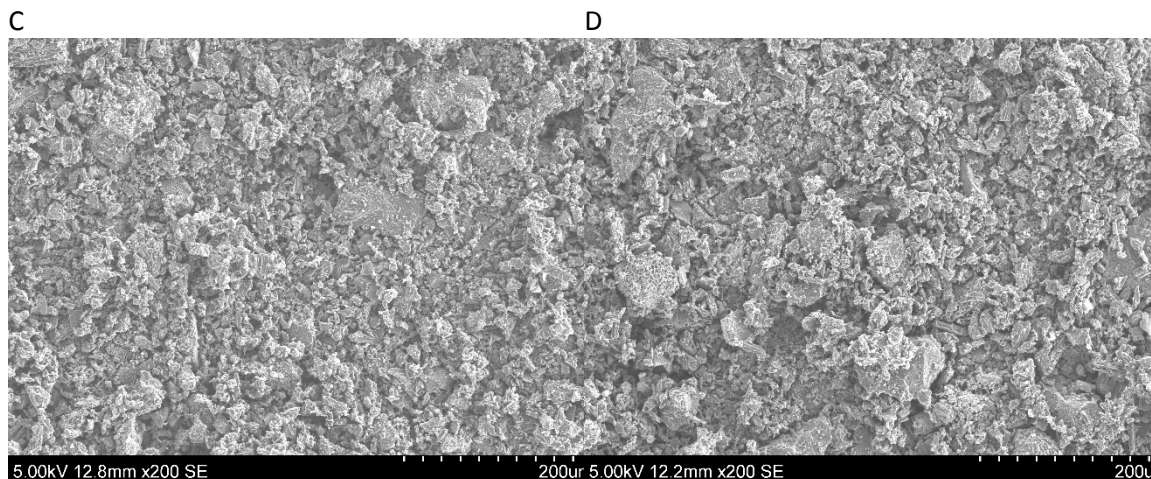
Fig. 6. 5. SEM images of the ACs. (A) Unmodified AC; (B) 120-AC; (C) 150-AC; (D) 180-AC.

The kinds and amounts of surface functional groups on unmodified AC and 180-AC were more quantitatively determined by the XPS method. Fig. 6.6 shows the C 1s and O 1s XPS spectra of unmodified AC and 180-AC. After baseline correction using Shirley's method, the C 1s peak of these two samples can be deconvoluted into five peaks centered at 284.6, 286.0, 287.3, 288.9, and 290.3 eV, which are ascribed to the graphitic C=C bond, -C-O, -C=O, O-C=O, and CO_3 groups, respectively [164-166]. The O 1s peak of each sample contains contributions from two Gaussian deconvoluted peaks centered at 532.0 and 534.0 eV, which are attributed to =O and -O- species, respectively [167]. Table 6.3 shows the molar ratio distribution of surface functional groups on unmodified AC and 180-AC from a comparison of each deconvoluted peak. By contrast, oxidation at 180 °C increased C-O group amount (199.8% higher than the unmodified AC) accompanied by

simultaneous increase in C=O, O-C=O (e.g., -COOH). The C1s spectra (Table 6.3)

displayed higher carbonyl (or quinone) and carboxylic (or ester or lactone) groups

contents in 180-AC (2.81% of C=O group; 2.81% of O–C=O groups) compared to the

unmodified AC sample (1.96% of C=O, and 2.25% of O–C=O). However, the nitric acid

modification slightly reduced the concentration of CO_3 from 3.10% to 2.90%, probably

due to the removal of carbonate existing in unmodified AC during the oxidation

treatment. The O1s spectra shows the intensity of the oxygen components in form of –O

and =O. As is shown in Fig. 6.6, the intensity of the 180-AC was higher than that of

unmodified AC. The oxygen content of 180-AC was 4.17% for =O and 5.67% for -O-,

which was significantly higher than unmodified AC (1.88% for =O and 2.15% for -O-).

Table 6. 3 Surface functional group molar ratio distributions obtained by XPS
measurement.

Sample	C 1s					O 1s	
	C=C	C-O	C=O	O-C=O	CO_3	=O	-O-
Unmodified AC	87.47	5.21	1.96	2.25	3.10	1.88	2.15
180-AC	81.06	10.41	2.81	2.81	2.90	4.17	5.67
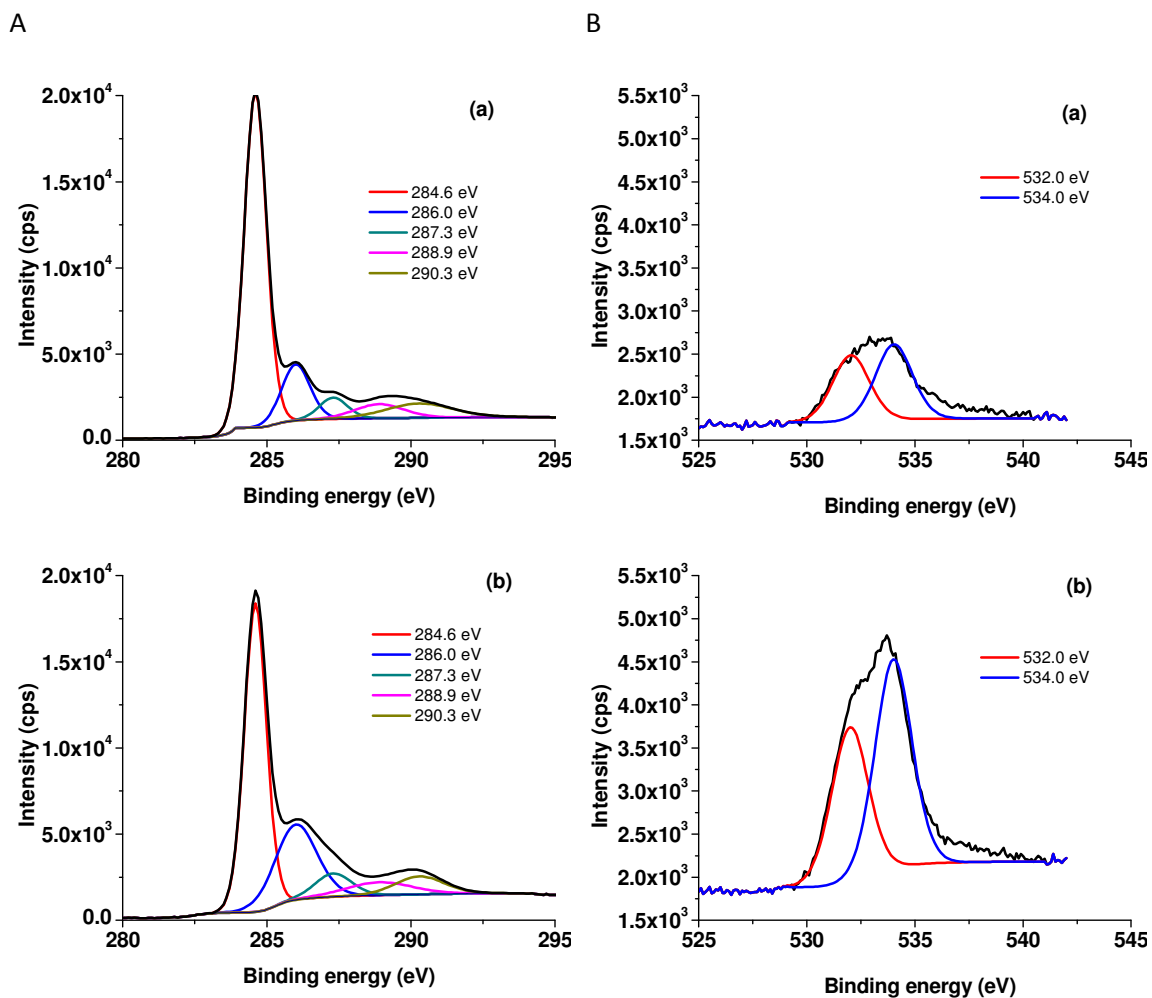
Fig. 6. 6. (A) C 1s and (B) O 1s XPS spectra of (a) unmodified AC, (b) 180-AC.

6.3.2 Equilibrium adsorption

Fig. 6.7A shows the equilibrium adsorption of creatinine onto the four AC samples with different concentrations. With the increasing initial concentration of creatinine, the equilibrium adsorption capacity for creatinine increased gradually until the equilibrium

condition is reached [168], showing the favourable adsorption of creatinine on AC samples at higher concentrations. It indicates that the AC-180 has the highest adsorption capacity among these four adsorbents. To compare the saturation adsorption capacity, we also investigated the saturation adsorption for ACs. As is shown in Fig. 6.7B, the creatinine adsorbed by the ACs was increasing until the creatinine solution volume increased to 80 ml. The 180-AC got the highest amount of creatinine adsorption at equilibrium (64.5 mg g^{-1}), which is 0.29 times more than the unmodified AC (50.0 mg g^{-1}).It indicates the modification greatly enhanced the creatinine adsorption capacity.

A

B
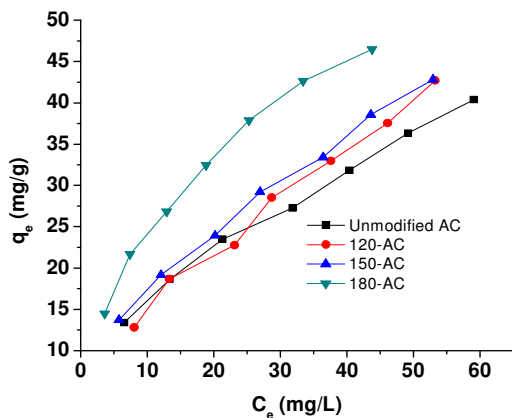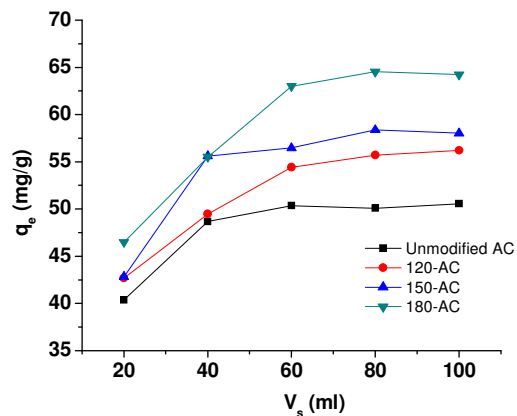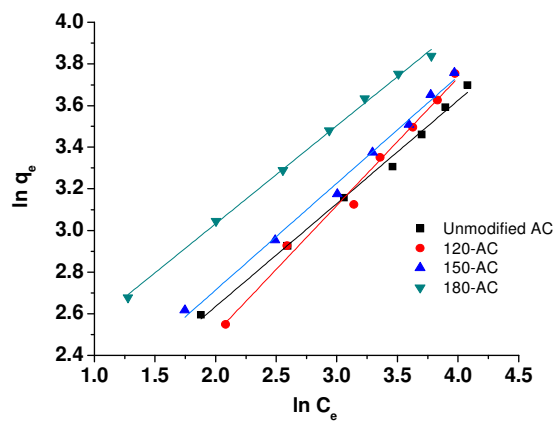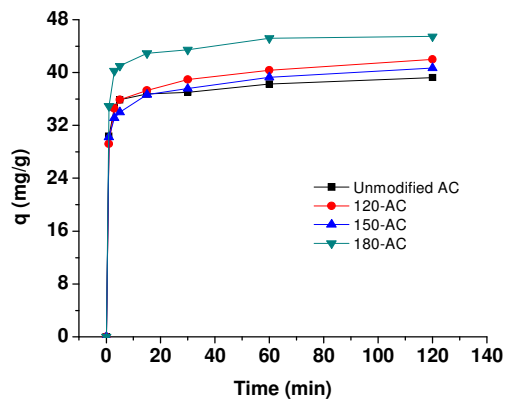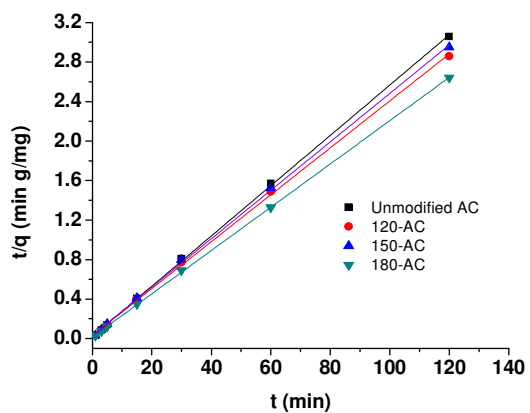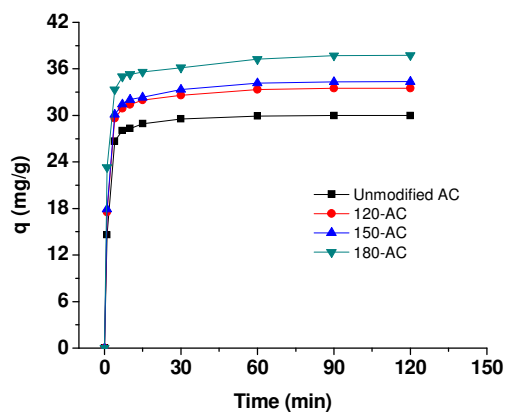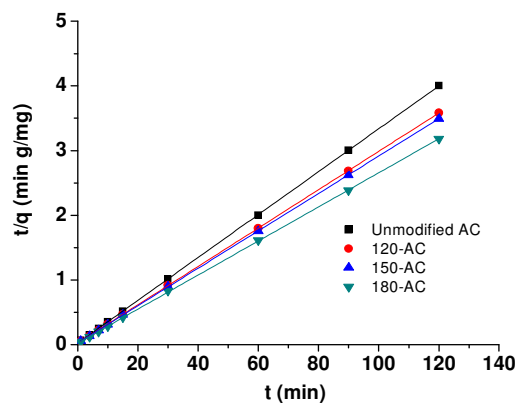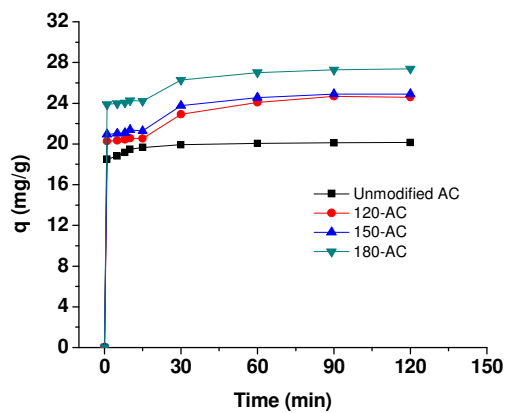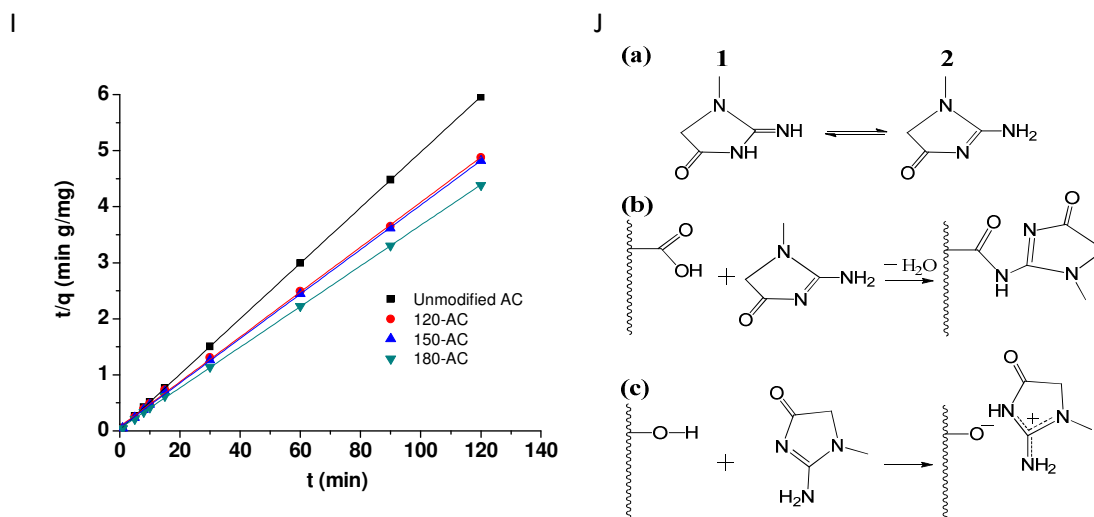
Fig. 6. 7. (A) Equilibrium adsorptions of creatinine onto AC samples; (B) Saturation adsorption capacities of creatinine at 160 mg L^{-1}; (C) Freundlich plots for AC samples. Adsorption kinetics of different initial creatinine concentrations: (D) 160 mg L^{-1}; (F) 120 mg L^{-1}; (H) 80 mg L^{-1}. Plots of pseudo second-order model of different initial creatinine concentrations: (E) 160 mg L^{-1}; (G) 120 mg L^{-1}; (I) 80 mg L^{-1}. (J) Tautomers of creatinine and possible reactions between HNO$_3$-modified AC and creatinine.

6.3.2.1 Langmuir isotherm

A linearized plot of C_e/q_e versus q_e was obtained from the model shown in Fig. 6.8. Q and b is computed from the slops and intercepts of different straight lines representing different AC samples. Table 6.4 lists the calculated results. It indicates that the computed maximum monolayer capacity Q of creatinine onto unmodified AC, 120-AC, 150-AC

and 180-AC are 55.6, 71.4, 62.5 and 62.5 mg g^{-1}, respectively. However, the fits are not quite well for the AC samples under the creatinine concentration ranges studied, and correlation coefficients of unmodified AC, 120-AC, 150-AC and 180-AC are 0.9422, 0.9070, 0.9335 and 0.9830, respectively. It indicates that the adsorption of creatinine was not typical monolayer [169].
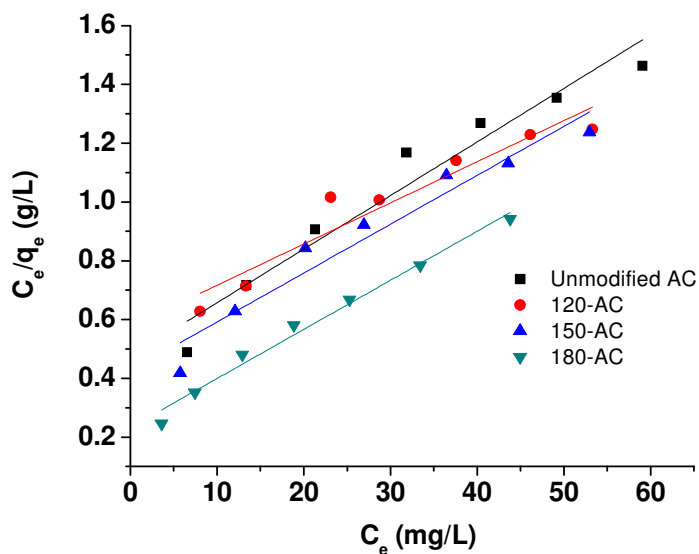
Fig. 6. 8. Langmuir plot for AC samples.

Table 6. 4 The parameters of Langmuir adsorption isotherm model and the Freundlich adsorption isotherm model.

Samples	Langmuir			Freundlich		
	R^2	Q (mg g^{-1})	b (L mg^{-1})	R^2	n	k_f (mg/g) (dm^3/mg)$^{1/n}$
Unmodified AC	0.9422	55.6	0.0379	0.9936	2.02	5.18
120-AC	0.9070	71.4	0.0243	0.9870	1.63	3.59
150-AC	0.9335	62.5	0.0376	0.9919	1.95	5.41
180-AC	0.9830	62.5	0.0690	0.9977	2.12	8.09

6.3.2.2. Freundlich isotherm

The values of the Freundlich adsorption isotherm constant n were 2.02, 1.63, 1.95 and 2.12 for the unmodified AC, 120-AC, 150-AC and 180-AC, respectively (Table 6.4). All the values were within 1-10, indicating that the adsorption for creatinine by these adsorbents were favorable [170, 171]. As a result, the Freundich adsorption model, which was considered to be the uneven adsorption mainly via monolayer chemical adsorption and a small amount of physical adsorption on the surface of the adsorbent, could be applied in the adsorption process for creatinine.

6.3.3 Kinetics of adsorption

Fig. 6.7D, F and H show the adsorption kinetics of creatinine onto AC samples at initial concentrations 160, 120 and 80 mg L^{-1} at 37 °C. It shows that adsorption was quick

in the first 15 min and the equilibrium was reached within 2 h for 160 mg L^{-1}. While it takes 90 and 60 min to reach the equilibrium at initial creatinine concentrations 120 and 80 mg L^{-1}, respectively. At initial concentration 160 mg L^{-1}, the adsorption capacity q_e at equilibrium is 40.3, 42.6, 42.8 and 46.5 mg g^{-1} for unmodified AC, 120-AC, 150-AC and 180-AC, respectively. It indicates that the adsorption capacity increased after nitric acid hydrothermal modification [160], which might due to the oxygen-containing functional groups such as strong carboxylic acids (-COOH), phenols (-OH) and carbonyls/quinones (=O) generated by oxidation [163]. Similar to the trends for initial concentration at 120 and 80 mg L^{-1}, AC modified by 4 M nitric acid with 180 °C obtained the fastest adsorption speed and highest adsorption capacity for creatinine.

6.3.4 Rate constant

As is shown in Fig. 6.9, log (q_e-q) versus t shows a poor agreement of experimental data with a first-order kinetic model with different initial creatinine concentrations (80, 120 and 160 mg L^{-1}). This suggests the adsorption of creatinine onto AC sample is not a first-order reaction.

A
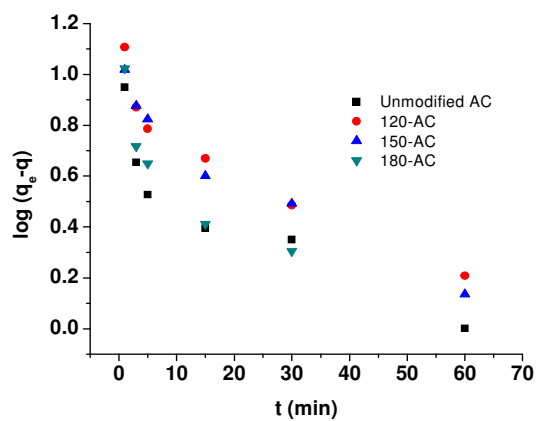
B
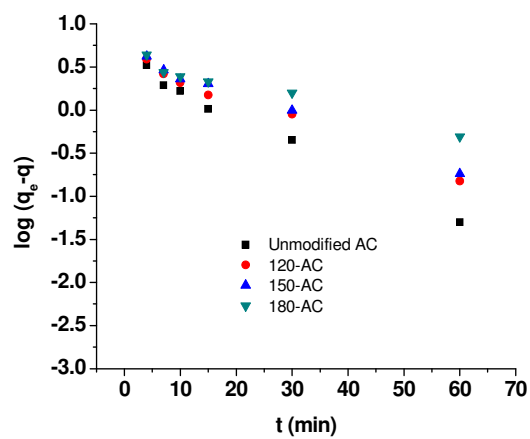
C
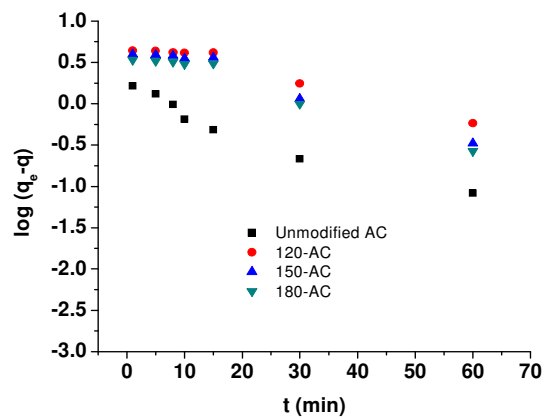
Fig. 6. 9. Plot of pseudo first-order model for AC samples. Initial creatinine

concentration: (A) 160 mg/L; (B) 120 mg/L; (C) 80 mg/L.

It can be seen from Fig. 6.7E, G and I that the plots of t/q versus t show a linear

relationship for each AC sample. The slops and intercepts of plots of t/q versus t were

used to calculate the second-order rate constant k_2 and q_e. The straight lines in plot of t/q

versus t (Fig. 6.7E, G and I) show a good agreement of experimental data with second-

order kinetic model for different AC samples with different initial creatinine

concentrations. Tables 6.5-7 list the calculated results obtained from the second-order

kinetic model. The correlation coefficients for the second-order kinetic model, which are

also presented in Tables 6.5-7, are higher than 0.99 for all the cases. These suggest that

the adsorption of creatinine onto AC samples follows the second-order kinetic model and

chemical adsorption might be the rate-limiting step [169]. Table 6.8 compares the

adsorption capacity of different types of adsorbents used for removal of creatinine [142,

143, 146]. It can be seen the AC-180 has higher adsorption ability than that of most

adsorbents reported in other literatures.

Table 6. 5 The parameters of second-order adsorption rate constants and calculated qe
for different AC samples at initial concentration (160 mg/L).

Samples	Second-order kinetic model		
	k_2(g mg^{-1} min^{-1})	$q_{e,cal}$ (mg g^{-1})	R^2
Unmodified AC	2.976E-2	40.0	0.9997
120-AC	1.707E-2	43.5	0.9990
150-AC	1.858E-2	41.7	0.9995
180-AC	2.940E-2	47.6	0.9990

Table 6. 6 The parameters of second-order adsorption rate constants and calculated qe for different AC samples at initial concentration (120 mg/L).

Samples	Second-order kinetic model		
	k_2(g mg^{-1} min^{-1})	$q_{e,cal}$ (mg g^{-1})	R^2
Unmodified AC	20.08	30.2	0.9999
120-AC	25.79	33.8	0.9999
150-AC	29.09	34.6	0.9999
180-AC	31.51	38.0	0.9999

Table 6. 7 The parameters of second-order adsorption rate constants and calculated q_e for different AC samples at initial concentration (80 mg/L).

Samples	Second-order kinetic model		
	k_2(g mg^{-1} min^{-1})	$q_{e,cal}$ (mg g^{-1})	R^2
Unmodified AC	6.83	20.2	0.9999
120-AC	45.20	25.0	0.9994
150-AC	37.08	25.2	0.9997
180-AC	31.66	27.6	0.9998

Table 6. 8 Adsorption capacities for the adsorption of creatinine onto various adsorbents.

Adsorbent	Adsorption capacity (mg g^{-1})	Reference
AC-180	64.5	This work
Poly(ether sulfone)/activated carbon	28.0	[142]
Zeolite	37.0	[143]
Carbon nanotube	24.0	[146]
Active carbon	26.0	[146]

Creatinine is one of the uraemic toxins in the blood, which is low molecular weight toxin. Some other middle molecular toxins could also be adsorbed by the active carbon

during the adsorption. By comparing the adsorption capacities for the adsorption of

creatinine onto various adsorbents such as carbon nanotube, zeolite, poly(ether

sulfone)/activated carbon, it indicates that the surface functioned active carbon obtained

by nitric acid hydrothermal modification get the highest adsorption capacity. Although

the adsorption by AC is non-selective, it can potentially be employed to clinic application

due to low cost without introducing any other substances into the blood [146].

Meanwhile, carbon filter and ion-exchange resin have been used to regenerate the

adsorbent after dialysis [172]. Therefore, we are trying to develop new surface functioned

AC adsorbents, and looking forward to collaborate with Sanford Healthcare to develop

some real tests with clinic dialysis liquid samples, and consider competition from other

biomolecules. In addition, one crucial factor impacting adsorption of creation by AC is

the depletion of adsorption sites [173], competition and pore blockage during active

carbon adsorption hampers the adsorption efficiency [174]. More work is needed to better

understand how to optimize the adsorption of creatinine and other toxins in the blood.

6.3.5 Mechanism of creatinine adsorption onto nitric acid modified AC

There are two possible tautomers of creatinine, the imine 1 and amine 2 forms [175],

as is shown in Fig. 6.7Ja. The amine 2 predominates in solution [176]. After HNO_3

oxidation, some carboxylic acid groups were generated by the treatment as discussed

above. Therefore, the amine (creatinine) and carboxylic acid reacted and formed covalent

bond (Fig. 6.7Jb), the water produced and an amide was formed. This reaction enhanced

the creatinine adsorption quantity by using the HNO_3-modified ACs as sorbents. A hydrogen ion can break away from the phenolic group on the surface of the modified AC. The creatinine molecule combined with the hydrogen ion and was protonated [144, 177], which would be "adsorbed" by the negatively charged site from the previous phenolic group. This mechanism is shown in Fig. 6.7Jc, which indicates the pyridine-N-oxide structure was formed. The N1 spectra of AC-180 and creatinine-adsorbed AC-180 verified these formations.

Fig. 6.10 shows the deconvoluted N 1s spectra of 180-AC and creatinine adsorbed 180-AC. The N 1s spectra of these samples can be deconvoluted into different peaks centered at 399.7 (N1 component), 400.6 (N2 component), 401.4 (N3 component), 403.0 (N4 component), and 406.5 eV (N5 component). According to the literature review, pyridinic-type nitrogen gives rise to a peak about 398.6 eV [178], the binding energy of nitrogen in amides can be at about 399.7 eV [179, 180]. Nitrogen in pyrrole and lactam groups was found to be at 400.3 [181] and 400.1 eV [182], respectively. The contribution at 401.5 eV has been assigned to various forms of quaternary nitrogen atoms [183]. Furthermore, the peak at 402-405 eV was identified to arise from pyridine-N-oxide[184]. The higher binding energy around 406.5 eV can be attributed to N 1s of $-NO_2$ [185]. Based on these literature reports, the N1 peak can be assigned to amide, and N2 peak to lactam and pyrrole groups. The N3 component can be assigned to highly coordinated nitrogen atoms bound to three C atoms in the bulk of a graphene layer and the N4 peak to the pyridine-N-oxide, which gives a peak above 402.0 eV [186]. Finally, the N5 peak can

be NO_2 group on the modified AC. As is shown in Table 6.9, the total nitrogen

concentration was increased from 0.74 to 2.58 % after adsorption. To assess the amount

of different types of N-species, the relative percentage of different N-groups was

calculated based on the deconvoluted N 1s spectra (Table 6.9). AC-180 shows two peaks:

a low binding energy component (N3) centered at 401.4 eV and a higher binding energy

component (N5) centered at 406.5 eV. In case of creatinine adsorbed 180-AC, three other

peaks (N1, N2 and N4) appeared. It indicates that nitrogen component N1 increased

0.91%, which agrees with the amide formed in Fig. 6.7Jb. The N2 species and the

increased amount of N3 species of creatinine adsorbed 180-AC, which may come from

the creatinine itself. N4-type-nitrogen species (0.15%) was from the pyridine-N-oxide

formed according to the combination shown in Fig. 6.7Jc. While the N5 component

remained the same after the adsorption since there was no reaction to the $-NO_2$ group

during the adsorption. The carboxyl and phenolic groups generated by HNO_3 oxidation

combined with the creatinine molecules, therefore, the creatinine adsorption capacity

increased after HNO_3 treatment.
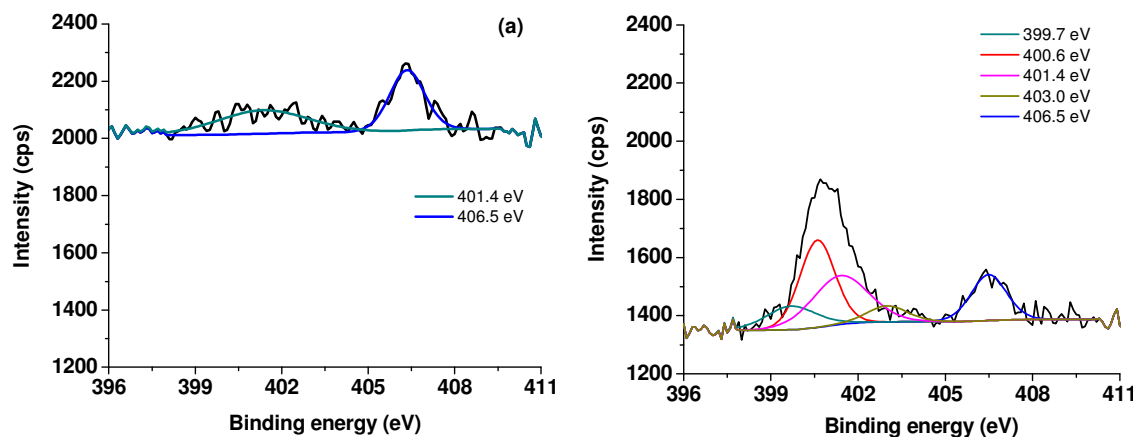
Fig. 6. 10. N 1s XPS spectra of (a) 180-AC, (b) creatinine adsorbed 180-AC.

Table 6. 9 Surface nitrogen composition of AC-180 and creatinine adsorbed 180-AC derived from XPS.

Sample	N%					
	N total	N1	N2	N3	N4	N5
180-AC	0.74	—	—	0.33	—	0.41
Creatinine adsorbed 180-AC	2.58	0.91	0.70	0.57	0.15	0.41

6.4 Conclusions

After 4M HNO_3 hydrothermal modification at 180 °C, the total surface oxygen content was increased 2.69 times. Although the BET surface area was decreased by 26 m^2 g^{-1}, the creatinine saturation adsorption capacity in 180-AC was 29% higher than the unmodified AC. The improvement of the adsorptive performance by the HNO_3 oxidation modification is dominantly through an increase of the oxygen-containing functional groups on the AC surface. N 1s XPS results indicate carboxyl and phenolic groups

generated by HNO_3 oxidation can potentially "adsorb" (reacted with) creatinine. Freundlich model and second-order kinetic model fitted very well to the equilibrium isotherm and the dynamical behavior for the adsorption of creatinine onto the HNO_3-modified ACs. These suggested that the rate-limiting step might be chemical adsorption but not mass transfer.

Chapter 7 General conclusions and recommendations for future work

The functional groups on activated carbon are very important for adsorption in both gas and aqueous phases. Functional groups generated by oxidation could interact with the butanol and creatinine. The hydrophilicity of the activated carbon was increased via hydrothermal modification by using hydrogen peroxide and nitric acid. However, the adsorption capacity of butanol vapor was decreased after modification of activated carbon. High BET surface area activated carbon was prepared from corn stalk, which shows high butanol vapor adsorption capacity. These results will provide some guidelines for the design of the separation process, selection and preparation of absorbent, which can be used in pilot or large scale butanol recovery. While the oxygen-containing functional groups from oxidation could react with the creatinine, which greatly decreased the concentration. Based on the research works which have been done, the following conclusions can be obtained:

1. In the present work, active carbons and ZSM-5 zeolite were employed to absorb the butanol vapor produced by gas stripping. It gives ideas for recovering butanol from fermentation. In order to investigate the adsorption behavior of active carbons with different surface functional groups, different concentrations of hydrogen peroxide were used to modify the original active carbon by hydrothermal reaction. It indicates that the active carbons have almost three times adsorption capacity higher than the ZSM-5. In addition, the butanol desorption is completed by heating to 150 ℃ after adsorption. It means that the active carbon can be potentially used for butanol recovery during gas stripping process. Moreover, hydrogen peroxide hydrothermal modification can increase

the BET surface area, oxygen functional groups and pore volume of the active carbon. However, these modifications decreased the adsorption capacity of the active carbons. This result demonstrates that adsorption heavily depends on the surface properties of carbon adsorbents, e.g. the interactions between the surface functional groups and butanol.

2. Active carbons modified by nitric acid were employed to adsorb the butanol vapor produced by gas stripping. It gives ideas for recovering butanol from fermentation. In order to investigate the adsorption behavior of active carbons with different surface functional groups, different concentrations of nitric acid were used to modify the original active carbon by hydrothermal reaction. It indicates that hydrothermal modification with 4 mol/L nitric acid increased BET surface area by 329 m^2 g^{-1}, micropore volume by 0.10 cm^3 g^{-1}, and mesopore volume by 0.12 cm^3 g^{-1}. However, these modifications decreased the adsorption capacity of the active carbons. This result demonstrates that adsorption heavily depends on the surface properties of carbon adsorbents, e.g. the interactions between the surface functional groups and butanol. In addition, the butanol desorption was completed by heating to 150 ℃ after adsorption. It means that the active carbon can be potentially used for butanol recovery during gas stripping process. These results will provide some guidelines for the design of the separation process and selection of absorbent, which can be used in pilot or large scale butanol recovery.

3. Active carbons were prepared from waste biomass-corn stalk and employed to adsorb the butanol vapor produced by gas stripping. It gives ideas for recovering butanol from fermentation. Active carbon with high surface area (2330 m^2 g^{-1}) was prepared from the whole corn stalk, which shows pretty high adsorption capacity (410.0 mg g^{-1}) for butanol vapor. It indicates that the active carbons (prepared from the whole corn stalk at 900 ℃) have 2.85 times adsorption capacity higher than the commercial active carbon from charcoal. It can be employed as low-cost adsorbent and considered as an alternative one to commercial AC. The adsorption capacity can be maintained at 94% for five cycles. There was a good correlation between the amount of butanol vapor adsorbed and pore volumes (<50 nm). It can be concluded that butanol adsorption was mainly governed by the pores smaller than 50 nm of the adsorbents.

4. In order to investigate the adsorption behavior of ACs with different surface functional groups, different reaction temperatures were used to modify the original AC by hydrothermal reaction. It indicates that hydrothermal modification with 180 °C was an efficient method in improvement of the adsorption performance of the AC for creatinine. The improved adsorption capacity can be attributed mainly to an increase in the acidic oxygen-containing functional groups. The adsorption of creatinine over AC may involve an interaction with the acidic oxygen-containing groups on AC. Langmuir and Freundlich adsorption models were applied to describe the experimental isotherm and isotherm constants. Equilibrium data fitted very well to the Freundlich model in the entire saturation range. Pseudo first-order and second-order kinetic models were used to

describe the kinetic data and the rate constants were evaluated. The experimental data fitted well to the second-order kinetic model, which indicates that the chemical adsorption is the rate-limiting step, instead of mass transfer.

We did a lot of oxidation of activated carbon via hydrogen peroxide and nitric acid modification. Plasma could also be used to modify the surface chemistry of the activated carbons. Different protection gases could be used for the plasma treatment, such as nitrogen, helium, methane, and oxygen, which could potentially generate oxygen-containing functional groups or decrease the hydrophilicity. Potassium hydroxide could be employed to treat the activated carbon, which could potentially generate more basic functional groups. It has been approved that hydrothermal modification could create a lot of functional groups on the activated carbon surface. Therefore, these modified activated carbon might have very strong adsorption capacity for heavy metal or organic pollutant from water.

A recommendation for future work for activated carbon preparation should focus on using different biomass as precursor, and use salts (potassium chloride or sodium chloride) as template to form porous structure, then the activation could be done to the porous biochar, which will generate high BET surface area carbons.

References

[1] W. Liao, R. Heijungs, G. Huppes, Natural resource demand of global biofuels in the Anthropocene: A review, Renewable and Sustainable Energy Reviews, 16 (2012) 996-1003.

[2] C. Xue, X.Q. Zhao, C.G. Liu, L.J. Chen, F.W. Bai, Prospective and development of butanol as an advanced biofuel, Biotechnology advances, 31 (2013) 1575-1584.

[3] M.O.S. Dias, L.G. Pereira, T.L. Junqueira, L.G. Pavanello, M.F. Chagas, O. Cavalett, R. Maciel Filho, A. Bonomi, Butanol production in a sugarcane biorefinery using ethanol as feedstock. Part I: Integration to a first generation sugarcane distillery, Chemical Engineering Research and Design, 92 (2014) 1441-1451.

[4] Z. Zhang, T. Wang, M. Jia, Q. Wei, X. Meng, G. Shu, Combustion and particle number emissions of a direct injection spark ignition engine operating on ethanol/gasoline and n-butanol/gasoline blends with exhaust gas recirculation, Fuel, 130 (2014) 177-188.

[5] S.S. Merola, G. Valentino, C. Tornatore, L. Marchitto, In-cylinder spectroscopic measurements of knocking combustion in a SI engine fuelled with butanol–gasoline blend, Energy, 62 (2013) 150-161.

[6] T. Venugopal, A. Ramesh, Experimental studies on the effect of injection timing in a SI engine using dual injection of n-butanol and gasoline in the intake port, Fuel, 115 (2014) 295-305.

[7] W. Jiang, J. Zhao, Z. Wang, S.T. Yang, Stable high-titer n-butanol production from sucrose and sugarcane juice by Clostridium acetobutylicum JB200 in repeated batch fermentations, Bioresource technology, 163 (2014) 172-179.

[8] H.T.M. Tran, B. Cheirsilp, B. Hodgson, K. Umsakul, Potential use of Bacillus subtilis in a co-culture with Clostridium butylicum for acetone–butanol–ethanol production from cassava starch, Biochemical Engineering Journal, 48 (2010) 260-267.

[9] A.S. Afschar, K. Schaller, Production of acetone and butanol from starch by continuous bioprocess, Journal of biotechnology, 18 (1991) 255-264.

[10] R. Marchal, M. Ropars, J. Pourquié, F. Fayolle, J.P. Vandecasteele, Large-scale enzymatic hydrolysis of agricultural lignocellulosic biomass. Part 2: Conversion into acetone-butanol, Bioresource technology, 42 (1992) 205-217.

[11] C. Moon, C.H. Lee, B.I. Sang, Y. Um, Optimization of medium compositions favoring butanol and 1,3-propanediol production from glycerol by Clostridium pasteurianum, Bioresource technology, 102 (2011) 10561-10568.

[12] J.T. Ellis, N.N. Hengge, R.C. Sims, C.D. Miller, Acetone, butanol, and ethanol production from wastewater algae, Bioresource technology, 111 (2012) 491-495.

[13] C.R. Shen, E.I. Lan, Y. Dekishima, A. Baez, K.M. Cho, J.C. Liao, Driving forces enable high-titer anaerobic 1-butanol synthesis in Escherichia coli, Applied and environmental microbiology, 77 (2011) 2905-2915.

[14] P. Dürre, New insights and novel developments in clostridial acetone/butanol/isopropanol fermentation, Applied microbiology and biotechnology, 49 (1998) 639-648.

[15] L.T.P. Trinh, Y.J. Lee, H.-J. Bae, H.-J. Lee, Pervaporative separation of butanol using

a composite PDMS/PEI hollow fiber membrane, Journal of Industrial and Engineering Chemistry, 20 (2014) 2814-2818.

[16] A. Oudshoorn, L.A.M. van der Wielen, A.J.J. Straathof, Assessment of Options for Selective 1-Butanol Recovery from Aqueous Solution, Industrial & Engineering Chemistry Research, 48 (2009) 7325-7336.

[17] A. Oudshoorn, L.A.M. van der Wielen, A.J.J. Straathof, Desorption of butanol from zeolite material, Biochemical Engineering Journal, 67 (2012) 167-172.

[18] A.P. Mariano, M.J. Keshtkar, D.I.P. Atala, F. Maugeri Filho, M.R. Wolf Maciel, R. Maciel Filho, P. Stuart, Energy Requirements for Butanol Recovery Using the Flash Fermentation Technology, Energy & Fuels, 25 (2011) 2347-2355.

[19] H. Janssen, C. Grimmler, A. Ehrenreich, H. Bahl, R.-J. Fischer, A transcriptional study of acidogenic chemostat cells of Clostridium acetobutylicum—Solvent stress caused by a transient n-butanol pulse, Journal of biotechnology, 161 (2012) 354-365.

[20] D.R. Nielsen, K.J. Prather, In situ product recovery of n-butanol using polymeric resins, Biotechnology and bioengineering, 102 (2009) 811-821.

[21] S.H. Ha, N.L. Mai, Y.-M. Koo, Butanol recovery from aqueous solution into ionic liquids by liquid–liquid extraction, Process Biochemistry, 45 (2010) 1899-1903.

[22] I.L. Borisov, A.O. Malakhov, V.S. Khotimsky, E.G. Litvinova, E.S. Finkelshtein, N.V. Ushakov, V.V. Volkov, Novel PTMSP-based membranes containing elastomeric fillers: Enhanced 1-butanol/water pervaporation selectivity and permeability, Journal of Membrane Science, 466 (2014) 322-330.

[23] T. de Vrije, M. Budde, H. van der Wal, P.A. Claassen, A.M. Lopez-Contreras, "In situ" removal of isopropanol, butanol and ethanol from fermentation broth by gas stripping, Bioresource technology, 137 (2013) 153-159.

[24] A.G. Fadeev, Y.A. Selinskaya, S.S. Kelley, M.M. Meagher, E.G. Litvinova, V.S. Khotimsky, V.V. Volkov, Extraction of butanol from aqueous solutions by pervaporation through poly(1-trimethylsilyl-1-propyne), Journal of Membrane Science, 186 (2001) 205-217.

[25] C. Xue, J. Zhao, F. Liu, C. Lu, S.T. Yang, F.W. Bai, Two-stage in situ gas stripping for enhanced butanol fermentation and energy-saving product recovery, Bioresource technology, 135 (2013) 396-402.

[26] N. Qureshi, H.P. Blaschek, Recovery of butanol from fermentation broth by gas stripping, Renewable Energy, 22 (2001) 557-564.

[27] J. Li, Z. Li, B. Liu, Q. Xia, H. Xi, Effect of Relative Humidity on Adsorption of Formaldehyde on Modified Activated Carbons, Chinese Journal of Chemical Engineering, 16 (2008) 871-875.

[28] A. Anfruns, M.J. Martin, M.A. Montes-Morán, Removal of odourous VOCs using sludge-based adsorbents, Chemical Engineering Journal, 166 (2011) 1022-1031.

[29] F. Gironi, V. Piemonte, VOCs removal from dilute vapour streams by adsorption onto activated carbon, Chemical Engineering Journal, 172 (2011) 671-677.

[30] Y.J. Tham, P.A. Latif, A.M. Abdullah, A. Shamala-Devi, Y.H. Taufiq-Yap, Performances of toluene removal by activated carbon derived from durian shell, Bioresource technology, 102 (2011) 724-728.

[31] A. Martínez de Yuso, M.T. Izquierdo, R. Valenciano, B. Rubio, Toluene and n-hexane adsorption and recovery behavior on activated carbons derived from almond shell wastes, Fuel Processing Technology, 110 (2013) 1-7.

[32] R.R. Gil, B. Ruiz, M.S. Lozano, M.J. Martín, E. Fuente, VOCs removal by adsorption onto activated carbons from biocollagenic wastes of vegetable tanning, Chemical Engineering Journal, 245 (2014) 80-88.

[33] C. Yin, M. Aroua, W. Daud, Review of modifications of activated carbon for enhancing contaminant uptakes from aqueous solutions, Separation and Purification Technology, 52 (2007) 403-415.

[34] N. Qureshi, H. Blaschek, Recovery of butanol from fermentation broth by gas stripping, Renewable Energy, 22 (2001) 557-564.

[35] W. Groot, R. Van der Lans, K.C.A. Luyben, Technologies for butanol recovery integrated with fermentations, Process Biochemistry, 27 (1992) 61-75.

[36] W. Groot, R. Lans, K.C.A. Luyben, Batch and continuous butanol fermentations with free cells: integration with product recovery by gas-stripping, Applied microbiology and biotechnology, 32 (1989) 305-308.

[37] K. Pi, M. Xia, P. Wu, M. Yang, S. Chen, D. Liu, A.R. Gerson, Effect of oxidative modification of activated carbon for the adsorption behavior of nicotine, Journal of Industrial and Engineering Chemistry, 31 (2015) 112-117.

[38] R.T. Yang, Adsorbents: fundamentals and applications, John Wiley & Sons, 2003.

[39] M.M. Maroto-Valer, I. Dranca, T. Lupascu, R. Nastas, Effect of adsorbate polarity on thermodesorption profiles from oxidized and metal-impregnated activated carbons, Carbon, 42 (2004) 2655-2659.

[40] A. Aburub, D.E. Wurster, Phenobarbital interactions with derivatized activated carbon surfaces, Journal of colloid and interface science, 296 (2006) 79-85.

[41] R.R.A. Rios, D.E. Alves, I. Dalmázio, S.F.V. Bento, C.L. Donnici, R.M. Lago, Tailoring activated carbon by surface chemical modification with O, S, and N containing molecules, Materials Research, 6 (2003) 129-135.

[42] J. Jaramillo, P.M. Álvarez, V. Gómez-Serrano, Oxidation of activated carbon by dry and wet methods, Fuel Processing Technology, 91 (2010) 1768-1775.

[43] M.F.R. Pereira, S.F. Soares, J.J. Órfão, J.L. Figueiredo, Adsorption of dyes on activated carbons: influence of surface chemical groups, Carbon, 41 (2003) 811-821.

[44] X. Song, H. Liu, L. Cheng, Y. Qu, Surface modification of coconut-based activated carbon by liquid-phase oxidation and its effects on lead ion adsorption, Desalination, 255 (2010) 78-83.

[45] B. Salas-Enríquez, A. Torres-Huerta, E. Conde-Barajas, M. Domínguez-Crespo, L. Díaz-García, M.d.l.L.X. Negrete, Activated carbon production from the Guadua amplexifolia using a combination of physical and chemical activation, Journal of Thermal Analysis and Calorimetry, 124 (2016) 1383-1398.

[46] I.I.G. Inal, S.M. Holmes, A. Banford, Z. Aktas, The performance of supercapacitor electrodes developed from chemically activated carbon produced from waste tea, Applied Surface Science, 357 (2015) 696-703.

[47] X. Li, W. Xing, S. Zhuo, J. Zhou, F. Li, S.Z. Qiao, G.Q. Lu, Preparation of

capacitor's electrode from sunflower seed shell, Bioresource technology, 102 (2011) 1118-1123.

[48] G. Ma, Q. Yang, K. Sun, H. Peng, F. Ran, X. Zhao, Z. Lei, Nitrogen-doped porous carbon derived from biomass waste for high-performance supercapacitor, Bioresource technology, 197 (2015) 137-142.

[49] Y. Fan, X. Yang, B. Zhu, P.-F. Liu, H.-T. Lu, Micro-mesoporous carbon spheres derived from carrageenan as electrode material for supercapacitors, Journal of Power Sources, 268 (2014) 584-590.

[50] X. He, P. Ling, J. Qiu, M. Yu, X. Zhang, C. Yu, M. Zheng, Efficient preparation of biomass-based mesoporous carbons for supercapacitors with both high energy density and high power density, Journal of Power Sources, 240 (2013) 109-113.

[51] Y. Lv, L. Gan, M. Liu, W. Xiong, Z. Xu, D. Zhu, D.S. Wright, A self-template synthesis of hierarchical porous carbon foams based on banana peel for supercapacitor electrodes, Journal of Power Sources, 209 (2012) 152-157.

[52] C. Zhong, S. Gong, L.e. Jin, P. Li, Q. Cao, Preparation of nitrogen-doped pitch-based carbon materials for supercapacitors, Materials Letters, 156 (2015) 1-6.

[53] S. Boufi, A. Chaker, Easy production of cellulose nanofibrils from corn stalk by a conventional high speed blender, Industrial Crops and Products, 93 (2016) 39-47.

[54] K.L. Kadam, J.D. McMillan, Availability of corn stover as a sustainable feedstock for bioethanol production, Bioresource technology, 88 (2003) 17-25.

[55] M.E. Walsh, R.L. Perlack, A. Turhollow, D. de la Torre Ugarte, D.A. Becker, R.L. Graham, S.E. Slinsky, D.E. Ray, Biomass feedstock availability in the United States: 1999 state level analysis, Bioenergy Information Network, Bioenergy Feedstock Development Program, Oak Ridge National Laboratory, (2000).

[56] J.-S. Lv, X.-Y. Liu, J.-X. Xu, Y.-F. Deng, Z. Wu, Y.-M. Wang, M.-Y. Fan, H. Xu, Preparation and properties of adsorption material from corn stalks core when used for enzyme immobilization and the subsequent activities of the adsorbed enzymes, Industrial Crops and Products, 50 (2013) 787-796.

[57] J. Sreńscek-Nazzal, W. Kamińska, B. Michalkiewicz, Z.C. Koren, Production, characterization and methane storage potential of KOH-activated carbon from sugarcane molasses, Industrial Crops and Products, 47 (2013) 153-159.

[58] J. Coresh, E. Selvin, L.A. Stevens, J. Manzi, J.W. Kusek, P. Eggers, F. Van Lente, A.S. Levey, Prevalence of chronic kidney disease in the United States, Jama, 298 (2007) 2038-2047.

[59] H. Abe, M. Otsuka, Comparison of physico-chemical characteristics among three pharmaceutical spherical carbon adsorbents, Colloids and Surfaces B: Biointerfaces, 100 (2012) 90-94.

[60] M.J. Berg, W.G. Berlinger, M.J. Goldberg, R. Spector, G.F. Johnson, Acceleration of the body clearance of phenobarbital by oral activated charcoal, New England Journal of Medicine, 307 (1982) 642-644.

[61] B. Lisowska-Myjak, Uremic toxins and their effects on multiple organ systems, Nephron Clinical Practice, 128 (2014) 303-311.

[62] N. Abdehagh, F.H. Tezel, J. Thibault, Separation techniques in butanol production: Challenges and developments, Biomass and Bioenergy, 60 (2014) 222-246.

[63] V. Saravanan, D.A. Waijers, M. Ziari, M.A. Noordermeer, Recovery of 1-butanol from aqueous solutions using zeolite ZSM-5 with a high Si/Al ratio; suitability of a column process for industrial applications, Biochemical Engineering Journal, 49 (2010) 33-39.

[64] Q.L. Zhuang, T. Kyotani, A. Tomita, The change of TPD pattern of O2-gasified carbon upon air exposure, Carbon, 32 (1994) 539-540.

[65] U. Zielke, K.J. Hüttinger, W.P. Hoffman, Surface-oxidized carbon fibers: I. Surface structure and chemistry, Carbon, 34 (1996) 983-998.

[66] B. Marchon, J. Carrazza, H. Heinemann, G.A. Somorjai, TPD and XPS studies of O2, CO2, and H2O adsorption on clean polycrystalline graphite, Carbon, 26 (1988) 507-514.

[67] J.L. Figueiredo, M.F.R. Pereira, M.M.A. Freitas, J.J.M. Órfão, Modification of the surface chemistry of activated carbons, Carbon, 37 (1999) 1379-1389.

[68] M. Ruta, N. Semagina, L. Kiwi-Minsker, Monodispersed Pd Nanoparticles for Acetylene Selective Hydrogenation: Particle Size and Support Effects, The Journal of Physical Chemistry C, 112 (2008) 13635-13641.

[69] P. Tribolet, L. Kiwi-Minsker, Palladium on carbon nanofibers grown on metallic filters as novel structured catalyst, Catalysis Today, 105 (2005) 337-343.

[70] L.A. Langley, D.E. Villanueva, D.H. Fairbrother, Quantification of Surface Oxides on Carbonaceous Materials, Chemistry of Materials, 18 (2005) 169-178.

[71] P.C.C. Faria, J.J.M. Órfão, M.F.R. Pereira, Adsorption of anionic and cationic dyes on activated carbons with different surface chemistries, Water Research, 38 (2004) 2043-2052.

[72] V. Gómez-Serrano, M. Acedo-Ramos, A.J. López-Peinado, C. Valenzuela-Calahorro, Oxidation of activated carbon by hydrogen peroxide. Study of surface functional groups by FT-i.r, Fuel, 73 (1994) 387-395.

[73] P. Chingombe, B. Saha, R.J. Wakeman, Surface modification and characterisation of a coal-based activated carbon, Carbon, 43 (2005) 3132-3143.

[74] M.F.R. Pereira, S.F. Soares, J.J.M. Órfão, J.L. Figueiredo, Adsorption of dyes on activated carbons: influence of surface chemical groups, Carbon, 41 (2003) 811-821.

[75] T. Borjigin, F. Sun, J. Zhang, K. Cai, H. Ren, G. Zhu, A microporous metal-organic framework with high stability for GC separation of alcohols from water, Chemical communications, 48 (2012) 7613-7615.

[76] L. Lin, Z. Cunshan, S. Vittayapadung, S. Xiangqian, D. Mingdong, Opportunities and challenges for biodiesel fuel, Applied Energy, 88 (2011) 1020-1031.

[77] L. Lin, Z. Cunshan, S. Vittayapadung, S. Xiangqian, D. Mingdong, Opportunities and challenges for biodiesel fuel, Applied Energy, 88 (2011) 1020-1031.

[78] L.D. Gottumukkala, B. Parameswaran, S.K. Valappil, K. Mathiyazhakan, A. Pandey, R.K. Sukumaran, Biobutanol production from rice straw by a non acetone producing Clostridium sporogenes BE01, Bioresource technology, 145 (2013) 182-187.

[79] H.M. Kim, S.G. Wi, S. Jung, Y. Song, H.J. Bae, Efficient approach for bioethanol production from red seaweed Gelidium amansii, Bioresource technology, 175C

(2014) 128-134.

[80] S. Manickam, V.N.D. Arigela, P.R. Gogate, Intensification of synthesis of biodiesel from palm oil using multiple frequency ultrasonic flow cell, Fuel Process. Technol., 128 (2014) 388-393.

[81] X. Zhao, L. Wei, J. Julson, Z. Gu, Y. Cao, Catalytic cracking of inedible camelina oils to hydrocarbon fuels over bifunctional Zn/ZSM-5 catalysts, Korean J. Chem. Eng., 32 (2015) 1528-1541.

[82] C. Xue, X.Q. Zhao, C.G. Liu, L.J. Chen, F.W. Bai, Prospective and development of butanol as an advanced biofuel, Biotechnol. Adv., 31 (2013) 1575-1584.

[83] C. Bellido, M. Loureiro Pinto, M. Coca, G. Gonzalez-Benito, M.T. Garcia-Cubero, Acetone-butanol-ethanol (ABE) production by Clostridium beijerinckii from wheat straw hydrolysates: efficient use of penta and hexa carbohydrates, Bioresource technology, 167 (2014) 198-205.

[84] H.W. Yen, Y.C. Wang, The enhancement of butanol production by in situ butanol removal using biodiesel extraction in the fermentation of ABE (acetone-butanol-ethanol), Bioresource technology, 145 (2013) 224-228.

[85] M. Setlhaku, S. Heitmann, A. Gorak, R. Wichmann, Investigation of gas stripping and pervaporation for improved feasibility of two-stage butanol production process, Bioresour. Technol., 136 (2013) 102-108.

[86] K. Kraemer, A. Harwardt, R. Bronneberg, W. Marquardt, Separation of butanol from acetone–butanol–ethanol fermentation by a hybrid extraction–distillation process, Comput. Chem. Eng., 35 (2011) 949-963.

[87] A. Oudshoorn, L.A.M. van der Wielen, A.J.J. Straathof, Assessment of Options for Selective 1-Butanol Recovery from Aqueous Solution, Ind. Eng. Chem. Res., 48 (2009) 7325-7336.

[88] A. Plaza, G. Merlet, A. Hasanoglu, M. Isaacs, J. Sanchez, J. Romero, Separation of butanol from ABE mixtures by sweep gas pervaporation using a supported gelled ionic liquid membrane: Analysis of transport phenomena and selectivity, J. Membr. Sci., 444 (2013) 201-212.

[89] J. Kujawski, A. Rozicka, M. Bryjak, W. Kujawski, Pervaporative removal of acetone, butanol and ethanol from binary and multicomponent aqueous mixtures, Sep. Purif. Technol., 132 (2014) 422-429.

[90] A. Oudshoorn, L.A.M. van der Wielen, A.J.J. Straathof, Adsorption equilibria of bio-based butanol solutions using zeolite, Biochemical Engineering Journal, 48 (2009) 99-103.

[91] J. Cousin Saint Remi, G. Baron, J. Denayer, Adsorptive separations for the recovery and purification of biobutanol, Adsorption, 18 (2012) 367-373.

[92] J.C. Saint Remi, T. Remy, V. Van Hunskerken, S. van de Perre, T. Duerinck, M. Maes, D. De Vos, E. Gobechiya, C.E. Kirschhock, G.V. Baron, J.F. Denayer, Biobutanol separation with the metal-organic framework ZIF-8, ChemSusChem, 4 (2011) 1074-1077.

[93] S.H. Ha, N.L. Mai, Y.-M. Koo, Butanol recovery from aqueous solution into ionic liquids by liquid–liquid extraction, Process Biochem., 45 (2010) 1899-1903.

[94] Y.C. Liao, K.M. Lu, S.Y. Li, Process parameters for operating 1-butanol gas

stripping in a fermentor, J. Biosci. Bioeng., 118 (2014) 558-564.

[95] L. Luo, D. Ramirez, M.J. Rood, G. Grevillot, K.J. Hay, D.L. Thurston, Adsorption and electrothermal desorption of organic vapors using activated carbon adsorbents with novel morphologies, Carbon, 44 (2006) 2715-2723.

[96] A. Subrenat, P. Le Cloirec, Adsorption onto Activated Carbon Cloths and Electrothermal Regeneration: Its Potential Industrial Applications, J. Environ. Eng., 130 (2004) 249-257.

[97] C. Yin, M. Aroua, W. Daud, Review of modifications of activated carbon for enhancing contaminant uptakes from aqueous solutions, Sep. Purif. Technol., 52 (2007) 403-415.

[98] N. Soudani, S. Souissi-najar, A. Ouederni, Influence of Nitric Acid Concentration on Characteristics of Olive Stone Based Activated Carbon, Chin. J. Chem. Eng., 21 (2013) 1425-1430.

[99] Y. Cao, K. Wang, X. Wang, Z. Gu, W. Gibbons, H. Vu, Butanol vapor adsorption behavior on active carbons and zeolite crystal, Applied Surface Science, 349 (2015) 1-7.

[100] A.M.T. Silva, B.F. Machado, J.L. Figueiredo, J.L. Faria, Controlling the surface chemistry of carbon xerogels using HNO3-hydrothermal oxidation, Carbon, 47 (2009) 1670-1679.

[101] Q. Wang, X. Liang, W. Qiao, C. Liu, X. Liu, R. Zhang, L. Ling, Modification of polystyrene-based activated carbon spheres to improve adsorption of dibenzothiophene, Applied Surface Science, 255 (2009) 3499-3506.

[102] A. Khelifi, M.C. Almazán-Almazán, M. Pérez-Mendoza, M. Domingo-García, F.J. López-Domingo, L. Temdrara, F.J. López-Garzón, A. Addoun, Influence of nitric acid concentration on the characteristics of active carbons obtained from a mineral coal, Fuel Process. Technol. , 91 (2010) 1338-1344.

[103] Q.L. Zhuang, T. Kyotani, A. Tomita, The change of TPD pattern of O2-gasified carbon upon air exposure, Carbon, 32 (1994) 539-540.

[104] U. Zielke, K.J. Hüttinger, W.P. Hoffman, Surface-oxidized carbon fibers: I. Surface structure and chemistry, Carbon, 34 (1996) 983-998.

[105] B. Marchon, J. Carrazza, H. Heinemann, G.A. Somorjai, TPD and XPS studies of O2, CO2, and H2O adsorption on clean polycrystalline graphite, Carbon, 26 (1988) 507-514.

[106] J.L. Figueiredo, M.F.R. Pereira, M.M.A. Freitas, J.J.M. Órfão, Modification of the surface chemistry of activated carbons, Carbon, 37 (1999) 1379-1389.

[107] M. Ruta, N. Semagina, L. Kiwi-Minsker, Monodispersed Pd Nanoparticles for Acetylene Selective Hydrogenation: Particle Size and Support Effects, J. Phys. Chem. C, 112 (2008) 13635-13641.

[108] P. Tribolet, L. Kiwi-Minsker, Palladium on carbon nanofibers grown on metallic filters as novel structured catalyst, Catal. Today, 105 (2005) 337-343.

[109] L.A. Langley, D.E. Villanueva, D.H. Fairbrother, Quantification of Surface Oxides on Carbonaceous Materials, Chem. Mater., 18 (2005) 169-178.

[110] T. Borjigin, F. Sun, J. Zhang, K. Cai, H. Ren, G. Zhu, A microporous metal-organic framework with high stability for GC separation of alcohols from water, Chem.

Commun., 48 (2012) 7613-7615.

[111] X. Zhao, L. Wei, J. Julson, Z. Gu, Y. Cao, Catalytic cracking of inedible camelina oils to hydrocarbon fuels over bifunctional Zn/ZSM-5 catalysts, Korean Journal of Chemical Engineering, 32 (2015) 1528-1541.

[112] X. Zhao, L. Wei, S. Cheng, E. Kadis, Y. Cao, E. Boakye, Z. Gu, J. Julson, Hydroprocessing of carinata oil for hydrocarbon biofuel over Mo-Zn/Al2O3, Applied Catalysis B: Environmental, 196 (2016) 41-49.

[113] S. Cheng, L. Wei, X. Zhao, E. Kadis, Y. Cao, J. Julson, Z. Gu, Hydrodeoxygenation of prairie cordgrass bio-oil over Ni based activated carbon synergistic catalysts combined with different metals, New biotechnology, 33 (2016) 440-448.

[114] J. Cousin Saint Remi, G. Baron, J. Denayer, Adsorptive separations for the recovery and purification of biobutanol, Adsorption, 18 (2012) 367-373.

[115] J.C. Saint Remi, T. Remy, V. Van Hunskerken, S. van de Perre, T. Duerinck, M. Maes, D. De Vos, E. Gobechiya, C.E. Kirschhock, G.V. Baron, J.F. Denayer, Biobutanol separation with the metal-organic framework ZIF-8, ChemSusChem, 4 (2011) 1074-1077.

[116] A. Oudshoorn, L.A.M. van der Wielen, A.J.J. Straathof, Adsorption equilibria of bio-based butanol solutions using zeolite, Biochemical Engineering Journal, 48 (2009) 99-103.

[117] J. Niemistö, W. Kujawski, R.L. Keiski, Pervaporation performance of composite poly(dimethyl siloxane) membrane for butanol recovery from model solutions, J. Membr. Sci. , 434 (2013) 55-64.

[118] K. Kraemer, A. Harwardt, R. Bronneberg, W. Marquardt, Separation of butanol from acetone–butanol–ethanol fermentation by a hybrid extraction–distillation process, Computers & Chemical Engineering, 35 (2011) 949-963.

[119] Y. Chen, H. Ren, D. Liu, T. Zhao, X. Shi, H. Cheng, N. Zhao, Z. Li, B. Li, H. Niu, W. Zhuang, J. Xie, X. Chen, J. Wu, H. Ying, Enhancement of n-butanol production by in situ butanol removal using permeating-heating-gas stripping in acetone-butanol-ethanol fermentation, Bioresource technology, 164 (2014) 276-284.

[120] K.-M. Lu, S.-Y. Li, An integrated in situ extraction-gas stripping process for Acetone–Butanol–Ethanol (ABE) fermentation, Journal of the Taiwan Institute of Chemical Engineers, 45 (2014) 2106-2110.

[121] L. Luo, D. Ramirez, M.J. Rood, G. Grevillot, K.J. Hay, D.L. Thurston, Adsorption and electrothermal desorption of organic vapors using activated carbon adsorbents with novel morphologies, Carbon, 44 (2006) 2715-2723.

[122] Y.C. Liao, K.M. Lu, S.Y. Li, Process parameters for operating 1-butanol gas stripping in a fermentor, Journal of bioscience and bioengineering, 118 (2014) 558-564.

[123] Y. Cao, K. Wang, X. Wang, Z. Gu, W. Gibbons, H. Vu, Adsorption of butanol vapor on active carbons with nitric acid hydrothermal modification, Bioresour. Technol., 196 (2015) 525-532.

[124] Y. Cao, K. Wang, X. Wang, Z. Gu, W. Gibbons, H. Vu, Butanol vapor adsorption behavior on active carbons and zeolite crystal, Applied Surface Science 349

(2015) 1-7.

[125] M.A. Yahya, Z. Al-Qodah, C.W.Z. Ngah, Agricultural bio-waste materials as potential sustainable precursors used for activated carbon production: A review, Renewable Sustainable Energy Rev., 46 (2015) 218-235.

[126] J.i. Hayashi, T. Horikawa, I. Takeda, K. Muroyama, F. Nasir Ani, Preparing activated carbon from various nutshells by chemical activation with K2CO3, Carbon, 40 (2002) 2381-2386.

[127] J. Sreńscek-Nazzal, W. Kamińska, B. Michalkiewicz, Z.C. Koren, Production, characterization and methane storage potential of KOH-activated carbon from sugarcane molasses, Industrial Crops and Products 47 (2013) 153-159.

[128] V.O. Njoku, B.H. Hameed, Preparation and characterization of activated carbon from corncob by chemical activation with H3PO4 for 2,4-dichlorophenoxyacetic acid adsorption, Chemical Engineering Journal, 173 (2011) 391-399.

[129] Z. Wang, J. Wu, T. He, J. Wu, Corn stalks char from fast pyrolysis as precursor material for preparation of activated carbon in fluidized bed reactor, Bioresource technology, 167 (2014) 551-554.

[130] H. Deng, L. Yang, G. Tao, J. Dai, Preparation and characterization of activated carbon from cotton stalk by microwave assisted chemical activation--application in methylene blue adsorption from aqueous solution, Journal of hazardous materials, 166 (2009) 1514-1521.

[131] N. Bagheri, J. Abedi, Preparation of high surface area activated carbon from corn by chemical activation using potassium hydroxide, Chemical Engineering Research and Design, 87 (2009) 1059-1064.

[132] W.T. Tsai, C.Y. Chang, S.Y. Wang, C.F. Chang, S.F. Chien, H.F. Sun, Cleaner production of carbon adsorbents by utilizing agricultural waste corn cob, Resources, Conservation and Recycling, 32 (2001) 43-53.

[133] C.J. Peterson, R.M. Hixon, Chemical examination of the tissue of the cornstalk, Industrial and Engineering Chemistry, Analytical Edition, 1 (1929) 64-67.

[134] Z. Gu, X. Wang, Carbon Materials from High Ash Bio-char: A Nanostructure Similar to Activated Graphene, American Transactions on Engineering & Applied Sciences, 2 (2013) 15-34.

[135] X. Xie, B. Goodell, D. Zhang, D.C. Nagle, Y. Qian, M.L. Peterson, J. Jellison, Characterization of carbons derived from cellulose and lignin and their oxidative behavior, Bioresource technology, 100 (2009) 1797-1802.

[136] Y. Cao, K. Wang, X. Wang, Z. Gu, Q. Fan, W. Gibbons, J.D. Hoefelmeyer, P.R. Kharel, M. Shrestha, Hierarchical porous activated carbon for supercapacitor derived from corn stalk core by potassium hydroxide activation, Electrochimica Acta, 212 (2016) 839-847.

[137] S. Tanada, T. Nakamura, N. Kawasaki, J. Izawa, T. Tokimoto, Y. Torii, T. Tamura, Adsorption Characteristics of Trichloroethylene Removal by 16 Kinds of Granular Activated Carbons in Gaseous Phase, Chemical and Pharmaceutical Bulletin, 42 (1994) 2146-2149.

[138] K. Kosuge, S. Kubo, N. Kikukawa, M. Takemori, Effect of Pore Structure in Mesoporous Silicas on VOC Dynamic Adsorption/Desorption Performance,

Langmuir, 23 (2007) 3095-3102.

[139] T. Panasyuk-Delaney, V.M. Mirsky, O.S. Wolfbeis, Capacitive Creatinine Sensor Based on a Photografted Molecularly Imprinted Polymer, Electroanalysis, 14 (2002) 221-224.

[140] G. Yushin, E.N. Hoffman, M.W. Barsoum, Y. Gogotsi, C.A. Howell, S.R. Sandeman, G.J. Phillips, A.W. Lloyd, S.V. Mikhalovsky, Mesoporous carbide-derived carbon with porosity tuned for efficient adsorption of cytokines, Biomaterials, 27 (2006) 5755-5762.

[141] D.J. Malik, G.L. Warwick, M. Venturi, M. Streat, K. Hellgardt, N. Hoenich, J.A. Dale, Preparation of novel mesoporous carbons for the adsorption of an inflammatory cytokine (IL-1 beta), Biomaterials, 25 (2004) 2933-2940.

[142] X. Deng, T. Wang, F. Zhao, L. Li, C. Zhao, Poly(ether sulfone)/activated carbon hybrid beads for creatinine adsorption, Journal of Applied Polymer Science, 103 (2007) 1085-1092.

[143] V. Wernert, O. Schäf, H. Ghobarkar, R. Denoyel, Adsorption properties of zeolites for artificial kidney applications, Microporous and Mesoporous Materials, 83 (2005) 101-113.

[144] D. Bergé-Lefranc, H. Pizzala, R. Denoyel, V. Hornebecq, J.-L. Bergé-Lefranc, R. Guieu, P. Brunet, H. Ghobarkar, O. Schäf, Mechanism of creatinine adsorption from physiological solutions onto mordenite, Microporous and Mesoporous Materials, 119 (2009) 186-192.

[145] D. Bergé-Lefranc, O. Schäf, R. Denoyel, J.-L. Bergé-Lefranc, R. Guieu, P. Brunet, V. Hornebecq, The extraction of creatinine from a physiological medium by a microporous solid and its quantification by diffuse reflectance UV spectroscopy, Microporous and Mesoporous Materials, 129 (2010) 144-148.

[146] C. Ye, Q. Gong, F. Lu, J. Liang, Adsorption of uraemic toxins on carbon nanotubes, Separation and Purification Technology, 58 (2007) 2-6.

[147] H.A. Tsai, M.J. Syu, Synthesis of creatinine-imprinted poly(beta-cyclodextrin) for the specific binding of creatinine, Biomaterials, 26 (2005) 2759-2766.

[148] H.-A. Tsai, M.-J. Syu, Synthesis and characterization of creatinine imprinted poly(4-vinylpyridine-co-divinylbenzene) as a specific recognition receptor, Analytica Chimica Acta, 539 (2005) 107-116.

[149] Y.-S. Chang, T.-H. Ko, T.-J. Hsu, M.-J. Syu, Synthesis of an Imprinted Hybrid Organic−Inorganic Polymeric Sol−Gel Matrix Toward the Specific Binding and Isotherm Kinetics Investigation of Creatinine, Analytical Chemistry, 81 (2009) 2098-2105.

[150] C.-X. Yang, C. Liu, Y.-M. Cao, X.-P. Yan, Metal–organic framework MIL-100(Fe) for artificial kidney application, RSC Advances, 4 (2014) 40824-40827.

[151] M. Mydlík, J. Buček, K. Derzsiová, J. Jarčuška, M. Takáč, Influence of charcoal haemoperfusion on platelet count in acute poisoning and during regular dialysis treatment, International Urology and Nephrology, 13 (1981) 387-389.

[152] J.F. Winchester, J. Silberzweig, C. Ronco, V. Kuntsevich, D. Levine, T. Parker, J.A. Kellum, J.A. Salsberg, P. Quartararo, N.W. Levin, Sorbents in acute renal failure and end-stage renal disease: middle molecule and cytokine removal, Blood

purification, 22 (2004) 73-77.

[153] S.R. Ash, T.A. Sullivan, D.J. Carr, Sorbent Suspensions vs. Sorbent Columns for Extracorporeal Detoxification in Hepatic Failure, Therapeutic Apheresis and Dialysis, 10 (2006) 145-153.

[154] S.R. Sandeman, C.A. Howell, G.J. Phillips, A.W. Lloyd, J.G. Davies, S.V. Mikhalovsky, S.R. Tennison, A.P. Rawlinson, O.P. Kozynchenko, H.L. Owen, J.D. Gaylor, J.J. Rouse, J.M. Courtney, Assessing the in vitro biocompatibility of a novel carbon device for the treatment of sepsis, Biomaterials, 26 (2005) 7124-7131.

[155] J. Yu, Y. Wu, S. Wang, X. Ma, The preparation of cellulose nitrate derivatives and their adsorption properties for creatinine, Carbohydrate polymers, 70 (2007) 8-14.

[156] E.A. Friedman, Bowel as a kidney substitute in renal failure, American Journal of Kidney Diseases, 28 (1996) 943-950.

[157] G. Brunori, B.F. Viola, P. Maiorca, G. Cancarini, How to Manage Elderly Patients with Chronic Renal Failure: Conservative Management versus Dialysis, Blood purification, 26 (2008) 36-40.

[158] N. Soudani, S. Souissi-najar, A. Ouederni, Influence of Nitric Acid Concentration on Characteristics of Olive Stone Based Activated Carbon, Chinese Journal of Chemical Engineering, 21 (2013) 1425-1430.

[159] A. Zhou, X. Ma, C. Song, Effects of oxidative modification of carbon surface on the adsorption of sulfur compounds in diesel fuel, Applied Catalysis B: Environmental, 87 (2009) 190-199.

[160] Z.P. Liang, Y.Q. Feng, S.X. Meng, Z.Y. Liang, Equilibrium and kinetic modeling of adsorption of urea nitrogen onto chitosan coated dialdehyde cellulose, Process Biochemistry, 40 (2005) 3218-3224.

[161] S. Brunauer, L.S. Deming, W.E. Deming, E. Teller, On a Theory of the van der Waals Adsorption of Gases, Journal of the American Chemical Society, 62 (1940) 1723-1732.

[162] Q. Wang, X. Liang, W. Qiao, C. Liu, X. Liu, R. Zhang, L. Ling, Modification of polystyrene-based activated carbon spheres to improve adsorption of dibenzothiophene, Applied Surface Science, 255 (2009) 3499-3506.

[163] A.M.T. Silva, B.F. Machado, J.L. Figueiredo, J.L. Faria, Controlling the surface chemistry of carbon xerogels using HNO3-hydrothermal oxidation, Carbon, 47 (2009) 1670-1679.

[164] Z.M. Wang, N. Yamashita, Z.X. Wang, K. Hoshinoo, H. Kanoh, Air oxidation effects on microporosity, surface property, and CH4 adsorptivity of pitch-based activated carbon fibers, Journal of colloid and interface science, 276 (2004) 143-150.

[165] A. Zhou, X. Ma, C. Song, Liquid-phase adsorption of multi-ring thiophenic sulfur compounds on carbon materials with different surface properties, The Journal of Physical Chemistry B, 110 (2006) 4699-4707.

[166] H. Guedidi, L. Reinert, J.-M. Lévêque, Y. Soneda, N. Bellakhal, L. Duclaux, The effects of the surface oxidation of activated carbon, the solution pH and the temperature on adsorption of ibuprofen, Carbon, 54 (2013) 432-443.

[167] Y.-Q. Wang, H. Viswanathan, A.A. Audi, P.M. Sherwood, X-ray photoelectron spectroscopic studies of carbon fiber surfaces. 22. Comparison between surface treatment of untreated and previously surface-treated fibers, Chemistry of Materials, 12 (2000) 1100-1107.

[168] Y. Zhang, Y. Cheng, N. Chen, Y. Zhou, B. Li, W. Gu, X. Shi, Y. Xian, Recyclable removal of bisphenol A from aqueous solution by reduced graphene oxide-magnetic nanoparticles: adsorption and desorption, Journal of colloid and interface science, 421 (2014) 85-92.

[169] W. Kong, Q. Dai, J. Ren, N. Ma, Homogeneous acylation of xylan with 3,5-dinitrobenzoyl in ionic liquid and the adsorption property, Carbohydrate polymers, 128 (2015) 105-111.

[170] R.L. Tseng, F.C. Wu, Inferring the favorable adsorption level and the concurrent multi-stage process with the Freundlich constant, Journal of hazardous materials, 155 (2008) 277-287.

[171] N. Ahalya, R.D. Kanamadi, T.V. Ramachandra, Biosorption of chromium (VI) from aqueous solutions by the husk of Bengal gram (Cicer arientinum), Electronic Journal of Biotechnology, 8 (2005) 258-264.

[172] R. Bellmann, I.W. Graziadei, C. Feistritzer, H. Schwaighofer, F. Stellaard, E. Sturm, C.J. Wiedermann, M. Joannidis, Treatment of refractory cholestatic pruritus after liver transplantation with albumin dialysis, Liver Transplantation, 10 (2004) 107-114.

[173] J. Hu, R. Shang, B. Heijman, L. Rietveld, Influence of activated carbon preloading by EfOM fractions from treated wastewater on adsorption of pharmaceutically active compounds, Chemosphere, 150 (2016) 49-56.

[174] J. Hu, A. Martin, R. Shang, W. Siegers, E. Cornelissen, B. Heijman, L. Rietveld, Anionic exchange for NOM removal and the effects on micropollutant adsorption competition on activated carbon, Separation and Purification Technology, 129 (2014) 25-31.

[175] J. Simon Craw, M. D. Cooper, I. H. Hillier, The structure and intermolecular interactions of a creatinine designed-receptor complex, studied by ab initio methods, Journal of the Chemical Society, Perkin Transactions 2, (1997) 869-872.

[176] T. Bell, Z. Hou, Y. Luo, M. Drew, Detection of creatinine by a designed receptor, Science, 269 (1995) 671.

[177] R.E. Reddick, G.L. Kenyon, Syntheses and NMR studies of specifically labeled [2-15N]phosphocreatine, [2-15N]creatinine, and related 15N-labeled compounds, Journal of the American Chemical Society, 109 (1987) 4380-4387.

[178] G.S. Szymański, T. Grzybek, H. Papp, Influence of nitrogen surface functionalities on the catalytic activity of activated carbon in low temperature SCR of NOx with NH3, Catalysis Today, 90 (2004) 51-59.

[179] J. Lahaye, G. Nanse, A. Bagreev, V. Strelko, Porous structure and surface chemistry of nitrogen containing carbons from polymers, Carbon, 37 (1999) 585-590.

[180] L. Radovic, I. Silva, J. Ume, J. Menendez, C.L.Y. Leon, A. Scaroni, An experimental and theoretical study of the adsorption of aromatics possessing electron-withdrawing and electron-donating functional groups by chemically

modified activated carbons, Carbon, 35 (1997) 1339-1348.

[181] B.J. Meldrum, C.H. Rochester, In situ infrared study of the modification of the surface of activated carbon by ammonia, water and hydrogen, Journal of the Chemical Society, Faraday Transactions, 86 (1990) 1881-1884.

[182] K. Liu, Y. Suzuki, Y. Fukuda, Surface analysis of (NH2) 2CS-treated GaP (001) by AES and XPS, Surface and Interface Analysis, 36 (2004) 966-968.

[183] J. Pels, F. Kapteijn, J. Moulijn, Q. Zhu, K. Thomas, Evolution of nitrogen functionalities in carbonaceous materials during pyrolysis, Carbon, 33 (1995) 1641-1653.

[184] H. Wang, R. Côté, G. Faubert, D. Guay, J.P. Dodelet, Effect of the Pre-Treatment of Carbon Black Supports on the Activity of Fe-Based Electrocatalysts for the Reduction of Oxygen, The Journal of Physical Chemistry B, 103 (1999) 2042-2049.

[185] Q. Pan, H. Wang, Y. Jiang, Natural graphite modified with nitrophenyl multilayers as anode materials for lithium ion batteries, Journal of Materials Chemistry, 17 (2007) 329-334.

[186] A. Golzhauser, C. Woll, Interfacial systems chemistry: out of the vacuum--through the liquid--into the cell, Physical Chemistry Chemical Physics, 12 (2010) 4273-4274.